STRUCTURE IN EVOLUTIONARY TRANSITIONS IN INDIVIDUALITY: MECHANICS, GEOMETRY, AND TOPOLOGY

A Dissertation
Presented to
The Academic Faculty

By

Shane Joseph Jacobeen

In Partial Fulfillment
of the Requirements for the Degree
Doctor of Philosophy in the
School of Physics

Georgia Institute of Technology

December 2018

STRUCTURE IN EVOLUTIONARY TRANSITIONS IN INDIVIDUALITY: MECHANICS, GEOMETRY, AND TOPOLOGY

Approved by:

Prof. Peter J. Yunker, Advisor
School of Physics
Georgia Institute of Technology

Prof. William C. Ratcliff
School of Biological Sciences
Georgia Institute of Technology

Prof. Daniel I. Goldman
School of Physics
Georgia Institute of Technology

Prof. James C. Gumbart
School of Physics
Georgia Institute of Technology

Prof. Simon Sponberg
School of Physics
Georgia Institute of Technology

On: October 23, 2018

Two are better than one, because they have a good return for their labor

King Solomon, Ecclesiastes 4:9

ACKNOWLEDGEMENTS

First and foremost, I thank my advisor, Prof. Peter J. Yunker for taking me on as his first graduate student. When I arrived at Georgia Tech in 2014, the collaboration which I have had the fortune to be a part of did not yet exist, and I initially had only limited interest in soft matter and biophysics. Instead, I was drawn to Peter's easy-going and encouraging personality, and his patient guidance, passion for science, and constant optimism have played a pivotal role in my success.

I also thank Prof. Will C. Ratcliff–co-PI on the aforementioned collaboration–for his guidance and wisdom throughout the years. My work would have been impossible without the guidance of his biological expertise. In addition, I thank the remaining members of my thesis committee, Daniel Goldman, James Gumbart, and Simon Sponberg for taking the time to guide and review my thesis research.

One of my favorite parts of my Ph.D. experience was being able to collaborate with intelligent and motivated people in tackling complex scientific questions. I have had the privilege of working with numerous individuals over the years, but I thank in particular my collaborators and co-authors Colin G. Brandys, Thomas C. Day, Elyes C. Graba, Pedro Márquez-Zacaría, and Jennifer T. Pentz for their contributions.

Additionally, I thank my fellow members of the Yunker lab for their feedback and various suggestions. These include the numerous undergraduate and high school researchers who have passed though the lab over the years, and fellow graduate students Arben Kalziqi, Jonathan Michel, David Yanni, and Thomas C. Day, as well as post-doctoral researchers Skanda Vivek and Gabi Steinbach.

Finally, a word of thanks to my family and friends who have offered their encouragement during my Ph.D.. While I have enjoyed a largely positive experience, it has not been without difficulty, and I owe a word of thanks to all those outside of academia who supported and encouraged me.

TABLE OF CONTENTS

LIST OF FIGURES

‘

SUMMARY

In the history of life on earth, Evolutionary Transitions in Individuality (ETIs) have played a transformative role, increasing complexity and creating new hierarchies of organization. Examples of ETIs–in which previously independent individuals form groups and forgo their autonomy in the creation of new, higher-level individuals–include the formation of chromosomes from unlinked replicators, multicellular organisms from single cells, and eusocial colonies from solitary insects. In this thesis, I address the fundamental role of structure in two aspects of ETIs: the mechanics and geometry in the evolution of increased size in nascent multicellular clusters, and the role of interaction topology in the evolution of specialization.

The first step in the evolution of multicellularity–an example of an ETI–is thought to be the formation of large clusters. In the first part of my thesis, we show that the size of experimentally evolved snowflake yeast clusters is limited by the accumulation of internal stress during growth. We then show that snowflake yeast mitigate this challenge and increase their size by reducing intercellular contacts within the cluster. This is achieved by a geometric, cell-level change that further work reveals is among the most efficient routes to increased size, suggesting that physically-imposed geometric constraints may guide the evolution of increased size in nascent multicellular clusters. Additionally, we evolved snowflake yeast under various physical selection protocols to study the role of the environment on their evolutionary trajectory.

In the second part of my thesis, I turn to a universal hallmark of ETIs, the evolution of functionally-specialized individuals–that is, members of the group that exclusively perform a specific function. Such specialization often results in an increase of fitness for the group, but renders specialists dependent on the rest of the group for survival, thus completing the shift in the level of individuality from the individual to the collective. To explore the role of interaction topology, we created an individual based model in which individuals interact

via specified networks. We found that certain sparse topologies allow complementary specialists to be linked, thus favoring the evolution of specialization for a much wider range of individual investment-return profiles than previously thought.

CHAPTER 1
INTRODUCTION AND BACKGROUND

1.1 Overview

The nearly 4-billion-year history of life on earth has been characterized by an ever-changing and increasingly complex struggle for existence. This is the struggle by which natural selection has rewarded those organisms which, through innovation, cooperation, or mere chance, gain a competitive advantage within their environment [1]. Thus, our biological history could be written in terms of advantage-bestowing variations which resulted in the origin and destruction of countless species.

While a complete history of evolutionary adaptations is unattainable due to their immense number and gaps in the fossil record, we can nonetheless learn a great deal about the history of life on earth by focusing on the most transformative changes. Among the most fundamental of these major evolutionary transitions are those involving the formation of new levels of individuality from previously independent units. Known as Evolutionary Transitions in Individuality (ETIs), such transitions have occurred in numerous systems of varying size and complexity, including at the molecular (eukaryogenesis), cellular (multicellularity), and community levels (eusociality) [2]. Regardless of nomenclature or categorization, these transitions have played a large role in forming lifes hierarchical structure [3, 4], and thus have indisputably caused qualitatively momentous shifts in the nature of life on earth.

While the fundamental advantages bestowed by ETIs–such as improved reproductive efficiency, protection from predation and toxins, and improved access to resources [2]–are largely agreed upon, how they take place is much less clear. How do independent individuals suddenly forgo their autonomy in the formation of a new level of individuality?

What conditions favor the commencement of such a remarkable process? What features are general to all ETIs, and which are unique?

According to a traditional division of the scientific disciplines, these questions clearly fall in the realm of biology. However, to consider them apart from the physical forces at play would be to greatly obscure our understanding thereof. While the fundamental jiggling and wiggling of atoms [5] takes place at a length scale too far removed to be directly relevant, various physical principles play fundamental roles in ETIs. For example, emergent behavior associated with marginally connected particles on a wide range of relevant length scales has long been a topic of interest in soft matter physics [6]. Therefore, the study of ETIs is best conducted without concern for traditional disciplinary boundaries.

In this thesis, I present interdisciplinary work on the role of structure in ETIs. First, using experimental evolution, we explore the physical underpinnings of the evolution of increased group size, a critical first step in the evolution of multicellularity [3, 7, 8, 9, 10]. To obtain large size, groups of cells must overcome fundamental challenges that result from their novel physical structure. Independent advances in model biological systems and our understanding of the physical principles that govern cellular interactions set the stage for a deeper understanding of the mechanics and structure of nascent multicellular clusters. I then take a general, system-agnostic perspective, and use modeling and simulation techniques to explore the role of topological structure in the evolution of specialization–a hallmark of ETIs.

1.2 Multicellularity

1.2.1 Background

The evolution of multicellularitywhich has occurred at least 25 independent timesis a classic example an ETI [9, 11]. Multicellularity transformed life on earth, as individual cells came together to form larger, multicellular organisms, and in doing so forfeited their ability to exist independently. Thus the evolution of multicellularity is demarcated by a shift in the

unit of selection from the cell to the multicellular group [3, 12, 13, 14]. This shift has often been attributed to high relatedness within groups [15, 16, 17, 18, 19], which minimizes within group competition and facilitates the heritability of group-level adaptations [20, 21, 22]. Others, however, posit that relatedness does not favor specialzation [23]. And while a universal definition of what it means to be multicellular rather than a clump of multiple cells is not yet agreed upon, a common characteristic of multicellular organisms is the presence of function-specific cells. Such specialization benefits the group by increasing its overall efficiency, and is an characteristic feature of multicellularity as single cells are required to perform all tasks related to survival, such as feeding and reproduction.

The first step in the transition to multicellularity long preceding the evolution of specialization or complexity is believed to have been the formation of simple clusters [3, 7, 8, 9, 10]. Cluster formation confers protection from predation [24, 25] or environmental toxins exposure[26], or increased cooperative efficiency [27, 28]. However, direct experimental investigation of this evolutionary transition have historically been challenging, largely because these transitions occurred approximately a billion years ago, and the evolutionary path to multicellularity has been obscured by extinction in most extant lineages [11, 29].

Recently, however, the veil of mystery over the evolution of multicellularity has been eroded by several complementary advances, including the genetic reconstruction of early events [30], experiments comparing extant multicellular taxa to their unicellular relatives [31, 32], and experimental evolution of novel multicellular organisms [33, 34, 35, 27]. Yet each of these approaches has limitations: phylogenetic maps have missing pieces and lack information on environmental factors, while the similarity between model systems and true ancestors of extant species is impossible to ascertain.

Nonetheless, the tractability and simplicity of experimental evolution has provided a particularly valuable arena for the study of the first step in the evolution of multicellularity. While model systems may not provide a direct window into our past, they can nonetheless reveal general features common to the evolution of multicellularity. For example, partnered

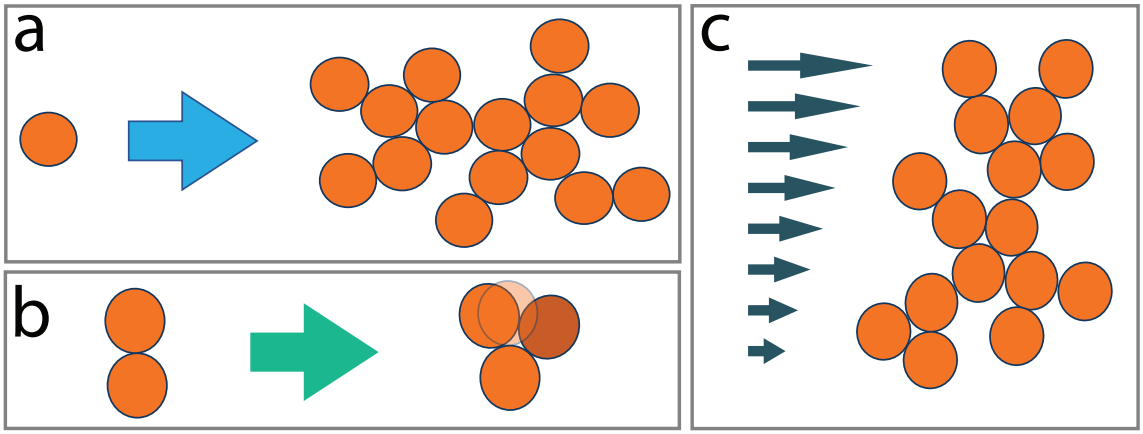

Figure 1.1: (a) Upon cluster formation, groups of cells probe the universe on new, longer length scales too large to have been relevant for their unicellular ancestors. (b) Internal force due to crowding during growth; existing cell is displaced from its equilibrium position by the addition of a new (dark orange) cell. (c) A group of cells in a graduated flow field, such as at may be found in a moving body of water. This is an example of an external force that may challenge cluster formation, growth, or evolution.

with phylogenetic analysis, experimental research has illuminated the transition from single cells to clusters with functional specialization in volvocine algae [36, 37, 38]. Additionally, the work of the Ratcliff lab and others has shown that under selection for large size, the bakers yeast Saccharomyces cerevisae readily evolves simple multicellular clusters. Detailed study of these simple snowflake clusters has provided profound insight into the genotypic and phenotypic changes associated with early multicellularity [33, 34, 35, 39].

Despite these advances, a critical aspect of cluster formation had been largely overlooked: how does physical structure affect the function and evolutionary trajectory of nascent multicellular clusters? As they probe the universe on new length scales (Fig. 1.1a), clusters of cells experience physical forces–both internal and external (Fig. 1.1b, c)–that act on length scales that were too long to be relevant to their single-celled ancestors. These evolutionarily novel forces may limit cluster size by breaking intercellular bonds, or otherwise impeding the evolution of further complexity.

The structure of multicellular groups also plays a critical role in the transition of individuality from the low-level units to the group. Upon group formation, constituent cells

are subjected to novel selective pressures acting at the group level. Frequently, these forces are in conflict with selection at the individual-level [21], and group structure is a key factor in determining the interplay between these levels of selection [40]. Furthermore, it is not obvious how simple multicellular clusters that lack developmental control networks can evolve novel multicellular complexity; that is, without evolved intercellular communication, how can selection acting exclusively at the group level effect adaptive changes which necessarily take place at the level of the cell?

1.2.2 Physical structure

We first explored the physical underpinnings of increased group size in snowflake yeast–a strain of diploid *saccharomyces cerevisiae* that remain attached to their parent after budding via a circular chitin bond. [33, 34, 35]. Snowflake yeast clusters–which get their name from their fractal-like structure–grow via the addition of new cells and reproduce via fracturing (Fig. 1.2). Over seven weeks ($\sim$ 291 generations) of daily selection for large size [33], snowflake clusters evolve to increase their radius 70%. Using microscopy and mechanical measurements, we discovered that this increase in cluster radius is the result of delayed fracturing, which occurs due to stress that accumulates within the cluster during growth.

The mechanism of this reduction in stress is a structural change within snowflake clusters. As is the case with non-living ellipsoidal packings [41], the aspect ratio of cells within the clusters plays a significant role in how they pack together–in the case of snowflake yeast, packing fraction (that is, the volume of cells enclosed within a given region divided by the total volume of the enclosing region) decreases as cells become more elongated. With more available space, clusters consisting of more elongated cells experience fewer intercellular interactions, and thus a slower rate of internal stress accumulation. Modeling of snowflake yeast clusters with a geometric simulation confirms that an increase in cellular aspect ratio slows the accumulation of internal stress that limits cluster size [42].

Simulations also reveal that changing cluster structure via cellular aspect ratio is a far

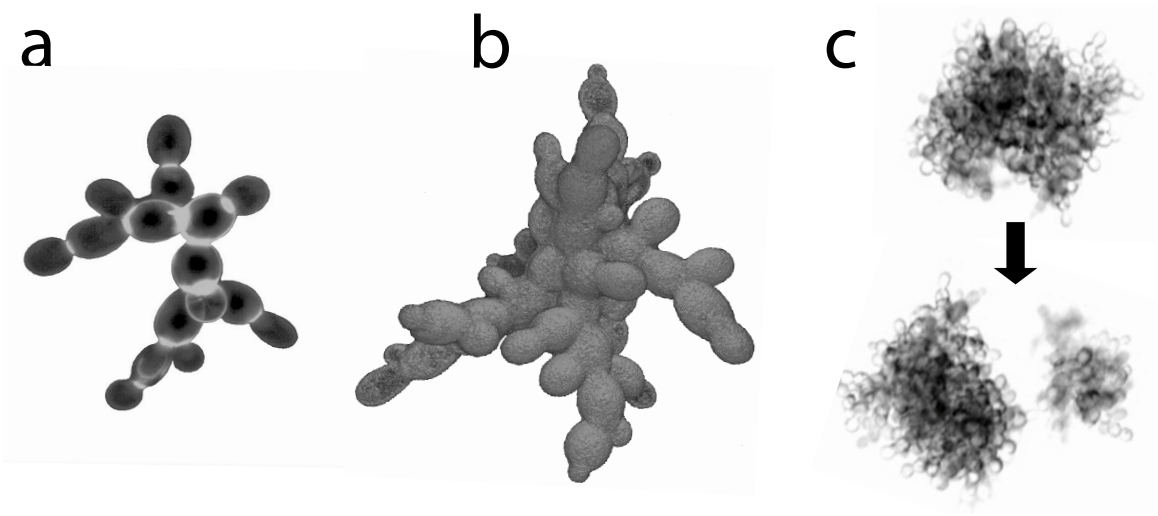

Figure 1.2: (a) Transmission image of a juvenile snowflake yeast cluster. (b) 3D confocal image of a moderate-sized snowflake yeast cluster. (c) A large cluster before and after fracture.

more efficient route to large size than increasing the strength of intercellular bonds. As cells reproduce, internal stress in the cluster increases rapidly, so increasing bond strength provides diminishing returns in increasing cluster size. Changing cellular aspect ratio, however, has a significant effect on the rate at which stress accumulates within the cluster. Thus, changing cellular geometry is a significantly more efficient route to large size than increased intercellular adhesion. Even modifying the geometric arrangement of cellular connections within clusters had a larger effect on cluster size than increasing bond strength [43]. While separating geometric effects from biological processes in the determination of causation is often impossible [44], it appears likely that the superior efficiency of modifying cluster structure over bond strength may have been a guiding force in the early stages of multicellular evolution.

We have shown how fundamental physical constraints play a critical role in the evolution of multicellularity. Simultaneously, we have gained fundamental insight into the parameters that control the packing efficiency of ellipsoidal particles bounded in a fractal-like network. While bodies of work on ellipsoidal packing and fractal networks exist independently [41, 45, 46], snowflake yeast provided a unique system in which to study their

combination. Beyond their independent contributions to physics and biology, these discoveries regarding the physical underpinnings of the size increase in nascent multicellular clusters demonstrate the intertwined and inseparable nature of biology and physics [47].

1.2.3 Environmental influence

So far, our studies have been limited to snowflake yeast that evolve large size under selection for settling in liquid media [33, 34, 35]. While this system has proven to be a powerful tool for studying the first steps in multicellular evolution [3, 7, 8, 9, 10, 33, 34, 35, 42, 43], it is necessarily far more simple than selection *in vivo*, where numerous, often competing selective pressures are at play [48]. To explore the effect of a more challenging physical environment on the evolutionary trajectory of snowflake yeast, we developed a selection protocol in which clusters are compressed prior to size selection. Large clusters are susceptible to fracture; thus compression largely deprived them of their competitive advantage under selection for large size.

We find that the same large size is achieved under both selection regimes over eight weeks of evolution. However, the population dynamics differ significantly in the two regimes, with gradual, consistent changes observed in the presence of compression, in contrast to the more abrupt change observed under negatively-frequency dependent selection. Ongoing work on this project is aimed at understanding how the presence of compression has such a significant effect on evolutionary dynamics, yet results in the same maximum cluster size.

1.3 Specialization

1.3.1 Background

Our work on snowflake yeast focused on the physical mechanism of increased cluster size, a critical step in the early evolution of simple multicellularity [3, 7, 8, 9, 10]. While several conflicting definitions of true multicellularity exist, a feature generally often associated

with complex multicellularity is the presence of functionally specialized cells [49, 50]. Functional specialization occurs when cells within a group become experts at one function (*e.g.* viability or fecundity) to the neglect of other functions requisite for survival. Thus in a group consisting solely of specialized cells, the level of individuality has shifted entirely from the cell to the multicellular organism [3, 4]. While such a transition can substantial increase the fitness of the group, many questions remain about how cells–that have been existed as individuals for millions of years–can suddenly come together and forgo their individuality for the benefit of the group.

This shift in the of the level of organismal individuality that results from specialization of the lower-level units is not unique to multicellularity; rather, it is a hallmark of all ETIs [51]. Additional examples of ETIs include the formation of the genome from unlinked replicators, eukaryogenesis, and eusocial insect colonies [52, 53]. Some even speculate that corporations [54] and humans [55] are specialized units in the high-level entity of modern society. Regardless of the system in question, many fundamental questions remain about the conditions that favor these transformational evolutionary transitions.

Much of the previous work on ETIs has employed simple models in which individuals face a trade-off between two functions (such as viability and fecundity), both of which are necessary for survival [56, 57, 58, 59, 60]. Such models reveal that as group size increases, functional specialization becomes increasingly adaptive [58, 61, 8] and requires a super-linear return on functional investment [62, 61, 63, 64, 57, 65]–that is, as an individual invests more of its limited resources in a specific function, its fitness return from that function increases to a disproportionately large degree.

The majority of prior work, however, has focused on systems in which all individuals interact with each other, and thus failed to consider the critical role of group interaction structure [62, 61, 63, 64, 57, 65]. Our work demonstrates that this is a critical feature of groups of interacting individuals; *how* the products of specialization are shared among individuals is a key aspect in determining the adaptivity of specialization. In a well-mixed pop-

ulation or fully-connected group, the fitness benefit of increased investment in one function are complemented by the loss of production of the other; hence the need for super-linear returns. However, not all interactions within the group contribute equally to fitness, so the adaptivity of specialization depends essentially on the interaction topology of the group.

1.3.2 Topological structure

To explore the role of topology in the evolution of specialization, we created an individual-based evolutionary simulation in which individuals must perform two generic functions. Groups of individuals interact via specified topologies and are selected on collective fitness. Here, topology refers simply to the interactions between individuals; while these interactions may be imposed by physical structure (Fig. 1.3), here we consider interactions of any type. We found that for certain biologically-relevant topologies, specialization can be achieved even for linear and sublinear functional returns. This is a significant result because it sheds light on how individuals that have evolved as generalists (for which sublinear returns are adaptive) for millions of years may undergo the transition to multicellularity. Thus this work contributes to a growing body of work suggesting that ETIs may have been more readily accessible than previously thought [33, 10, 49, 66].

1.4 Discussion

Evolutionary transitions in individuality are largely responsible for the complex hierarchy of life on earth today; likewise, our approach to understanding these transitions has itself been hierarchical in its scope and focus. We began with a very focused and specific problem–the evolution of increased size in snowflake yeast. In our exploration of the early steps of multicellularity–one example of an ETI–we discovered fundamental principles of cellular packings that likely apply to all similarly structured systems. We then took the opposite approach, and considered ETIs from an abstract perspective, allowing us to gain insight into the role of topological structure in the evolution of specialization.

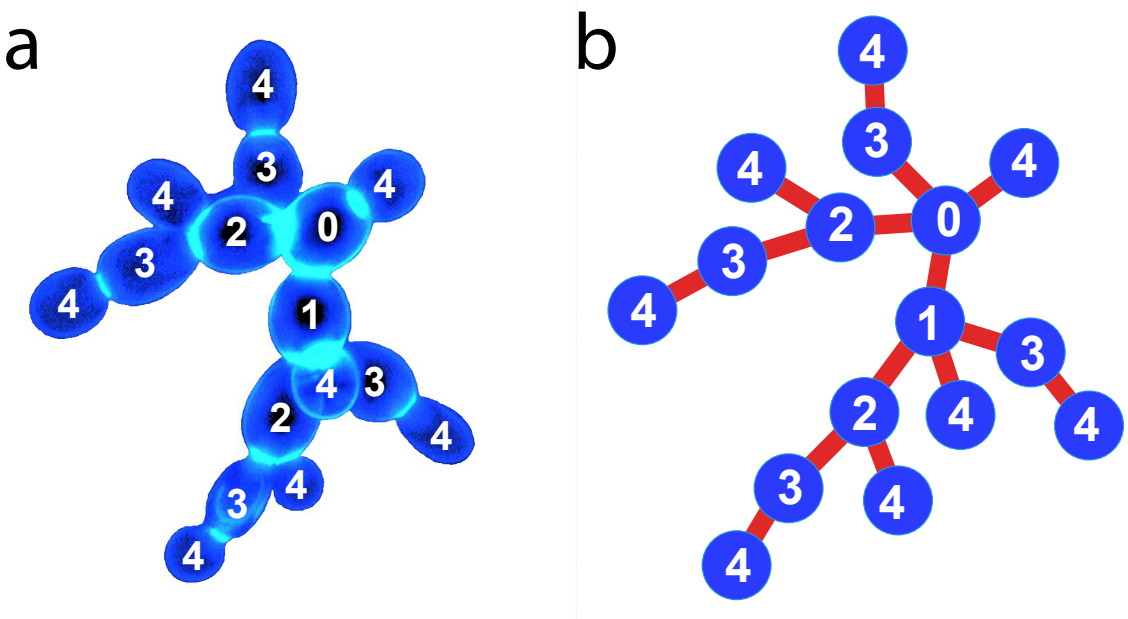

Figure 1.3: Physically-imposed group topology; an image of a juvenile snowflake yeast cluster (a) and a schematic illustrating the topology of the group defined by its intercellular bonds (b). While our study of topological structure is not limited to physically-imposed topologies, spacial proximity between individuals often promotes interaction.

This work combines experimental, computational, and theoretical approaches to a complex problem. Without the snowflake yeast model system–in which the first steps toward multicellularity are recapitulated in the lab–we could have only speculated at the mechanics underpinning increased size. Correspondingly, without a computational model to test the role of cellular aspect ratio on cluster volume fraction and internal energy accumulation, untangling various effects and validating our hypothesis would have been far more challenging, if not impossible. Furthermore, evolutionary simulations allowed us to make discoveries about theoretical requirements for the evolution of specialization that would have been impossible had our methods been confined to laboratory experiments.

Finally, the success of this work in elucidating fundamental features of ETIs is a testament to the power of combining various scientific perspectives. Drawing primarily from the disciplines of soft matter physics and evolutionary biology, this work also used tools and techniques from materials science, graph theory, and topology. This eclectic combination has yielded significant progress in our understanding not only of evolutionary transitions,

but also of the general structures at play therein, such as the packing of ellipsoidal particles in fractal networks and the role of topology in the evolution of groups of interacting individuals. While work in each of these areas is far from complete, our combination of tools from a wide variety of disciplines has yielded fundamental insights into the workings and history of the natural world.

CHAPTER 2
CELLULAR PACKING, MECHANICAL STRESS, AND THE EVOLUTION OF MULTICELLULARITY

2.1 Chapter Summary

The evolution of multicellularity set the stage for sustained increases in organismal complexity [3, 7, 8, 9, 10]. However, a fundamental aspect of this transition remains largely unknown: how do simple clusters of cells evolve increased size when confronted by forces capable of breaking intracellular bonds? Here we show that multicellular snowflake yeast clusters [33, 34, 35] fracture due to crowding-induced mechanical stress. Over seven weeks (~ 291 generations) of daily selection for large size, snowflake clusters evolve to increase their radius 1.7-fold by reducing the accumulation of internal stress. During this period, cells within the clusters evolve to be more elongated, concomitant with a decrease in the cellular volume fraction of the clusters. The associated increase in free space reduces the internal stress caused by cellular growth, thus delaying fracture and increasing cluster size. This work demonstrates how readily natural selection finds simple, physical solutions to spatial constraints that limit the evolution of group size–a fundamental step in the evolution of multicellularity. This work was conducted in collaboration with Jennifer T. Pentz, Elyes C. Graba, Colin G. Brandys, William C. Ratcliff and Peter J. Yunker and first published in *Nature Physics* on November 27, 2017.

2.2 Introduction

The first step in the transition to multicellularity–prior to the origin of cellular division of labour, genetically regulated development and complex multicellular forms–was the evolution of simple multicellular clusters [3, 7, 8, 9, 10]. Long before simple clusters of cells

can evolve traits characteristic of complex multicellularity, they must contend with physical forces–both internal and external–that are capable of breaking cell-cell bonds and thus limit cluster size. This physical challenge is critical for several reasons. First, large size is a likely prerequisite to the evolution of complex multicellularity [7, 8]. Second, these forces act on long length scales that were probably irrelevant to a single-cell ancestor, and are thus evolutionarily novel. Finally, it is unclear how simple multicellular clusters that do not yet possess genetically regulated developmental systems can evolve novel multicellular morphology.

Direct experimental investigation of the early steps in the transition to multicellularity has been challenging, largely because these transitions occurred long ago, and the evolutionary path to multicellularity has been obscured by extinction in most extant lineages [11, 29]. Recently, however, this constraint has been circumvented through experimental evolution of novel multicellular organisms [33, 34, 35, 27], genetic reconstruction of early events [30] and experiments comparing extant multicellular taxa with their unicellular relatives [31, 32].

2.3 Results

To examine the biophysical basis of the evolution of increased size in a nascent multicellular organism, we employed the tractable snowflake yeast model system [33, 34, 35]. Multicellular snowflake clusters evolved from the unicellular bakers yeast *Saccharomyces cerevisiae* under daily selection for rapid settling speed in liquid media [33]. The resulting snowflake growth form is the consequence of a single mutation in the ACE2 gene [35]. This mutation prevents cell separation after budding division, and hence causes the growth of fractal-like groups of cells (Fig. 1a). Snowflake yeast readily adapt to selection for large size, settling 28% more rapidly [34] by increasing their average radius at fracture by a factor of 1.7 ± 0.4 (Fig. 1bd) after eight weeks of selection (~ 330 generations). Although individual cells are larger in week-8 clusters than in their week-1 counterparts–their major

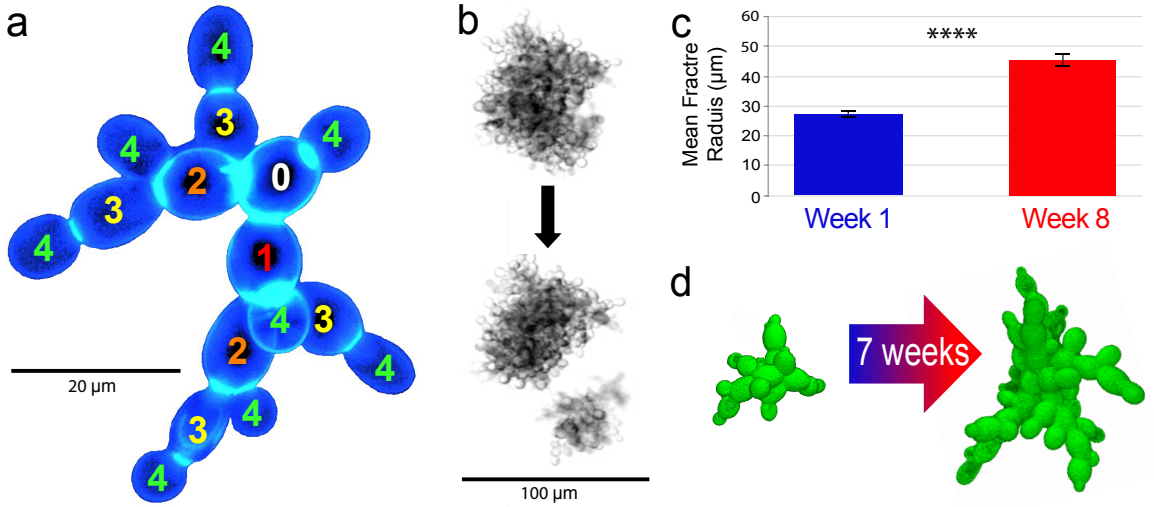

Figure 2.1: SNOWFLAKE YEAST EVOLVE LARGER SIZE. (a) Snowflake yeast form fractal-like branched clusters, imaged via fluorescence microscopy. The numbers indicate the relative generational age of cells in this cluster. (b) Bright-field images of snowflake yeast fracturing into two independently viable clusters. (c) Over seven weeks (~ 291 generations) of selection for large size, snowflake yeast clusters increase their average maximum radius by a factor of 1.7. (d) Three-dimensional confocal images show that week-8 snowflake yeast (right) contain a greater number of larger, more elongate cells than week-1 (left). The error bars in c denote one standard error of the mean; $^{****}P < 0.0001$.

axis is, on average, 23% larger–this change is insufficient to explain the observed increase in cluster size. For the present study, we utilize genotypes isolated from evolving populations after 1, 4, 6 and 8 weeks of selection, as first reported in *Ratcliff et al.* [33]. Cluster radius is calculated from the in-plane cluster area, A, by computing an effective radius $\sqrt{\frac{A}{\pi}}$.

Snowflake yeast clusters grow by the budding of existing cells, and reproduce by fracturing into two or more independently viable clusters (Fig. 1b). Fracturing limits cluster size, so elucidating the evolution of larger size in snowflake yeast requires first understanding the fracture process. Unfortunately, clusters at the point of spontaneous fracture are too large and dense for light to penetrate, so directly imaging all cells during fracture with optical microscopy is impossible. We circumvented this limitation by using a combined atomic force-brightfield microscope (AFM Workshop LS-AFM) to image and compress individual clusters. Cluster sizes were measured via bright-field microscopy before compression by an AFM cantilever at a rate of $\sim 7.5\mu m$ (~ 1 cell diameter) every 42s, during

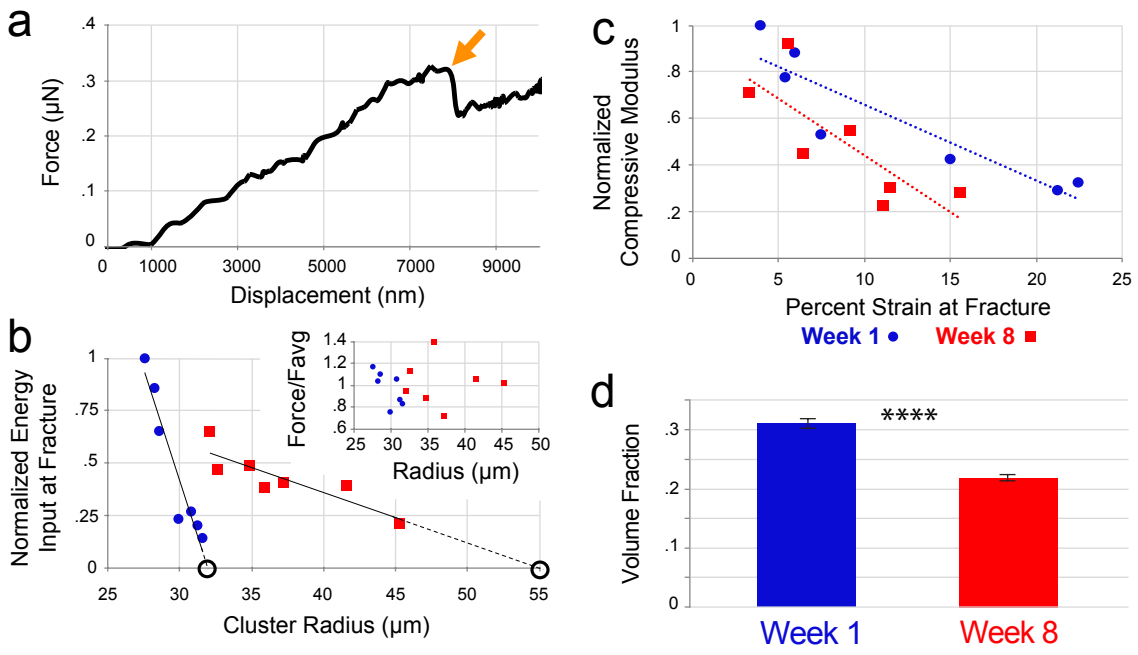

Figure 2.2: SNOWFLAKE YEAST FRACTURE DUE TO GROWTH-INDUCED MECHANICAL STRESS (a) Sample AFM forcedisplacement scan of an individual cluster. The sharp reduction in force (arrow) is indicative of a fracturing event. (b) Normalized energy input versus cluster radius for week 1 (blue) and week 8 (red) clusters, with linear extrapolations to the point of zero energy input markedthese extrapolated sizes correspond to expected spontaneous fracture sizes, and are in agreement with independent measurements thereof. Energy input normalized by the maximum measured value. The inset shows force at fracture, normalized by the average. (c) Normalized compressive modulus versus percentage of strain at fracture for week-1 (blue) and week-8 (red) clusters. Compressive modulus normalized by the maximum measured value. (d) Mean experimentally measured volume fraction for week-1 (blue) and week-8 (red) clusters. Error bars indicate standard error of the mean; $^{****}P < 0.0001$.

which the applied force was recorded. Precise forcedisplacement curves were collected for clusters of week-1 (newly multicellular) and week-8 genotypes. Fracture events are readily discernible in these curves by a sudden reduction in applied force of 20% or more (Fig. 2a), allowing for measurements of the applied force and energy input at fracture for a wide range of cluster sizes. Note, the energy input is the work done by the cantilever, calculated by estimating the integral of the force-displacement curve from zero displacement up to the point of fracture.

The applied force at fracture remained relatively constant across both genotypes and

all cluster sizes (Fig. 2b, week 1 versus week 8 $t = 0.55, P = 0.60$, two-tailed t-test). This differs from the behaviour of normal bulk materials, wherein the applied force at fracture–and the number of bonds that must fail to cause fracture–scales with sample size. With snowflake yeast, however, the fractal-like branching structure dictates that breaking a single bond is sufficient to fracture a cluster. These intercellular bonds fail when the force required to further strain them exceeds their ultimate strength6. Thus, the constant force at fracture suggests that bond strength does not vary significantly with cluster size or genotype, in agreement with independent confocal measurements of bond size (Appendix A Fig. A.3a).

These mechanical measurements also show that as cluster size increases, energy input at the point of fracture decreases approximately linearly for both week-1 and week-8 clusters, but with different slopes ($F_{3,13} = 29.2, P < 0.0001$, main effect of cluster radius in an analysis of covariance with normalized energy input at fracture as the response variable and yeast strain as the cofactor, overall $r^2 = 0.9$. The interaction with the cofactor was highly significant, $P < 0.0001$, indicating that two strains have different regression slopes). This behaviour deviates from that of normal bulk materials, in which the energy input required for fracture increases with size. Strikingly, these linear trends extrapolate to cross zero energy input at cluster sizes that are within one standard deviation of mean spontaneous fracture sizes (Appendix A Fig. A.5a). As a decrease in energy input at fracture is often a sign of residual stress in a material [67], this suggests that strain accumulation during growth plays a dominant role in determining fracture size (the comparison between snowflake yeast and bulk materials is further explored in appendix A). We thus sought to investigate whether fracture occurs due to the local accumulation of internal mechanical stress.

By directly observing the fracture process with bright-field microscopy, we found that the propagule–the smaller of two pieces post-fracture–has a mean radius 61% and 62% of the cluster radius prior to fracture, for week 1 and week 8, respectively (Appendix A

Fig. A.2a). This indicates that fracture events tend to occur deep in the cluster interior. Since we cannot directly observe these events, we instead confined clusters between glass plates with a separation of $\sim 15\mu m$, and focused on cells that were not in contact with the glass plates. In doing so, we could directly observe stress relaxation associated with intercellular bond failure (see, for example, Appendix A Fig. A.2d). Finally, we measured the compressive modulus of clusters of both genotypes. Previous studies demonstrated that the elastic modulus of individual yeast cells is relatively constant with respect to cell size[68]; if individual snowflake yeast cells behave similarly, the compressive modulus may be expected to increase if interior volume fraction increases [69, 70]. It is important to note that the distribution of cells within clusters is very heterogeneous [35, 71]; cells in the cluster interior are much more crowded than those at the periphery (Fig. 1b,d). We find that week-1 and week-8 snowflake yeast genotypes follow similar trend lines relating compressive modulus to percentage of strain at fracture (Fig. 2c) where percentage of strain is the distance the cluster is compressed divided by the cluster diameter–indicating that clusters closer to fracture are stiffer. Although indirect, these measurements are all consistent with fracture occurring due to the accumulation of internal stress from cellular growth.

To directly test whether fracture causes clusters to release accumulated stress, we utilize a microscopy-strain-gauge test, common in materials science [67]. Specifically, we measure the volume of the cluster before fracture, and the combined volume of the cluster (the larger piece post-fracture) and its propagule after fracture. If cells experience little or no mechanical stress, the total volume should remain constant or increase after fracture. However, if clusters experience repulsive mechanical stress due to cellular crowding, then branches of cells may be mechanically straightened, and the total volume should decrease after fracture as these branches are allowed to relax. Analysis of fracture events reveals that the total volume of the cluster and propagule–measured using the effective radius defined above–decreases to 94% for both genotypes ($P = 0.010$ and $P = 0.005$, for the compar-

ison to the null hypothesis that total volume after fracture is 100%, for week 1 and week 8, respectively, two-tailed t-tests). This decrease in total volume after fracture is consistent with the presence of internal stresses from cellular crowding.

Having established that cluster size is limited by fracture-inducing internal stress, we next investigated whether the large cluster-forming week-8 genotype had evolved mechanisms to ameliorate internal stress. While this could be achieved in a myriad of ways, the simplest include raising the fracture threshold or reducing the cellcell interactions that generate stress. While the former is not observed (Appendix A Fig. A.3a), the latter may well result from the measured decrease in volume fraction; that is, the total volume of cells in a cluster divided by the total volume of the cluster itself (Fig. 2d). We find that from week 1 to week 8, the volume fraction of clusters decreases substantially, from 0.32 ± 0.04 to 0.22 ± 0.03 ($t = 8.3$, $P = 6 \times 10^{10}$, two-tailed t-test). Decreasing volume fraction may decrease the number of contacts between cells, reducing the amount of internal stress, as previously observed in collections of grains [70] and unicellular yeast [69]. Thus, by reducing the number of cellcell interactions in week-8 clusters, decreasing volume fraction may also reduce the rate of internal stress accumulation.

How have week-8 clusters evolved a lower volume fraction? A simple cell-level change appears to be largely responsible. Although all S. cerevisiae cells are ellipsoidal [72], week-8 cells possess, on average, an 8% larger majorminor aspect ratio than week-1 cells (Fig. 3a; $t = 26$, $P = 3 \times 10^{136}$). Particle shape has been shown to affect numerous systems from randomly packed colloids to biofilms [41, 73]; here we examine the role of cellular aspect ratio on packing within the fractal pole-budding geometry of snowflake yeast. As previous exhaustive experiments [35] have validated that the fractal-like snowflake yeast growth form holds for week-1 and week-8 clusters of any size, the role of cell shape becomes a question of geometry. Diploid snowflake yeast grow through axial budding, producing daughter cells on the pole opposite their own mother [33, 35]. Thus, for cells of equal volume, the distal pole of those with higher aspect ratios is further from their parent; this

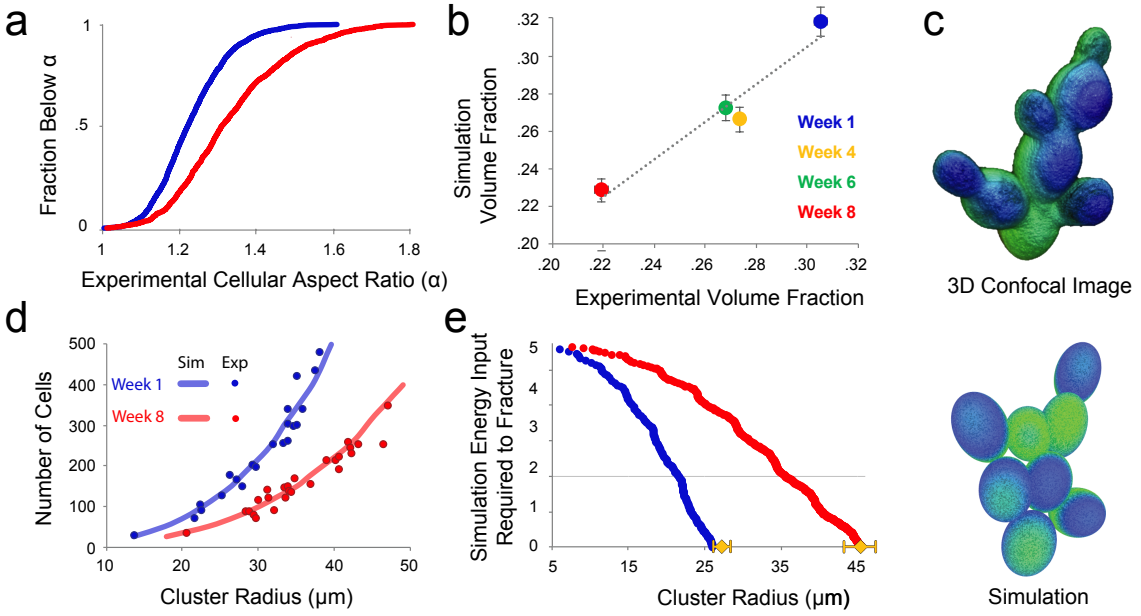

Figure 2.3: SNOWFLAKE YEAST EVOLVE TO MITIGATE MECHANICAL STRESSES BY INCREASING VOLUME FRACTION. (a) Experimentally measured fraction of cells with aspect ratio below for week-1 (blue) and week-8 (red) genotypes. (b) Volume fraction from experiment versus volume fraction from simulation. Week-4 (yellow circle) and week-6 (green circle) samples are included as well. Linear fit slope $= 0.998$, $r^2 = 0.94$; error bars indicate standard error. (c) Visual comparison of a confocal image of a snowflake (top) and a simulation-generated snowflake (bottom). (d) The simulation (continuous lines, averaged over 100 unique trials) accurately predicts the number of cells in a cluster observed in experiments (circles, each symbol is a measurement from a different cluster) as a function of radius for both genotypes. (e) Simulated energy input required to fracture versus cluster radius. The critical energy threshold was selected using the experimental value for week-8 spontaneous fracture size. Yellow diamonds show the experimentally measured spontaneous fracture size; error bars indicate standard error.

results in less cellular crowding and hence a decrease in volume fraction. Additionally, because the minimum cellcell spacing is set by the relatively invariant diameter of the circular intracellular chitin bond (Appendix A Fig. A.3b), as aspect ratio increases, the amount of deformation of minimally separated cells decreases–this may also contribute to the reduced rate of internal stress accumulation in week 8 clusters.

To formally investigate the effect of cell shape on volume fraction, we created a geometric model of the snowflake yeast growth form. Beginning from a single cell, new cells are added generation-by-generation; daughter cells are placed at a stochastic location with a polar angle of $45^\circ \pm 10\%$ with respect to the distal pole of the parent cell (Appendix A Fig. A.8a). Each generation, all cells in the cluster attempt to double. Cells, but not budding sites, may overlap; if a forbidden location is selected, no daughter cell is created and the parent cell does not attempt to reproduce again until the next generation (Appendix A Fig. A.8b). All cells have the same volume, and aspect ratio is randomly seeded from the experimentally measured distributions. Although this model lacks dynamics, simply changing the aspect ratio distribution in the simulation recapitulates the change in volume fraction observed experimentallythe slope of the best linear fit between experimental and simulated volume fractions is 0.998, with $r^2 = 0.94$ (Fig. 3b). To better validate our approach, we also measured the distribution of aspect ratios and global volume fractions for genotypes from week 4 and week (Appendix A Fig. A.6); it is interesting that the difference between week 8 and week 6 is much greater than that between week 6 and week 4, but a constant rate of change is not expected as evolution is highly stochastic and nonlinear [74, 75].

This simple model also exhibits remarkable agreement with experiment across several additional properties of snowflake yeast clusters. It reproduces clusters of cells that are structurally similar to snowflake yeast (Fig. 3c), and in addition to volume fraction, correctly predicts the number of cells as a function of radius (Fig. 3d, $N = 100$ for simulations of week 1 and week 8, $N = 21$ for week-1 experiments, $N = 26$ for week-8 experiments). Furthermore, we measured the square of the linear overlap between neighbouring cells,

essentially the sum of their radii minus their centre-to-centre separation (Appendix A Fig. A.8b). Linear overlap squared is a proxy for elastic energy storage from internal stress, as cells that overlap in the simulation would have displaced each other in a real cluster, and under a harmonic model the energetic cost is proportional to the displacement squared. For clusters created from the week-1 and week-8 aspect ratio distributions, the mean cumulative squared overlap at fracture sizes predicted by the linear extrapolation of the AFM data differs by only 6.5%, with standard error of the means of 2.2% and 2.1% for week 1 and week 8, respectively (week-1 versus week-8 cluster radius at fracture-inducing overlap squared, $P = 4.9 \times 10^{-63}$, two-tailed t-test). Thus, subtracting the cumulative squared overlap in the simulations from this threshold value (which gives the energy input required to fracture) produces a plot in which relative trends are consistent with the AFM experiments (Figs. 2b and 3e), and gives estimates of the spontaneous fracture size within error bars of experimentally measured values (Appendix A Fig. A.5a).

Finally, we investigated packing on a single parent cell; only the original cell adds daughters, but it does so until all available space is occupied. Intriguingly, week-8 parent cells can accommodate an average of only $\sim 5\%$ more daughter cells than week-1 parent cells. However, the total squared overlap of the week-8 daughter cells is $\sim 31\%$ smaller than that of week-1 daughter cells. This indicates that as aspect ratio increases, the amount of internal stress in a cluster decreases, even if the number of cells increases slightly

2.4 Discussion

By changing only the aspect ratio distributions from which new cells are seeded, our minimal model captures the observed phenotypic properties of evolving snowflake yeast. Despite the presence of numerous layers of biological complexity, these independent tests of our geometric model suggest that it captures critical aspects of snowflake yeast structure. While future experiments capable of directly probing the effect of cell shape on packing are necessary to prove causation, results from the current experiments and simulations offer

compelling evidence that cellular elongation plays a significant role in delaying snowflake fracture by decreasing the rate of internal stress accumulation (a more detailed discussion of the evidence for this claim is included in Appendix A).

Multicellularity has evolved in at least 25 independent lineages across a remarkable range of ecologies [9, 11]. Despite this diversity, there is general agreement that, at least initially, these lineages were under strong selection for increased size, due to ecological stresses such as predation [24, 25], toxin exposure[26] or for improved extracellular cooperation [27, 28]. Our work shows how a simple multicellular entity can overcome fundamental physical constraints on size, converging on a solution reminiscent of work on non-living ellipsoidal packings [41].

Snowflake yeast are an example of fixed-geometry multicellularity; cells have little ability to move within the organism after they are formed. This type of multicellularity has evolved numerous times (for example, land plants, red, brown and green algae, and fungi), and is one in which simple clusters of cells have relatively few ways in which they can generate novel multicellular morphology. While we observed a change in cell shape, one could imagine that, within the context of a specific multicellular geometry, novel multicellular traits could also be generated through changes in the strength of cellular attachment, budding angle or cell age-specific growth rates. Multicellular development, a key trait in the origin of complex multicellularity, may readily evolve in nascent multicellular lineages when these traits are plastically expressed in a location specific manner.

While no single model system can represent the diversity of routes to multicellularity, our work nonetheless highlights the central (and probably conserved) role that evolving novel materials properties play during this major evolutionary transition. Further, it demonstrates the physical basis of multicellular adaptation, showing how simple cell-level changes can guide the emergence of novel collective-level traits. The connections between evolution and mechanical fracture, biological fitness and volume fraction serve as another demonstration of the intertwined nature of biology and physics [47].

CHAPTER 3
GEOMETRY, PACKING, AND EVOLUTIONARY PATHS TO INCREASED MULTICELLULAR SIZE

3.1 Chapter Summary

The evolutionary transition to multicellularity transformed life on earth, heralding the evolution of large, complex organisms. Recent experiments demonstrated that laboratory-evolved multicellular snowflake yeast readily overcome the physical barriers that limit cluster size by modifying cellular geometry [42]. However, it is unclear why this route to large size is observed, rather than an evolved increase in intercellular bond strength. Here, we use a geometric model of the snowflake yeast growth form to examine the geometric efficiency of increasing size by modifying geometry and bond strength. We find that changing geometry is a far more efficient route to large size than evolving increased intercellular adhesion. In fact, increasing cellular aspect ratio is on average ~ 13 times more effective than increasing bond strength at increasing the number of cells in a cluster. Modifying other geometric parameters, such as the geometric arrangement of mother and daughter cells, also had larger effects on cluster size than increasing bond strength. Simulations reveal that as cells reproduce, internal stress in the cluster increases rapidly; thus, increasing bond strength provides diminishing returns in cluster size. Conversely, as cells become more elongated, cellular packing density within the cluster decreases, which substantially decreases the rate of internal stress accumulation. This suggests that geometrically imposed physical constraints may have been a key early selective force guiding the emergence of multicellular complexity. This work was conducted in collaboration with Elyes C. Graba, Colin G. Brandys, Thomas C. Day, William C. Ratcliff and Peter J. Yunker and published in *Physical Review E* on May 14, 2018.

3.2 Introduction

The evolution of multicellular organisms from single-celled ancestors set the stage for unprecedented increases in complexity, especially in plants and animals [7, 76]. In nascent multicellular organisms, size and complexity are strongly related [8, 7]; recent work has highlighted the potential for a size-complexity evolutionary feedback loop [76]. However, it is unclear how early, simple multicellular organisms evolved to be larger. Newly multicellular organisms lack genetically-regulated development, growing instead through the stochastic replication of physically-attached individual cells. At high cell densities, stochastic growth can result in large intercellular forces [69], fragmenting groups and limiting multicellular size [42]. Thus, mitigating internal mechanical stress is one of the first evolutionary challenges faced by nascent multicellular organisms. Though the transition to multicellularity occurred independently in at least 25 separate lineages [9, 11], we know little about the physical properties of early multicellular lineages due to their ancient origins and limitations of the fossil record.

Nonetheless, there are two clear routes to increased size in nascent multicellular clusters of cells whose size is limited by the accumulation of internal stress: an organism could evolve to withstand larger intercellular stresses, or, it could evolve to accumulate intercellular stresses at a slower rate during growth. The former strategy would likely involve evolving stronger intercellular bonds, while the later would involve changes to structural geometry. Geometrically-imposed physical constraints play key roles in the organization of numerous microbial systems, including growing biofilms and swarming or swimming communities [73, 77, 78, 79]. Separating geometric effects from biological processes is nontrivial [44], however, and little is known about how simple multicellular systems respond to selection for increased size.

Recently, model systems of simple multicellularity have allowed the early steps of this transition to be studied in the lab with unprecedented precision [33, 29, 27, 80]. In the

case of 'snowflake yeast' [33], simple multicellular clusters of *Saccharomyces cerevisiae* are subjected to daily selection for large size; they rapidly evolve to double their maximum number of cells per cluster in just seven weeks [42]. Snowflake yeast cluster size is limited by the fracturing of intercellular bonds under growth-induced stresses (Figure 3.1a). Larger size at fracture is accomplished primarily by a simple change to cluster geometry: over ~ 291 generations, snowflake yeast evolved to have more elongated cells. This increase in cellular aspect ratio decreases the cellular packing fraction, slowing the accumulation of internal stress and delaying fracture [42] (Figure 3.1b). Cellular elongation is a parallel evolutionary trait, evolving independently in replicate populations [34, 42]. However, it remains unclear *why* this evolutionary route to large size is repeatedly observed: do snowflake yeast clusters modify geometry because it is more effective than increasing the strength of cell-cell bonds, or for proximate reasons relating to the model system (e.g., it may be easier to modify geometry than bond strength)?

To investigate the roles of geometry and bond strength in the evolution of nascent multicellularity, we employ a geometric model of experimentally-evolved snowflake yeast [33, 34, 35], introduced and experimentally validated in Jacobeen *et. al.*, 2018 [42]. We find that modifying packing geometry, and thus slowing the accumulation of internal stresses, is a far more efficient route to large size than increasing intercellular bond strength. This result is likely general, as cells are capable of imparting tremendous forces during growth [69], and the resulting cell-cell forces increase rapidly in jammed aggregates. Thus, evolving physical robustness by modifying multicellular geometry may have been a key early selective force guiding the emergence of multicellular complexity.

3.3 Background

We simulate the growth of snowflake yeast clusters with a simple, three-dimensional geometric model [42] based on their fractal-like growth pattern [33]. The model is purely structural, *i.e.*, it lacks dynamics, yet it accurately reproduces many relevant experimentally-

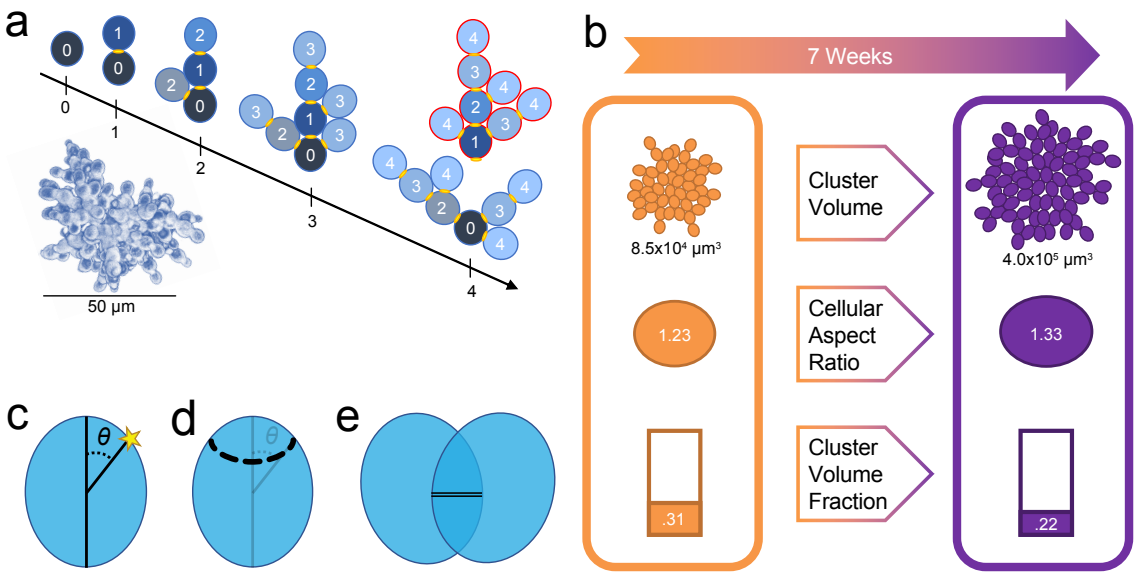

Figure 3.1: (a) 2D schematic of snowflake yeast growth morphology, showing fracture due to cellular crowding. Inset: 3D confocal image of a snowflake yeast cluster. (b) Changes over 7 weeks of experimental evolution in mean values of snowflake yeast cluster size, cellular aspect ratio, and cluster volume fraction. (c-e) describe the geometric simulation of cluster growth; (c) new cells are added on the surface of their parent at an attachment site (yellow star) defined by the polar angle θ from the major axis of the cell; this angle is referred to as the 'angle of attachment'. (d) Rotating θ around the major axis of the cell defines a ring on its surface along which daughter cells may be randomly placed (dashed line); this ring is termed the 'budding ring'. (e) The length of the double line illustrates the linear overlap between two cells.

measured structural properties of snowflake yeast [42] (for more details on experimental validation of the model, please see the Appendix B).

3.3.1 Model

Snowflake yeast cells reproduce via budding [33]; daughter cells remain attached to their mothers, creating a biologically and physically tractable multicellular cluster (Fig. 3.1a). In our simulation, cells are modeled as prolate spheroids (ellipsoids in which two 'equatorial' radii are equal and less than the polar radius), with major-minor axis aspect ratio α. Each generation, all cells in the cluster attempt to reproduce by adding a daughter cell of identical volume on their surface. Daughter cells are placed at a specified angle from the polar axis, called the angle of attachment, θ, where θ is the acute angle between the parent cell's major

axis and a vector that originates at the geometric center of the cell and passes through the point on its surface at which the daughter cell attaches (Fig. 3.1c). Thus, daughter cells are randomly placed along a 'budding ring' on their parent's surface (Fig. 3.1d). Additionally, cells other than the basal cell have an 80% chance of spawning at the pole opposite their parent (that is, with $\theta = 0$) on their initial reproduction attempt. Cellular bodies may overlap (Fig. 3.1e), but the center-to-center separation may not be less than 50% of their small diameter; this constraint is analogous to disallowing the overlap of bud scars (*i.e.*, attachment sites). If the randomly selected attachment site would cause too much ($>50\%$) overlap, the daughter cell is not created and the parent cell misses their chance to reproduce that generation.

Varying θ and α facilitate changes to cluster geometry. To vary bond strength, we first calculate the deformation energy (u) between the bodies of neighboring cells. That is

$$u_{ij} = (d - r_i - r_j)^2 \tag{3.1}$$

where d is the center-to-center distance between overlapping cells, and r_i and r_j are the equatorial radii of two neighboring cells. $u_{ij} = 0$ for non-overlapping cells, and the total 'deformation energy' (U) in a cluster is the sum of individual u_{ij}:

$$U = \sum_{i=1}^{N} \sum_{j \neq i}^{N} u_{ij} \tag{3.2}$$

where N is the number of cells in the cluster. In a real cluster, cells would bend at their cell-cell bonds rather than overlap, so linear overlap acts as a proxy for deformation and squared overlap is a proxy for deformation energy, or internal stress within the cluster (using a Hertzian, rather than a harmonic model for deformation energy does not qualitatively change the results of this simulation [42]). As clusters fracture due to an asymmetric accumulation of internal stress concentrated in the core of the cluster [42] (Fig S1d), we use a U threshold (U_c) to limit cluster size. Snowflake clusters fracture when their internal

stress exceeds the ultimate strength of the cell-cell bonds; thus, changing U_c is analogous to changing bond strength.

As previously reported in Jacobeen *et. al.*, 2018 [42], this geometric model recapitulates many key structural features observed in experiments. Experimentally evolved isolates were modeled by randomly picking each new cell's α from experimentally measured distributions. These simulations revealed that as mean cellular α increases, cluster volume fraction decreases. In fact, simulations closely replicate experimental observations: simulated and experimentally measured packing fractions are within 5% of each other for all four genotypes studied (the validation of the model via comparison with experimental results is detailed in Chapter 2 and revisited in Appendix B). As internal stress limits cluster size by fracturing intercellular bonds, the decrease in volume fraction due to cellular geometry modification likely plays a large role in the evolved increase in cluster volume over seven weeks [42] (Figure 3.1b).

3.4 Results

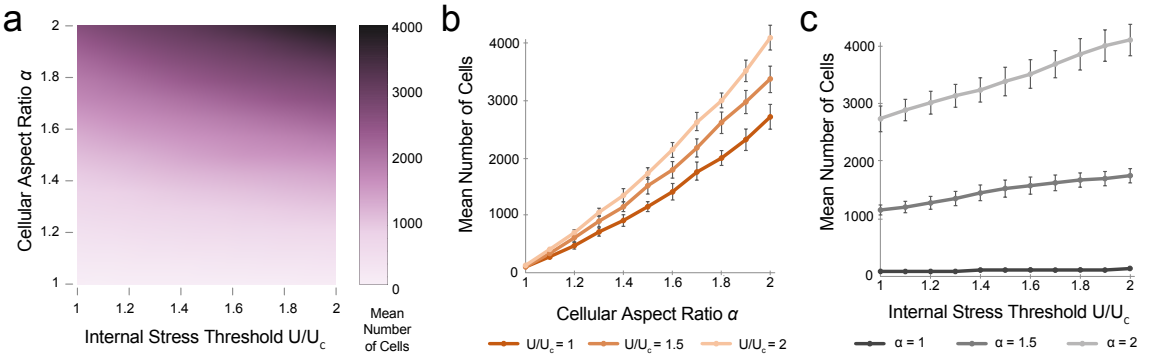

Figure 3.2: (a) Interpolated heat map of the mean number of cells in a cluster as a function of cellular aspect ratio (α) and deformation energy threshold (U_c). (b) Mean number of cells per cluster versus α for U_c (dark orange, bottom), $1.5U_c$ (medium orange, middle), and $2U_c$ (light orange, top). (c) Mean number of cells per cluster versus U_c for $\alpha = 1.0$ (dark gray, bottom), $\alpha = 1.5$ (medium gray, middle), and $\alpha = 2.0$ (light gray, top). Each data point is the average of 100 independent simulations. Error bars indicate standard deviation.

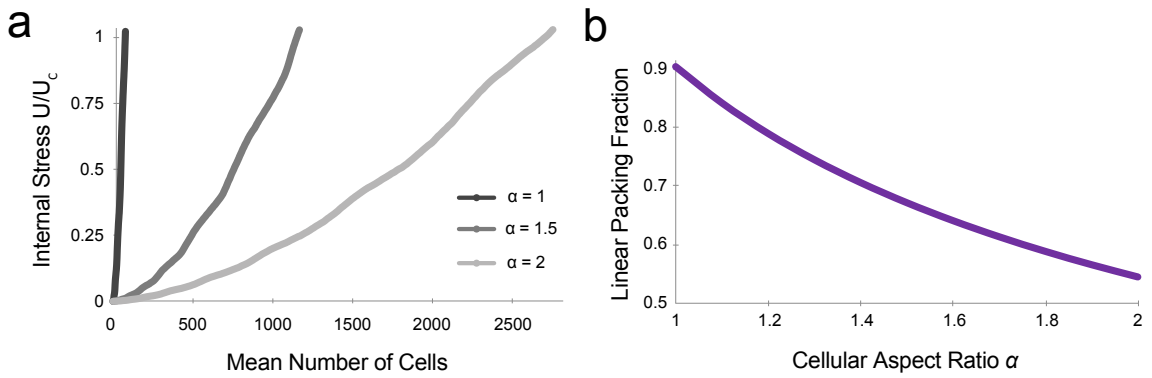

Figure 3.3: (a) As a cluster grows, total deformation energy, U,increases as well. This increase is rapid when $\alpha = 1$ (dark gray, left), moderate for $\alpha = 1.5$ (medium gray, middle), and slowest for $\alpha = 2$ (light gray, right). Each overlapping data point is the average of 100 independent simulations. (b) Linear packing fraction for 5 daughter cells on a single mother cell as a function of aspect ratio for $\theta = 54°$.

To directly compare the efficiency of increasing cluster size via cellular elongation and increased bond strength, we first simulated clusters with a wide range of α and U_c values (we set $\theta = 54°$, as cluster size is maximized for this value). We varied α and U_c between 1.0 and 2.0 in steps of 0.1, and simulated 100 clusters for each pair of parameters (Fig. 3.2a). The mean number of cells per cluster increases rapidly with increasing α for any value of U_c (Fig. 3.2a and b). In contrast, the mean number of cells increases much more slowly with increasing U_c (Fig. 3.2a and c). Thus increasing α is a more efficient path to large size than increasing U_c.

While increasing α always increases cluster size more then increasing U_c, the size of this disparity varies. For example, the smaller α is, the more beneficial it is to increase α than U_c. In fact, for clusters of spherical cells ($\alpha = 1.0$), it is on average ~ 59 times more effective to increase α than to increase U_c (*i.e.*, for small α, there is almost no discernible gradient along the U_c axis (Fig. 3.2a)). Thus, there is an especially large incentive to increase aspect ratio at least a little above 1.0. Further, increasing U_c always enlarges the incentive for increasing α; this is visible in Fig. 3.2a as the strength of the vertical gradient increases with U_c. Though the relative superiority of increasing α over U_c varies over the studied range of parameters – generally decreasing significantly with increasing α and

increasing with U_c – it is always at least 2.5 times more effective to increase α, and on average ~ 13 times more cells are added for an increase of $.1$ in α than for an increase of the same magnitude in U_c.

Why is increasing aspect ratio a more efficient route to large size than increasing bond strength? To investigate, we measured the deformation energy in simulated clusters as a function of the mean number of cells. U increases ∼quadratically with N for any value of α (Figure 3.3a). Thus, increasing U_c yields sub-linear returns ($N \sim \sqrt{U_c}$). However, increasing α causes U to increase at a slower rate, allowing more cells to be added before U_c is reached. The linear relationship between N and α (Fig. 3.2c) further demonstrates the superior returns on increasing α rather than U_c.

To understand how cellular aspect ratio affects internal stress accumulation, we calculated the linear packing fraction (*i.e.*, the occupied fraction of the budding ring) of 5 non-overlapping daughter cells on a parent cell for $\theta = 54^\circ$ (5 cells was chosen because it is the maximum number that can be placed at $\theta = 54^\circ$ for all values of α between 1 and 2) (Figure 3.3b). Considering that daughter cells maximize their available space when they are oriented perpendicular to the long axis of their parent, linear packing fraction ϕ, is

$$\phi = \frac{n \cdot 2 \cdot r_{min}}{2 \cdot \pi \cdot (r_\theta + \alpha \cdot r_{min})} \tag{3.3}$$

where n is the number of daughter cells, r_{min} is the minor radius, and r_θ is the radius at θ. Larger α daughter cells have smaller widths; smaller widths make it less likely for any two cells to overlap. Thus, more cells must be added to clusters with large α to obtain the same packing fraction - and U - as clusters with small α.

We also investigated other geometric parameters, to determine if the effects of α represented an isolated case. We varied θ between 30° and 90° in increments of 12° and again varied U_c from 1.0 to 2.0 in steps of 0.1. For each pair of parameters, 100 independent simulations were conducted with $\alpha = 1.5$, and the resulting mean values are shown in the interpolated heat map in figure 3.4a. As previously mentioned, cluster size is maximized

when $\theta = 54^\circ$ for all values of U_c (note, $\theta = 54^\circ$ is within the experimentally observed range [42]). This is due to a trade-off between local and global packing effects. The number of cells that can pack on a single parent increases with θ–up to $\theta = 90^\circ$–because the circumference around which daughters are packed is largest at $\theta = 90^\circ$. However, branches within a cluster interfere with each other less for smaller values of θ; 54° is the angle where the trade-off between these competing affects is maximized. Additionally, changing θ (moving it closer to $\theta = 54^\circ$) is generally a more efficient route to increase cluster size than increasing U_c, especially if θ is far from $\theta = 54^\circ$. However, since an optimal value of θ exists (unlike with α), when θ is close to 54°, increasing U_c is more beneficial. Note, the optimum angle is near the so-called 'magic angle', $\theta = 54.7^\circ$[81], suggesting that the snowflake yeast structure is analogous to packing cells in cones (see SI for more details).

Finally, we investigated the effect of heterogeneity in geometric parameters. Along with providing another geometric parameter to check, monodisperse values of α and θ are biologically unrealistic, as real snowflake yeast clusters feature polydispersity in both parameters [42]. First, a single pair of α and θ parameters was chosen; we selected $\alpha = 1.5$ because it is in the center of the range of values studied and is within the experimentally observed range, and $\theta = 54^\circ$ because it is the optimum value of θ. Variance is introduced in the form of a truncated Gaussian distribution centered on each selected parameter. For every cell added, the value of each parameter is chosen from a self-centered Gaussian distribution; however, if the value selected lies outside the relevant range (1.0 - 2.0 for α, 30° to 90° for θ), another value is randomly selected. We simulated 100 independent clusters for Gaussians with standard deviations of 0.05, 0.10, and 0.20 of the mean θ or α.

We find that variance in both α and θ has little effect on cluster size when it is relatively small (standard deviation / mean ≤ 0.1); larger variances, however, (> 0.1) decrease cluster size (Figure 3.4b). The inverse relationship between size and large variance is expected for θ; any deviation from the optimal value naturally leads to smaller clusters. However, the relationship between N and $alpha$ is highly linear (figure 3.2b), meaning that the detriments

of smaller aspect ratio cells must outweigh the benefits of longer aspect ratio cells within these disordered clusters. If the standard deviation in alpha decreases from 0.2 to 0.1, the resulting increase in cluster size is the same as that caused by an increase in α of $\sim .04$ or and increase in U_c of $\sim .26$, again supporting the idea that modifying geometry provides a larger return to the cluster size than modifying bond strength.

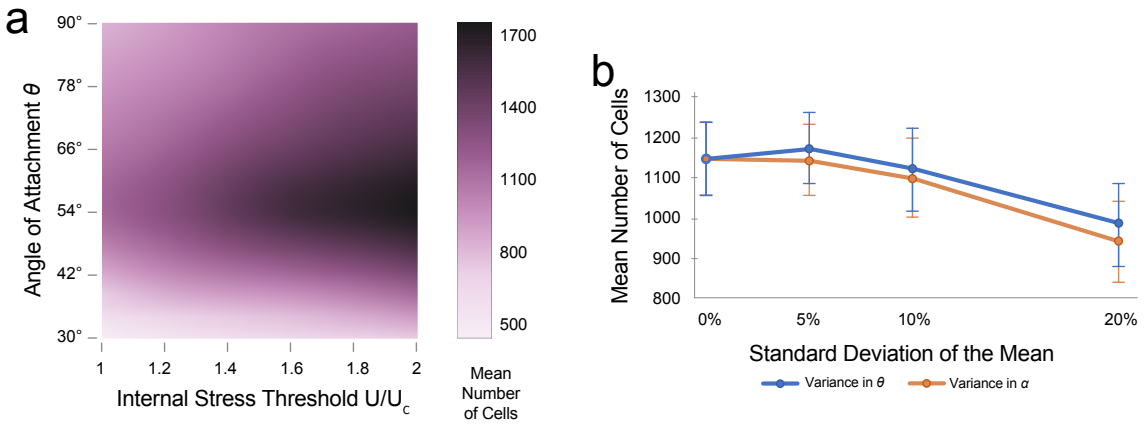

Figure 3.4: (a) Interpolated heat map of the mean number of cells in a cluster as a function of angle of attachment (θ) and deformation energy threshold (U_c). (b) Effect of variance in the angle of attachment(θ) and cellular aspect ratio(α) on cluster size. The number of cells in a cluster versus the standard deviation of the truncated Gaussian distribution for θ (blue, upper) and α (orange, lower). Each data point is the average of 100 independent simulations. Error bars indicate standard deviation.

3.5 Discussion

Evolutionary benefits stemming from size are thought to be a key driver of early multicellularity [9, 76], affording protection from common threats to microbial life (*e.g.*, predation and toxin exposure [26, 25, 24]). However, *how* large physical size could be achieved by newly multicellular organisms has remained poorly understood. Recent work revealed that snowflake yeast evolve increased size via modifications to cellular geometry[42]; here, we offer evidence for *why* this route was observed. Geometric modeling reveals that

modifying geometry – via three different parameters – is a significantly more effective means to achieve larger cluster size than increasing bond strength. Internal stress increases rapidly with cellular reproduction, so investing in bond strength produces diminishing returns. Conversely, modifying cell shape, budding angle, or the variance of these quantities changes how cells pack, slowing the accumulation of internal stress.

Our results highlight the absolute limit of spatial constraints. Two cells cannot overlap, so at high cell density the addition of new cells rapidly increases internal stress. The optimal strategy is not to increase bond strength in the face of vanishing free space, but to pack more efficiently so free space remains available longer. The rapid increase in internal stress with increasing cell number is reminiscent of the jamming transition of athermal grains, for which pressure increases with increasing packing fraction [82, 83]. Previously reported experiments on unicellular yeast demonstrated that reproduction in dense cellular packings can exert pressures on the order of 1 MPa [69]. Thus, a $\sim 3\mu m$ diameter bud scar may experience forces on the order of 10 μN. This is orders of magnitude larger than the ~ 100 pN force necessary to break mammalian intercellular bonds [84, 85] or tear bacteria from a biofilm [86]. Thus, resisting forces from growth at high cell density would require major innovations on known intercellular adhesion mechanisms.

While snowflake yeast is a lab-evolved model system, it possesses a number of features generally agreed to be common to naturally occurring nascent multicellular organisms. Snowflakes develop clonally, growing through mother-daughter cell adhesion with regular genetic bottlenecks[33, 35]. This facilitates multicellular adaptation, as it limits the potential for within-organism genetic conflict and promotes the emergence of novel, heritable multicellular traits [87]. Snowflake yeast readily adapt as multicellular individuals, evolving to be more complex by gaining novel multicellular traits [34, 33, 88]. Indeed, complex multicelluarity (*i.e.*, metazoans, land plants, red algae, brown algae and fungi) has only evolved in organisms that develop clonally[49]. Our geometric arguments are easily generalized to other organisms with fixed-geometry morphology. Interestingly, this appears to be

the dominant path to complexity: all independent transitions to complex multicellularity, with the exception of animals, grow with rigidly connected cells in a fixed-geometry body plan. Taken together, our results demonstrate that biophysical interactions play a critical role in the evolutionary transition to multicellularity.

CHAPTER 4
EVOLUTION OF LARGE CELLULAR CLUSTERS RESILIENT TO PHYSICALLY CHALLENGING ENVIRONMENT

4.1 Chapter Summary

Recent experiments have revealed that clonal snowflake yeast clusters readily evolve large size under selection for settling in liquid media. To explore the effect of a more challenging environment on the evolutionary trajectory of snowflake yeast, we created selection protocol in which clusters are compressed prior to being subjected to size selection. We find that the same large size is achieved under both selection regimes over eight weeks of evolution. However, the population dynamics differ significantly in the two regimes, with gradual, consistent changes observed in the presence of compression, in contrast to the more abrupt change observed in the control, compression-free population. This work is an ongoing collaboration with Thomas C. Day, Colin G. Brandys, William C. Ratcliff and Peter J. Yunker. Upon my departure from the lab in December of 2018, any outstading work will be concluded by Thomas Day, who will be co-first author on the publication.

4.2 Introduction

In recent studies of the evolution of multicellularity, 'snowflake' yeast clusters under selection for settling in liquid media respond by readily increasing their size via morphological changes at the cell level [34, 35, 42]. This selection–which rewards clusters that perform well in a race against time to the bottom of a vial (Fig. 4.1a,b)–imposes strong selection for large size, and results in rapid morphological changes that increase fitness. While this system has proved to be a powerful tool for studying the first steps in multicellular evolution [3, 7, 8, 9, 10, 33, 34, 35, 42, 43], it is necessarily far more simple than selection *in*

vivo, where numerous, often competing selective pressures are at play [48].

To explore how snowflake yeast respond when facing more complex selection, we added a step to the size selection protocol designed to challenge the evolution of larger clusters. This was achieved by compressing the clusters prior to subjecting them to selection for large size (Fig. 4.1a). Large clusters are susceptible to fracture by compression (Fig. 4.1c); as size selection was performed immediately after compression, large clusters that were fractured were deprived of their competitive advantage. Thus this protocol imposed a more complex challenge to the evolution of large size.

4.3 Results

To study how snowflakes respond to this selection with compression–as opposed to size selection alone–we evolved six replicate populations under both the 'compression' and 'control' protocols. These protocols are identical except that the former includes compression, while the later consists of size selection alone. Evolution was initiated on populations of nascent snowflake yeast clusters that had been genetically created by knocking out the ace2 gene as described in. Ratcliff *et. al.*[35]. We found that under both treatments, the largest clusters follow similar trajectories of increasing size (Fig 2a). This was unexpected, given that the presence of compression in the selection protocol fractures the vast majority of large clusters (Fig. 4.1c).

While the largest clusters evolve increased size similarly, the overall population dynamics differ significantly between compression and control strains. After two weeks of evolution, no significant differences are observable in their size distributions (Fig. 4.2b). After five weeks, however, the control populations have shifted to significantly larger mean sizes than the compression strains, even though their maxima are similar (Fig. 4.2c). And after eight weeks, the compression strains have nearly 'caught up' in size to the control strains (Fig. 4.2d).

How, then, has large size evolved similarly with and without compression, and what is

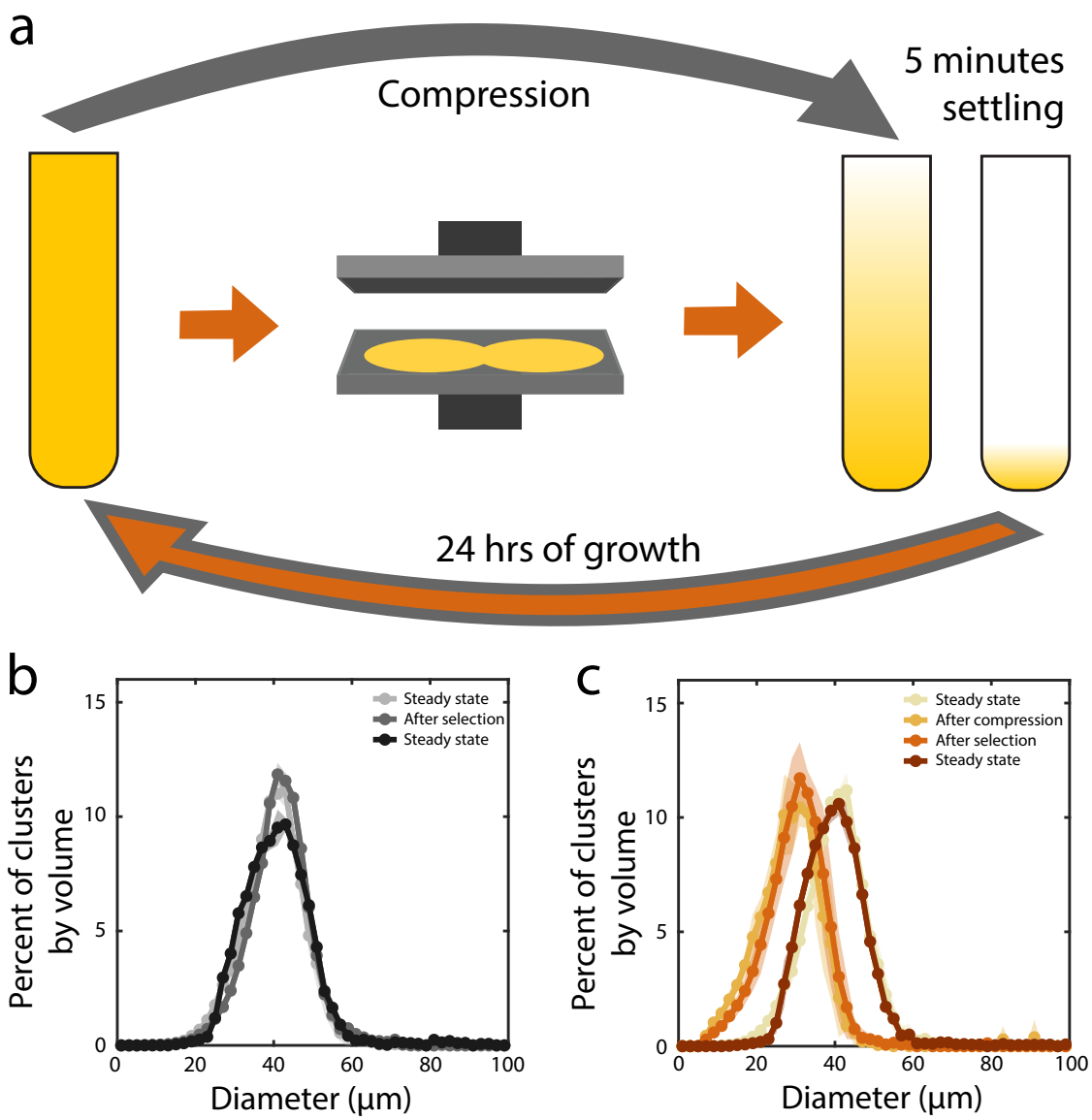

Figure 4.1: (a) Schematic of selection process for settling speed (gray path) and settling speed with crushing (orange path). (b) Histogram of cluster size distribution within a population after each step of the size selection protocol. (c) Histogram of cluster size distribution within a population after each step of the protocol with compression.

the cause of the substantial difference in population dynamics? First we tested the eight week evolved populations from both protocols for compressive resistance, and found them to be similar to each other and to their common ancestor in susceptibility to compression.

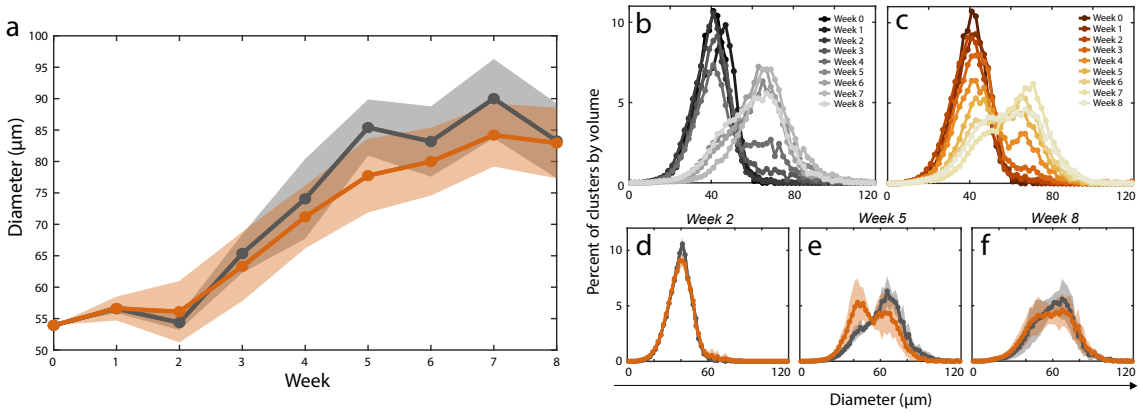

Figure 4.2: (a) Largest 2% of clusters in the population as a function of weeks of evolution for compression (orange) and control (gray) populations. The solid line represents the mean across 6 replicate populations, and the shaded area is the standard deviation. (b) Histograms of mean cluster size distribution for control (b) and compression (c) strains over 8 weeks of evolution. (d-f) Comparison of mean cluster size distribution histograms for control (gray) and compression (orange) populations at 2, 5 and 8 weeks of evolution.

CHAPTER 5
TOPOLOGICAL CONSTRAINTS IN THE ORIGINS OF ADAPTIVE SPECIALIZATION

5.1 Chapter Summary

Within-organism division of labor (e.g., cellular differentiation) is a key innovation underlying the origins of biological complexity, and is thus a hallmark of major evolutionary transitions. Despite its importance, little is known about the conditions under which specialization becomes adaptive. Long-standing theory posits that specialization will only evolve when the benefits of dividing labor exceed its costs (i.e., when there is a superlinear return on investment). Here we show that this result, while intuitive, is not general. Using an individual-based model and evolutionary algorithms, we examine how the manner in which entities within a group interact, defined mathematically by their network topology, affects the evolution of specialization. We show that by preferentially linking individuals investing primarily in complementary functions, a broad class of sparse networks strongly favor specialization–even when returns on investment are sub-linear. Furthermore, we find that the temporal consistency of group structure plays a critical role in facilitating the evolution of specialization by promoting complimentary interactions. Thus, for certain sparsely and consistently connected interaction network topologies, specialization can evolve under a broader class of benefit return functions than previously thought. Our results highlight the importance of restricted social interactions in the evolution of cooperation, and provide new insight into the key factors constraining - and catalyzing - major transitions in evolution.

5.2 Introduction

The hierarchical organization of life is largely the outcome of evolutionary transitions in individuality (ETIs), in which new levels of organization emerge from the integration of lower-level biological units [3, 4]. A common feature of ETIs is the evolution of specialization / division of labor between lower-level units [51], such as mitochondria with eukaryotic cells [2, 52, 53], and cellular differentiation in multicellular organisms [49, 50]. Thus specialization and functional integration are a key step in the evolution of organismal complexity. The mechanisms leading to the emergence and further evolution of functional integration, however, remain poorly understood [89].

The leading hypothesis for the evolution of specialization is that the integration of functionally diverse units has to yield higher fitness than the case in which the units are generalists to be favored by evolution [3, 90, 91, 92, 93, 94, 95, 96, 97, 98]. In economic terms, this means specialization will evolve only when it is a cost-effective strategy. Formally, this implies that functional specialization will only be favored by natural selection when the returns on investment in the specialized units are super-linear (that is, an increase in investment in a function yields a disproportionately large return), and therefore linear or sub-linear functional returns disfavor the evolution of specialization [62, 61, 63, 64, 57, 65].

A general feature of all ETIs is a shift in the level of individuality from the lower-level unit to the collective, regardless of the system or specific 'tasks' at hand [51, 99, 100]. However, many studies involving the evolution of functional specialization have focused on the reproductive division of labor in multicellular organisms [56, 57, 58, 59, 60], or are focused on comparative and morphological aspects of biological functions [101, 102, 103, 104]. Here, rather than focus on a specific type of specialization, we explore the general case of functional integration of specialized units within groups under various interaction topologies. While such topology may be imposed by physical structure, in

general it simply refers to the interactions between individuals within the group. This system-agnostic approach has yielded considerable insight into the critical, yet generally overlooked role of group structure in the evolution of specialization [105, 106].

In this paper, we show that network topology plays a key role in the evolution of specialization during major evolutionary transitions. Under a broad class of sparse, durable networks, complete functional specialization can be adaptive even when returns from dividing labor are sub-linear. Further, we show that specialization-promoting networks readily result from simple biophysical mechanisms underlying group formation in natural systems. Our results provide new insight into the conditions under which natural selection can favor the evolution of mutual-interdependence of units within a group, through functional specialization, a key step in evolutionary transitions.

5.3 Model

To study the evolution of specialization in groups of interacting individuals, we developed a minimal individual-based model, in which individuals may perform two functions, both of which are necessary for survival. For generality, we refer to these functions as A and B; they may represent any number of distinct functions, such as germ/soma differentiation in multicellular organisms [62], division of labor in social organisms [104], or photosynthesis/nitrogen fixation in multicellular cyanobacteria [107]. As both functions are necessary for survival; fitness can be modeled as a multiplicative function of A and B, and non-interacting individuals must perform both functions [61, 108]. In our model, the values of A and B represent the individual's fitness benefit from each function, which is calculated by raising their investment in each to a 'specialization power', α. That is, $A, B = (I_{A,B})^{\alpha}$, where resources are constrained by $I_A + I_B = 1$ for each individual. All members of the group are given the same value of α.

Using this model, we study how the interactions within a group change the way individual investment in A and B maximize group fitness. When there are no interactions

between individuals, the fitness of the group is simply the sum of the self-interaction fitness values of its constituent members, A_iB_i, where i is an index representing different individuals. When there are interactions between individuals, this sum includes interaction terms $A_iB_j\beta$, where i and j are indices representing the interacting individuals, and β is the fraction of their functional output that individuals share in the interaction, or functional interaction strength. Like α, the value of β is the same for all members of the group. To ensure that increasing the number of individuals or connections in the group does not spuriously increase fitness through multiple-counting, each individual's functional production is divided between itself and its connections. For additional details on the simulation, see section 'simulation: structure' in the supplement.

We started with populations of groups whose constituents invest equally in parameters A and B. During each round of selection, the fittest groups replicate ten times to replace the less fit groups. During replication, each individual in the group redistributes its investments by a random amount up to 10% of its total available resources (figure 1a). If this redistribution either increases group fitness, or decreases it by less than 1%, it is preserved; otherwise the distribution from the previous round is retained. To quantify the degree of specialization within each group, we define a mean quantity called 'specialization' that ranges from 0 (for groups consisting of individuals investing equally in functions A and B) to 1 (for groups consisting of individuals investing exclusively in either function; see section 'specialization' in the supplement for additional information).

We evolved populations of 100 groups for 100 steps; these parameters were sufficient for all of the populations we considered to reach equilibrium (Fig. S2). Note that we are interested in the final configuration of the groups, and not the evolutionary dynamics; we find that while their dynamics may differ, a variety of approaches allow the system to reach the same equilibria (see section 'Simulation: Evolution Parameters' in the supplement for details). We chose a group size of $n = 10$ for several reasons. While division of labor in some METs often occurs in groups with many members (i.e. multicellularity and

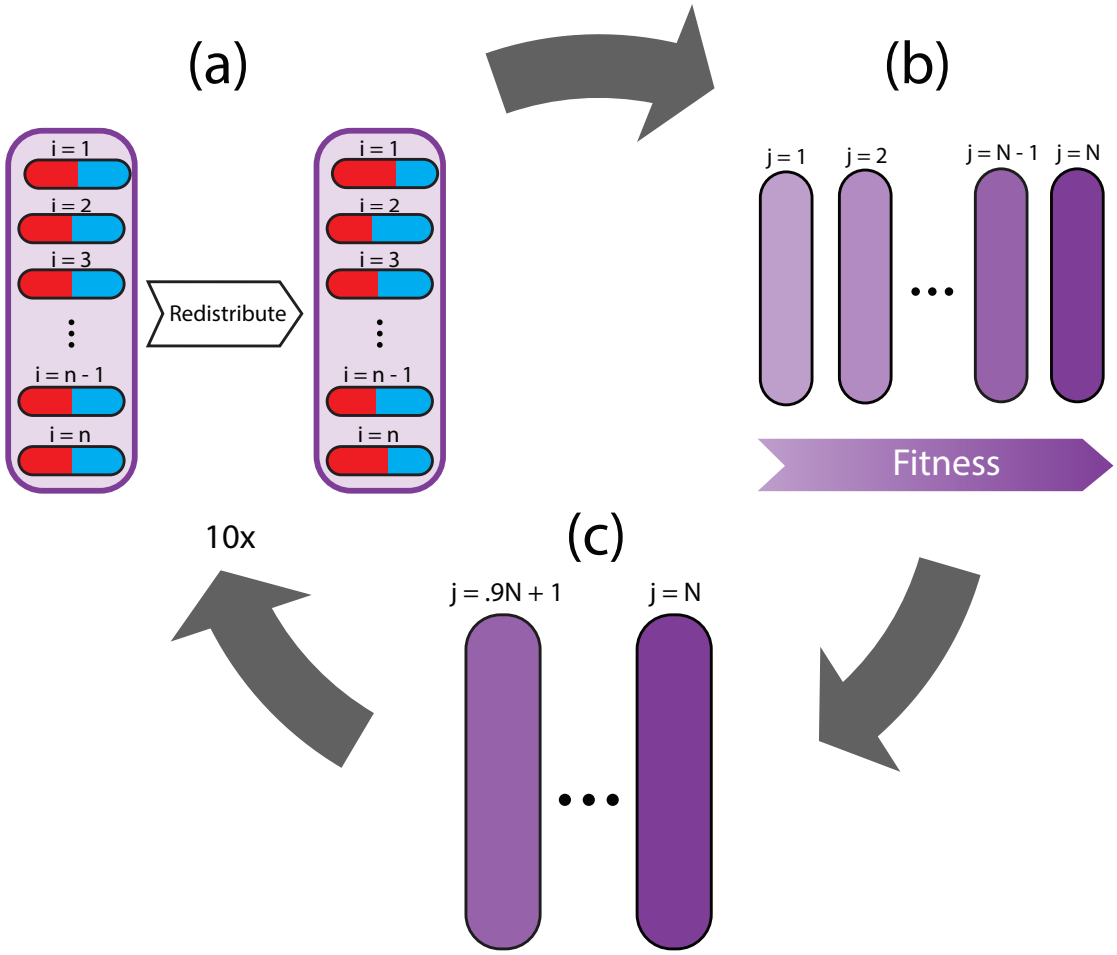

Figure 5.1: EVOLUTION PROTOCOL. (a) We simulated evolution in a population of N groups consisting of n individuals initially investing equally in parameters A and B. Each individual then redistributes its investment distribution by a random amount between 0 and 10 percent of its total available resources. (b) Selection is performed on groups; the fittest 10% of groups are selected and reproduced (with resource redistribution) 10 times to create a new population (c).

super-organismality), the example of eukaryogenesis provides evidence that small numbers of functional units can readily be integrated [2, 10, 109]. Thus, our choice of $n = 10$ serves as a midway point between the hundreds of individuals observed in simple multicellular organisms and eusocial insect colonies, and the handful of individuals involved in eukaryogenesis. Additionally, previous work has demonstrated that specialization becomes increasingly favored as groups become larger [58, 61, 8], so studying small groups ensures that our results are driven by topological rather than size effects (which have been studied

elsewhere [110, 10]).

5.4 Results

5.4.1 Topological Structure of Groups

We initially consider the simplest group topologies: groups with no connections and groups that are maximally connected. They represent, respectively, the case in which all individuals within the group are autonomous and the case in which every individual interacts with all others (i.e. a 'well-mixed' group). In each case we vary the return on investment, α, between 0.1 and 2.0, and the functional interaction strength, β, between 0.0 and 1.0, both in increments of 0.1. In the absence of interactions, individuals cannot benefit from functions performed by others and therefore must perform both functions A and B; hence specialization is thus not favored, and does not evolve (figure 2a). In the fully connected case, a high degree of specialization is observed for many values of α and β (figure 2b). Consistent with classic results [62, 61, 63, 64, 57, 65], specialization is only achieved in the fully connected case for $\alpha > 1$. Note that when complete specialization is achieved, the self-fitness terms ($A_i B_i$) in the fitness sum necessary go to zero; mathematically, this means that group fitness no longer depends on the fitness of individuals. This is analogous to the shift in individuality from the lower-level units to the higher-level organism associated with evolutionary transitions in individuality [65].

Next, we consider a simple sparse network in which each individual within a group is connected to only 2 other individuals (Fig. 2c); we refer to this as the two-neighbor topology. Surprisingly, specialization evolves even when the returns on investment are sub-linear, i.e., when there are diminishing returns on further investment. In our simulations, this topology leads to an alternating chain of specialists in A and B. We can maximize the range of parameters for which specialization is possible by connecting each of the even-numbered individuals in the group to all of the odd-numbered ones, and vice-versa (Fig. 2d). Note that we observe specialization with $\alpha < 1$ not when the group is maximally

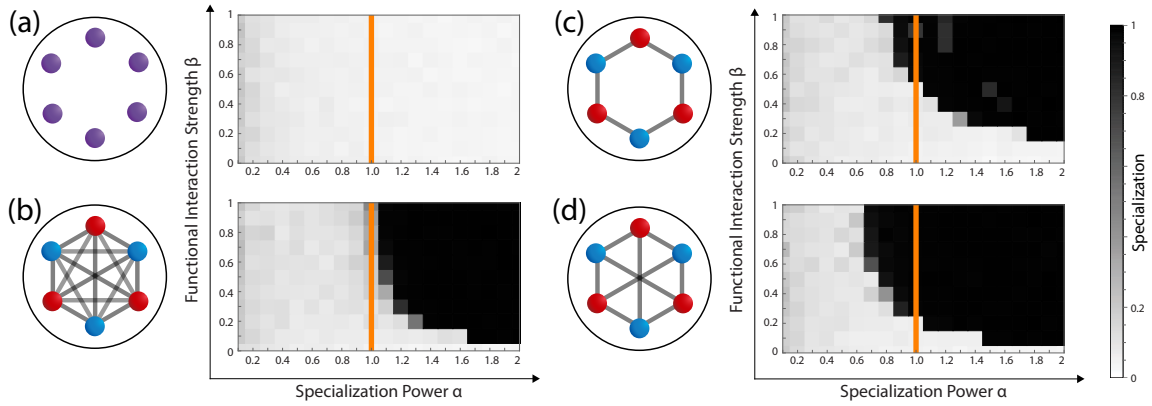

Figure 5.2: TOPOLOGICAL STRUCTURE OF GROUPS (a) Dependence of specialization on functional interaction strength and specialization power in groups without individual interactions; in the absence of interactions, individuals must perform both functions, and specialization does not evolve. (b) In the fully-connected group, however, specialization only evolves–but only when the returns from division of labor are super-linear (to the right of the orange line). (c) When each member of the group is connected to only two other members, however, specialization evolves even more readily–in some cases even when the returns from specialization are sub-linear ($\alpha < 1$). (d) The range of parameters over which specialization is possible is maximized when even numbered individuals are connected to all odd numbered individuals, and vice-versa. Simplified schematics illustrate topological structure for groups of 6 individuals. All results reported for stable equilibrium configurations of the system.

connected, but rather when connections are fairly sparse.

The benefit of specialization, despite sub-linear returns on investment, is not the result of 'double counting' the products of each individual's functional production by sharing it without consumption; a normalization step in the simulation prevents this by distributing each individual's products across its connections. Neither is it a result of group-size, as control simulations with 100 individuals revealed similar results (Fig. S2). Rather, it is the result of topologies that preferentially connect complementary specialists. In a well-mixed population or fully-connected group, the fitness benefit of increased investment in one function are complemented by the loss of production of the other; hence the need for super-linear returns. Not all interactions within the group contribute equally to fitness, however, as the value of those between individuals investing preferentially in opposite functions are increased by specialization, whereas those between individuals favoring the same func-

tion are decreased. Thus if the interactions that would be diminished by specialization do not exist, the cost to specialization is reduced, and even sub-linear returns on investment are sufficient for functional specialization to be adaptive.

5.4.2 Connection Types

To explore the role of topology in the evolution of specialization, consider a group of generalists and a group of specialists with $\alpha = \beta = 1$ interacting via identical topologies. The fitness ratio $\frac{W_{spc}}{W_{gen}}$ determines if specialists or generalists are favored ($\frac{W_{spc}}{W_{gen}} > 1$ and $\frac{W_{spc}}{W_{gen}} < 1$, respectively). In a group of generalists, each connection increases fitness by an equal amount (Fig. 3a, top). This is because each identical individual invests equally in both parameters, so the product $A_i B_j \beta$ is the same for any pair (i.e., any i, j where $i \neq j$). For a group of specialists, however, the fitness contribution of connections depends on the identity of individuals who are connected; connections between A and B specialists increase group fitness, but connections between like specialists ($A - A$ or $B - B$) do not (Fig. 3a, bottom).

The effect of adding like- versus unlike-specialist connections in a 10-individual group with $\alpha = \beta = 1$ is shown in figure 3b; if unlike-specialist connections are exclusively added first, the ratio $\frac{W_{spc}}{W_{gen}}$ quickly rises above 1, and continues to rise until only like-specialist connections remain and are added (Fig. 3b, orange line). If connections are added in the opposite order, with like-specialist connections added first, $\frac{W_{spc}}{W_{gen}}$ never exceeds 1 and specialization is never favored (Fig. 3b, purple line). This is because for $\alpha > .5$, unlike-specialist connections contribute more to fitness than do generalist connections, so adding specialist connections increases the ratio $\frac{W_{spc}}{W_{gen}}$, while adding like-specialist connections decreases it (see supplement section 'Connection Types' for more details). Randomly adding connections also results in a situation that–on average–never favors specialization (Fig. 3b, gray line). Additionally, as the total number of possible beneficial interactions scales with group size, large groups are capable of more strongly favoring specialization when

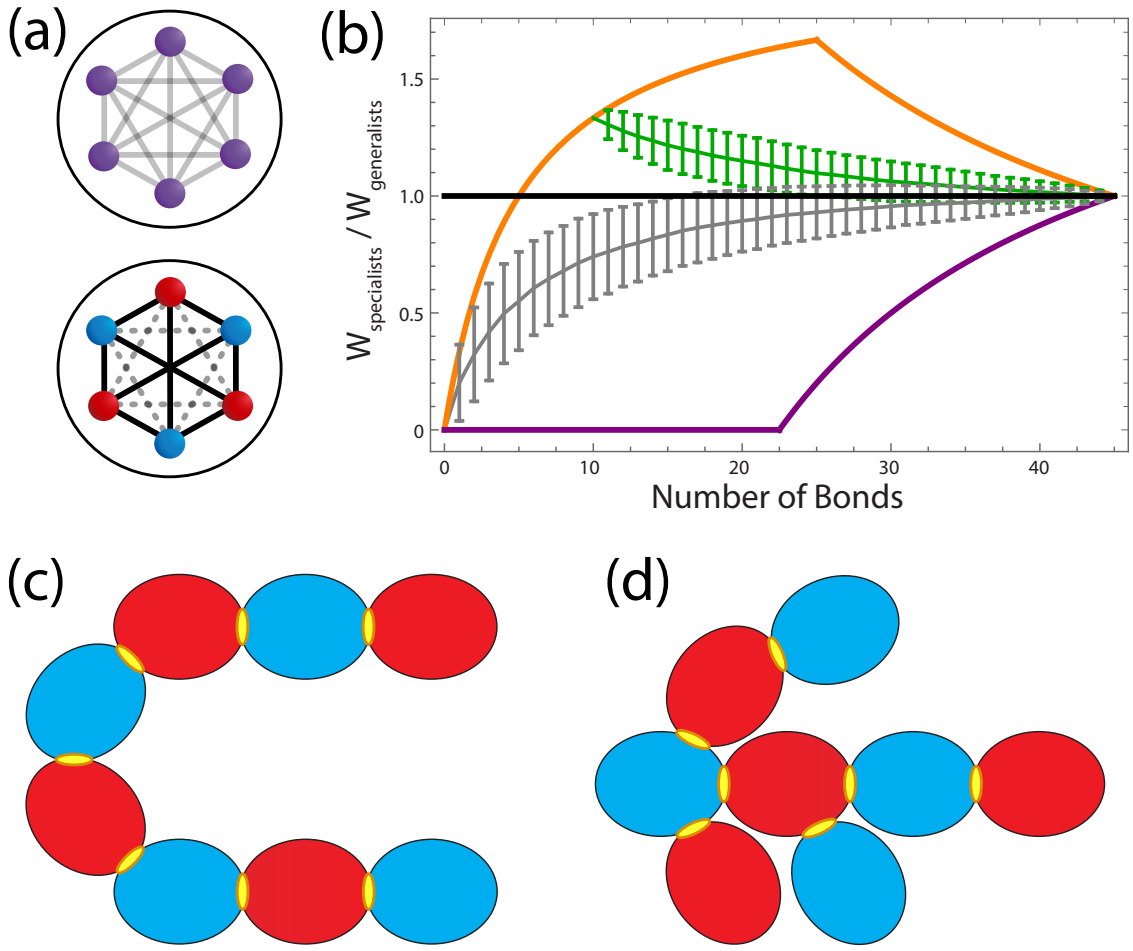

Figure 5.3: CONNECTION TYPES (a) Schematics show connection structure for a simplified 6-individual system, with generalists on the top (purple nodes) and specialists on the bottom (red and blue nodes). Dashed lines indicate interaction terms that do not contribute to fitness. (b) The ratio $\frac{W_{spc}}{W_{gen}}$ for a group of 10 individuals with $\alpha = \beta = 1$ for all *i,j*. If connections that contribute to W_{spc} are exclusively added first to a group of non-interacting individuals, specialization rapidly becomes favored (orange line). On the other hand, if connections that contribute only to W_{gen} are exclusively added first, specialization is never favored (purple line). If connections are randomly added, specialization can be favored, but on average it is not (gray line). Beginning with the two-neighbor topology and adding random connections reveals that this configuration is stable for the evolution of specialization (green line). Error bars indicate standard deviation across 1000 trials. Examples of two-neighbor ('specialization topology') chains of cells (c) and branching fractals (d) that are observed in early multicellularity fossil records [111, 112].

optimally connected.

Thus a group of interacting individuals will evolve specialization if its connections

allow for unlike specialists to be preferentially linked (given that α and β are sufficiently large). This is the case for scenario in which each individual is connected to two neighbors– such emergent patterns resulting in alternating A and B specialists result in a $\frac{W_{spc}}{W_{gen}}$ ratio greater than 1. Furthermore, two-neighbor connected configurations are relatively stable for the evolution of specialization; randomly adding additional connections to such networks decreases the ratio $\frac{W_{spc}}{W_{gen}}$, but it does so asymptotically to the crucial value of 1, so that specialization remains favored on average (Fig. 3b).

Using this analytic approach, we can calculate the relative fitnesses of generalists and specialists interacting via any topology, and thus determine whether specialization will be favored. Alternately, we may consider a given topology and determine the parameters for which individuals interacting thereby may evolve specialization. Consider, for example, the case in which each individual is connected to two neighbors. If we set $\beta = 1$, the fitness contribution of each individual in a group of generalists is

$$w_i = 3 \cdot a \cdot A_i^{\alpha} B_j^{\alpha} \tag{5.1}$$

where a is the normalization constant, and $A_i = B_i = .5$ for all i, j. The factor of 3 comes from the fact that resources are shared among 3 individuals (individual i and its two neighbors).

For specialists, the fitness contribution is given by

$$w_i = a \cdot A_i^{\alpha} B_i^{\alpha} = 1a \tag{5.2}$$

where A_i is the specialty of the individual i, and B_j the specialty of the individuals to which it is connected; hence A_i and B_j are both equal to 1. There is no factor of three here because the number of unlike-specialist bonds equals the number of individuals in the group.

We can find the minimum value of α for which specialization can evolve for the two-

neighbor topology by setting equation 5.1 equal to $1a$ and solving for α. Doing so yields $\alpha_{critical} = \frac{\log 3}{2 \log 2} \approx .79$, in agreement with our simulation results in figure 2c. Note that for this two-neighbor configuration, the value of $\alpha_{critical}$ does not depend on the size of the group.

Finally, it is worth highlighting that in addition to being a simple representation of the role of topology in the evolution of specialization, the two-neighbor configuration has significant biological relevance. A first step in the evolution of multicellularity is the formation of groups off cells [3, 7, 8, 9, 10]. Simple groups readily form through cell division without cytokynesis forming either 2D filaments (figure 3c) or branching patterns (figure 3d) [111, 112, 107, 33]. Cases from experimental evolution show that a single mutation can be enough to produce this phenotype [35, 113]. These cellular configurations (figures 3c and 3d) are equivalent from our topological perspective, resulting in sparse connection topologies that strongly favor differentiation. Specifically, they favor specialization and exchange with directly attached cells (parents and offspring). While these topologies differ slightly from the two-neighbor configuration because they have one fewer bond than cells, this difference rapidly becomes negligible with increasing n. We have previously reported that simple and easily accessible routes to multicellular group formation can readily evolve in response to selection for organismal size [33], and this process may also strongly favor the evolution of cellular differentiation [114, 115, 116, 9].

5.4.3 Temporal Consistency

While group topology plays a critical role in the evolution of specialization, our above models made a crucial assumption: that the composition of groups was constant across generations other than variation created by redistribution of investment. This reflects the life history of simple groups that grow through 'staying together'; creating new groups through fission / fragmentation [117]. However, what if the composition of the group is not constant, but instead membership changes within a single life-cycle, as with aggregative

multicellularity [118, 119, 120]? To explore the role of temporal consistency of interactions in the evolution of specialization, we simulated a scenario in which the topology is constant–each individual is connected to two neighbors–but the neighbors are randomly selected each round. As shown in figures 4a and b, the addition of temporal variance on this topology significantly impedes the evolution of specialization. This occurs because when neighbors are randomly chosen, on average only 50% of connections are unlike-specialist connections–that is, connections between individuals who took steps toward specializing in opposite tasks in the previous round. Specialization can only occur if the fitness benefits of unlike-specialist connections outweigh those of like-specialist connections, and this can only occur for well-mixed groups when $\alpha > 1$. Thus, randomly selecting neighbors prevents the evolution of specialization when functional returns are sub-linear. Note that because the two-neighbor topology is quite stable (even if a few unlike-specialist connections are removed, or a few like-specialist connections are added, it still favors specialization; Fig. 3b), it will favor specialization as long as the probability of preferentially forming unlike specialist connections is sufficiently high.

Specialization is further impeded when the existence of interactions is temporally unstable. If we prevent individuals from interacting every other round, only partial specialization evolves, even when the network topology would otherwise strongly promote specialization (Fig. 4c). This is because without consistent interactions, complete specialization is disincentivized by the need to perform both functions when connections are absent. This effect is not restricted to the two-neighbor topology; it is also observed when groups alternate between having no connections and being fully connected (figure 4d). Thus, the temporal component of group structure also plays an important role in determining the equilibrium configuration of groups by restricting the parameter space in which the evolution of functional specialization is favorable.

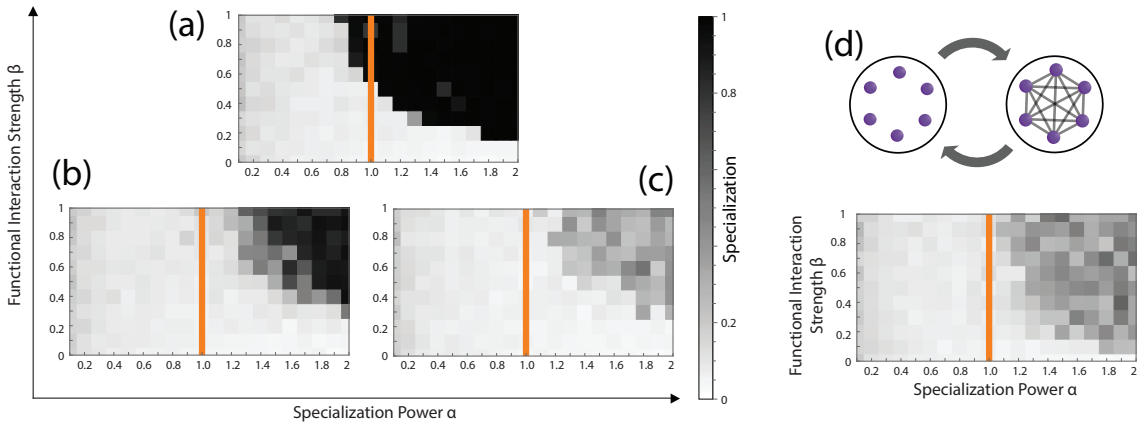

Figure 5.4: TEMPORAL STRUCTURE OF GROUPS. (a) Heat map of specialization as a function of specialization power and functional interaction strength for two constant neighbors. When two neighbors are randomly chosen each round, specialization is impeded (b). (c) When groups alternate between having constant neighbors and having no interactions, only partial specialization is achieved. (d) This effect is not unique to the two-neighbor topology; when alternating between the fully connected (Fig. 2b) and unconnected (Fig. 2a) scenarios, individuals must optimize fitness in two environments, and again only partial specialization is achieved.

5.5 Discussion

During an evolutionary transition in individuality (ETI), formerly autonomous units evolve into functionally-integrated parts of a new higher-level organism [65, 59]. ETIs are an important subset of major evolutionary transitions, as they are both a major route through which organisms evolve greater complexity [121, 122], and create the hierarchically-nested pattern of life seen on Earth [3, 4, 116]. Division of labor among component parts has long been thought to play a central role in ETIs, for good reason: groups of interacting organisms can often benefit from specialization of component parts, and once specialized, members of groups are often prevented from resuming a free-living existence [59, 108, 123]. Specialization thus can play a causal role in the shift in biological individuality to higher-level units [57, 64, 58].

Evolutionary game theory [92, 124, 125] argues that functional specialization should only evolve when greater investment in trade concomitantly increases absolute productiv-

ity (i.e., the returns from specialization are super-linear) [3, 90, 91, 92, 93, 94, 95, 96, 97, 98]. While this idea is intuitive, it is also overly restrictive. In this paper, we explore how social interactions within groups, measured by their network topology, affect the evolution of specialization. Indeed, when all individuals within groups interact (with equal functional interaction strength), benefits must be super-linear for specialization to evolve (figure 2b) [3, 90, 92, 62]. Yet for a broad class of sparsely-connected networks, in which individuals interact primarily with trading partners dividing labor appropriately, complete specialization can evolve even when the fitness function is sub-linear (figure 2 c&d).

Rather than being unusual, networks favoring specialization readily arise as a consequence of physical processes structuring simple groups [105]. For example, septin defects during cell division create groups with simple 2 or 3D graph structures (figure 3 c&d), where cells are connected only to parents and offspring [111, 112, 33, 34]. If cells share resources only with physically-attached neighbors, then the physical topology of the group describes its interaction topology, and these networks strongly favor specialization. Indeed, one of the earliest transitions to multicellularity occurred as early as 2.42 billion years ago in chain-forming cyanobacteria [126, 127], which evolved cellular differentiation to compartmentalize processes underlying nitrogen fixation and photosynthesis into separate cells [107]. Remarkably, even ancient fossils with cell-cell connections show cell differentiation reproductive division of labor [126].

The role of temporal variance is also significant in real systems. For instance, in the case of multicellular evolution, it is known that groups can be formed by 'staying-together' or by 'coming-together' mechanisms [117, 128]. In the former case, the body structure of the multicellular organism is temporally-stable, and in the latter case it is not. Notably, it is known that all the complex forms of multicellularity that have evolved develop clonally, showing higher degrees of cell specialization and functional integration, compared to groups formed via aggregation [11, 129]. As clonal groups have structures that persist across generations while aggregative groups do not, this is consistent with our result that

the addition of temporal variance can negate the benefits of specialization. Another example of the relevance of temporal consistency is observed in symbiont inheritance. When symbionts are acquired from the environment each generation, strong specialization is not observed. However, when symbionts are transmitted with the host's reproduction (*e.g.* mitochondria), strong specialization readily evolves [130]. Interesteingly, it has been reported that topologically stable networks can favor cooperation in human societies [131].

Our model does not consider the genetic relatedness of individuals within a group. High within-group relatedness is important for some ETIs, favoring the evolution of cooperation by aligning the fitness interests of individuals within the group [129, 90, 19, 132, 133, 134]. Yet relatedness, per-se, is not required for the evolution of cooperation, as other mechanisms, such as phenotypic assortment [135, 73] or repeated interactions among individuals [23, 136, 105, 106], can also align the fitness interests of group members. For example, recent work has shown that certain network topologies act as amplifiers favoring cooperation, independent of relatedness [105, 106]. Indeed, these networks share similar characteristics to those that we find favor specialization during an ETI, namely sparse connections and repeated interactions between cooperative partners. Network-based approaches are attractive for studying ETIs because they apply broadly, allowing one to analyze both fraternal transitions of highly-related individuals (e.g., the evolution of multicellular organisms from clonal groups of cells [129, 49]), and egalitarian transitions of unrelated partners (e.g., the evolution of eukaryotes from the symbiosis between independent prokaryotic cells [137]).

5.6 Conclusion

Using a minimal model, we explored the evolution of specialization in groups of individuals capable of specializing in one of two functions necessary for survival. Although the role of group structure in evolutionary processes has been explored by others, our results suggest that group structure can overcome the need for super-linear returns on specialization, which is in direct contrast to the prevalent view about the evolution of specialization

in evolutionary transitions [62, 61, 63, 64, 57, 65].

This new insight demonstrates that specialization can be an optimal strategy for a wider set of conditions than what was previously thought. Our results support the emerging consensus that evolutionary transitions in individuality may have been more readily achievable [33, 87, 10, 49, 66]. Furthermore, our result that super-linear functional returns are unnecessary for specialization to be adaptive is particularly consequential for understanding how group formation can be favored among individuals that have existed as generalists for millennia. While further work is required to find general patterns in the evolution of biological complexity and the major evolutionary transitions, our results suggest that some non-adaptive processes–such as temporal and topological group-level structure–are fundamental mechanisms upon which natural selection and other adaptive processes can act, paving the way to the evolution of new levels of organization.

CHAPTER 6
CONCLUSION

6.1 Summary of Findings

Physical structure plays an important role in the first steps in the evolution of multicellularity, as clusters of cells contend with novel, physical forces acting on length scales too large to have been relevant for their single-celled ancestors. Using snowflake yeast, we showed that these forces can limit cluster size. As clusters grow by the addition of new cells, intercellular contacts are formed and the resulting forces deform cells from their equilibrium positions. Energy is stored in these deformations, and stress accumulates within the cluster until it exceeds the adhesion strength of the intercellular bonds, and the cluster fractures.

We discovered that snowflake yeast overcome this challenge and achieve increased cluster size by increasing their cellular aspect ratio. This decreases the volume fraction of the cluster and thus the frequency of intercellular contacts and the magnitude of the energy stored therein. As such, the internal stress within the cluster accumulates more slowly, and thus clusters can achieve larger sizes before fracturing. We also found that this route to increased size is far more efficient than increasing intercellular bond strength. Indeed, we experimentally observed that bond strength remains constant while aspect ratio increases, indicating that evolution has followed the geometrically-optimum path.

The critical role of structure is not limited to snowflake yeast, or even the evolution of multicellularity. A key feature of evolutionary transitions is the functional specialization of the lower-level individuals. We discovered that the topological structure of interactions within a group plays a fundamental role in determining when the evolution of specialization is favored. Importantly, for certain interaction topologies, specialization can be favored even when returns from investing exclusively in one function are diminishing. As dimin-

ishing functional returns are adaptive for autonomous individuals, this insight is important for understanding how specialization can be favored in groups of individuals that had previously evolved for millennia as generalists.

6.2 Future Work

We have shown that cellular elongation allows for larger clusters in snowflake yeast. But several related questions remain about the limits of this benefit. What are the disadvantages to increasing cellular aspect ratio, and at what point do they surpass the fitness benefits of increased size? Is this equilibrium point a simple function of selection strength, or are there other factors at play? What further innovations may arise to overcome this trade-off between cellular elongation and increased cluster size? Future work is needed to answer these questions about the first step in the evolution of multicellularity. Snowflake yeast is an ideal experimental system with which to explore these questions, while complementary computational and theoretical work can speak to its generality.

In addition to furthering our understanding of the role of cellular shape on the structure and size of snowflake yeast clusters, a recently evolved form of snowflake yeast is raising new questions about the relationship between cellular properties and collective structure. Discovered by members of the Ratcliff lab, superflakes are large aggregates of cells (1mm; normal snowflakes are on the order of 100 m) that appear to consist of several smaller, snowflake-like modules. Some of the most fundamental questions surrounding these superflakes are inherently structural in nature: what mechanism allows the modules to remain attached to each other? What are their physical properties and fracture mechanics? How do the properties of their highly elongated cells differ from those of normal snowflake cells? These are just a few of the motivating questions driving ongoing research on the structure of early multicellular groups.

Finally, our work on the role of interaction topology has only begun to reveal structures role in the evolution of specialization. Potential future projects include studying time-

varying complex topologies, systems in which more than two functions are traded-off, and conducting detailed comparisons to real-world systems.

6.3 Final Thoughts

I conclude my thesis with a brief mention of how I have benefitted personally from my time as a student in the Yunker lab at Georgia Tech. My skills as a writer, researcher, presenter and analytical thinker have increased tremendously. Through collaboration, I have learned to quickly familiarize myself with unfamiliar concepts and to communicate effectively with others who do not share my background. I have learned to leverage available resources from numerous sources, and to use existing tools and ideas in new ways. I am thankful that I have had the opportunity to apply these skills to the advancement of science, and I look forward to applying them to new and diverse endeavors in the future.

Appendices

APPENDIX A

SUPPLEMENT TO CHAPTER 2

A.1 Snowfake yeast genotypes and growth

Genotypes used in this study were isolated from the evolution experiment conducted in Ratcliff *et al.*, 2012 [33] after 7, 28, 42 and 60 days of evolution. These genotypes are referred to throughout this manuscript as week-1, week-4, week-6 and week-8 genotypes, as they were isolated from an evolving population at these time points. During evolution, daily size selection was performed by selecting for fast settling in liquid media.

Daily selection and all measurements described in this paper were performed on clusters grown for approximately 24h in Yeast Peptone Dextrose (YPD) medium (10 $g \cdot l^{-1}$ yeast extract, 20 $g \cdot l^{-1}$ peptone and 20 $g \cdot l^{-1}$ dextrose) at $30°C$ and $250rpm$ in a Symphony Incubating Orbital Shaker Model 3500I. All experiments were performed on clusters from stationary phase (24h) culture to ensure consistency (except those requiring imaging during cluster growth).

To determine the aspect ratios of single cells, the aforementioned genotypes were reverted to unicellularity using the lithium acetate/polyethylene glycol/singlestranded carrier DNA method as described in Ratcliff *et al.*. 2015 [35] . Unicellular reversion was accomplished by replacing a single non-functional copy of ace2 (a mutation that arose during settling selection) with a functional, ancestral copy. These revertants are thus genetically identical to their snowflake counterparts, with the exception that they are capable of normal motherdaughter cellular separation after mitosis, allowing us to make precise measurements of cellular morphology that would have been far more difficult within three-dimensional snowflake clusters (statistics: week 1, $N = 2,128$; week 4, $N = 2,198$; week 6, $N = 2,219$; week 8, $N = 1,961$)

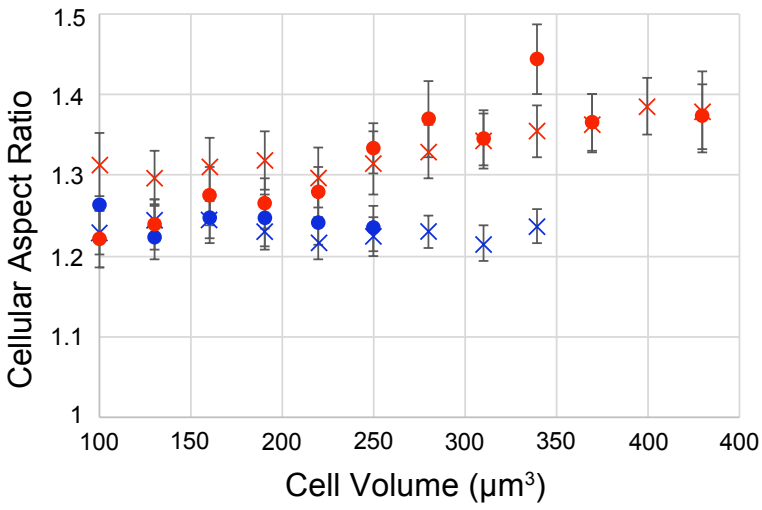

Figure A.1: Cellular aspect ratio vs cell volume for week 1 (blue) and week 8 (red) cells from revertant genotypes (circles) and cells sheared off clusters (xs). Bars denote one standard error of the mean.

To ensure that the revertant genotypes demonstrated the correct cellular properties (i.e. that growing in a cluster did not change cell shape), we disrupted snowflake clusters by shearing between glass slides, and compared the properties of individual cells to those of the revertant genotypes. To ensure that our results were not biased by small peripheral cells breaking off of clusters preferentially, we plotted aspect ratio as a function of cell volume (Figure A.1), and observe agreement between cells from the revertant genotypes and from crushed clusters. We excluded cell sizes that occurred less than 1% of the time in the crushed sample, as the statistics were too low to be significant. While the differences in all combinations of week 1 and week 8 aspect ratio distributions were statistically significant (week 1 crushed vs. week 8 crushed, $p = 3 \times 10^{-8}$; week 1 revertant vs. week 8 revertant, $p = 0.004$; week 1 revertant vs. week 8 crushed, $p = 2 \times 10^{-7}$; week 1 crushed vs. week 8 revertant, $p = 0.002$), the differences between crushed and revertant distributions for the same week were not statistically significant (week 1 crushed vs. week 1 revertant, $p = 0.1$; week 8 crushed vs. week 8 revertant, $p = 0.5$).

A.2 Chitin bond intensity

Intercellular chitin bonds were stained with calcoflour (Fluorescent Brightner 28 from MP Biomedicals, LLC) using the following procedure. Clusters from a steady-state culture were rinsed of media and diluted 1:10 with deionized water. Then calcoflour was added at a 1:100 dilution from a stock solution of $1mg/ml$ calcoflour/water, and this mixture was incubated in the dark at room temperature for at least 5 minutes. Lastly, the clusters were again rinsed with deionized water to remove any excess calcoflour (rinsing was performed using centrifugation to pellet the clusters and subsequent removal of the supernatant).

To measure bond intensity, confocal z-stack images consisting of nine images at a separation of 0.925 μm were collected on a Nikon A1R confocal. Using the image processing software Fiji, each slice was converted to 16-bit greyscale, so that each pixel had an intensity value between 0 and 65,535. Then the images were combined using the 'Sum Slices' command; after summation, none of the pixels reached saturation. Finally, the intensity of the bond was taken to be the total of all summed pixels constituting the image of the chitin bond.

A.3 Measurement of cluster sizes, growth, and propagule ejection

As snowflake yeast clusters are similarly compact (the number of cells in a cluster increases as $r^{2.80}$ and $r^{2.72}$ for week-1 and week-8 genotypes, respectively; Fig. 3d), and large clusters are relatively isotropic, a spherical approximation is a valid measure of cluster size (mean width-to-height ratios of 1.0 0.1 for week-1 and week-8 clusters, $N = 10$ for each, reported with standard error, $P = 0.45$ and $P = 0.63$, for week-1 and week8, respectively, for two-tailed t-test comparisons to the null hypothesis that the mean cluster aspect ratio is 1.00).

Cluster size when spontaneous fracture occurs (referred to throughout as spontaneous fracture size) and growth rate were obtained via time-series video captured on a Nikon

A1R confocal microscope, operating in bright-field mode. Images of unconfined clusters growing in nutrient-rich media were captured every few minutes.

From analysis of individual fracture events, spontaneous fracture size and size of the resulting propagules were obtained. Twenty and sixteen fracture events were analyzed for week-1 and week-8 genotypes, respectively. To observe fracture at the cellular level (impossible in large clusters due to light scattering), small clusters were confined to a chamber whose height was on the order of 3 cell diameters ($\sim 15 \mu m$).

The distributions of cluster sizes in a population were also measured via flow cytometry. A population of snowflake yeast clusters was grown for 24h in $10ml$ of YPD liquid media and then analyzed on the FL2 channel (580/50nm) of a Sysmex Cyflow Cube 6 flow cytometer. The samples analyzed contained 16,042 and 22,618 week-1 and week-8 clusters, respectively.

The mean spontaneous fracture size and standard deviation are shown in figures 1c and A.4a (W1 vs W8, $p = 7.6 \times 10^{-14}$, two-tailed t-test). Mean propagule radius as a percentage of cluster radius prior to fracture is shown in figure A.2a. Additionally, for the 20 W1 and 16 W8 clusters analyzed, the mean volume post-fracture is 94% (with a standard deviation of 10%) of the pre-fracture value ($p = 0.010$ and $p = 0.005$, for the comparison to the null hypothesis that total volume after fracture is 100%, for week 1 and week 8, respectively).

Growth rate was determined by measuring the size of a cluster at 5 time points over several hours. The average across 5 week 1 and 5 week 8 clusters is shown in Figure A.2b.

To confirm that cluster size is accurately measured via in-plane radius, 2 clusters were measured at several time points as they traversed a distance of approximately 10 cluster diameters. The measured radii were nearly invariant, and small changes observed were consistent with growth (Figure A.2c).

Figure A.2d shows the ejection of a propagule from a cluster grown in confinement. After ejection, the surrounding cells relax due to the alleviation of internal stress, decreasing the area subtended by the cells remaining in the initial cluster.

Figure A.2e illustrates the stress relaxation of a cluster post fracture; branches of cells mechanically straightened by crowding are allowed to relax, decreasing the total volume of the cluster and propagule relative to the volume of the cluster prior to fracture.

A.4 Measurement of cluster sizes, growth, and propagule ejection

We measured the fluorescence intensities of 30 randomly chosen chitin bonds (stained by the process described above) and diameters for each of the week 1 and week 8 genotypes. Average values and standard deviations are shown in figure A.3; average intensity values differ by only 3% (Figure A.3a), and diameters differ by $\sim 1\%$ (Figure A.3b) (Week 1 vs. week 8, $t = -.35$, $p = .72$ for intensities and $t = -.37$, $p = .71$ for diameters, respectively; two-tailed t-test).

A.5 AFM compression

The AFM measurements reported here were performed on an AFM Workshop Life Sciences model (LS-AFM) atomic force microscope by placing a dilute suspension of snowflake yeast clusters between a glass slide and a small piece of VWR plastic wrap (catalogue item number 46610-056) and compressing individual clusters with an AppNano AFM probe (SPM Probe model ACLA: $L = 225\mu m$, $W = 40\mu m$, $k = 36 - 90Nm^{-1}$). To ensure that our results were not impacted by the presence of the plastic wrap, the experiments were repeated in an aqueous environment using the LS-AFM Dunk n Scan attachment. For these experiments, Tipless AppNano cantilevers (part no. FORTA-TL: $L = 225\mu m$, $W = 27\mu m$, $k = 0.6 - 3.7Nm^{-1}$) were used to reduce extraneous interactions with a tip. On a glass surface, clusters readily slide out from beneath the cantilever during compression. To prevent this, clusters were confined in-plane by 54 and $90\mu m$ square Pelco TEM grid cells.

The plastic wrap method described above is similar to traditional materials testing techniques, wherein a sample may be compressed between two plates. Here, the glass slide

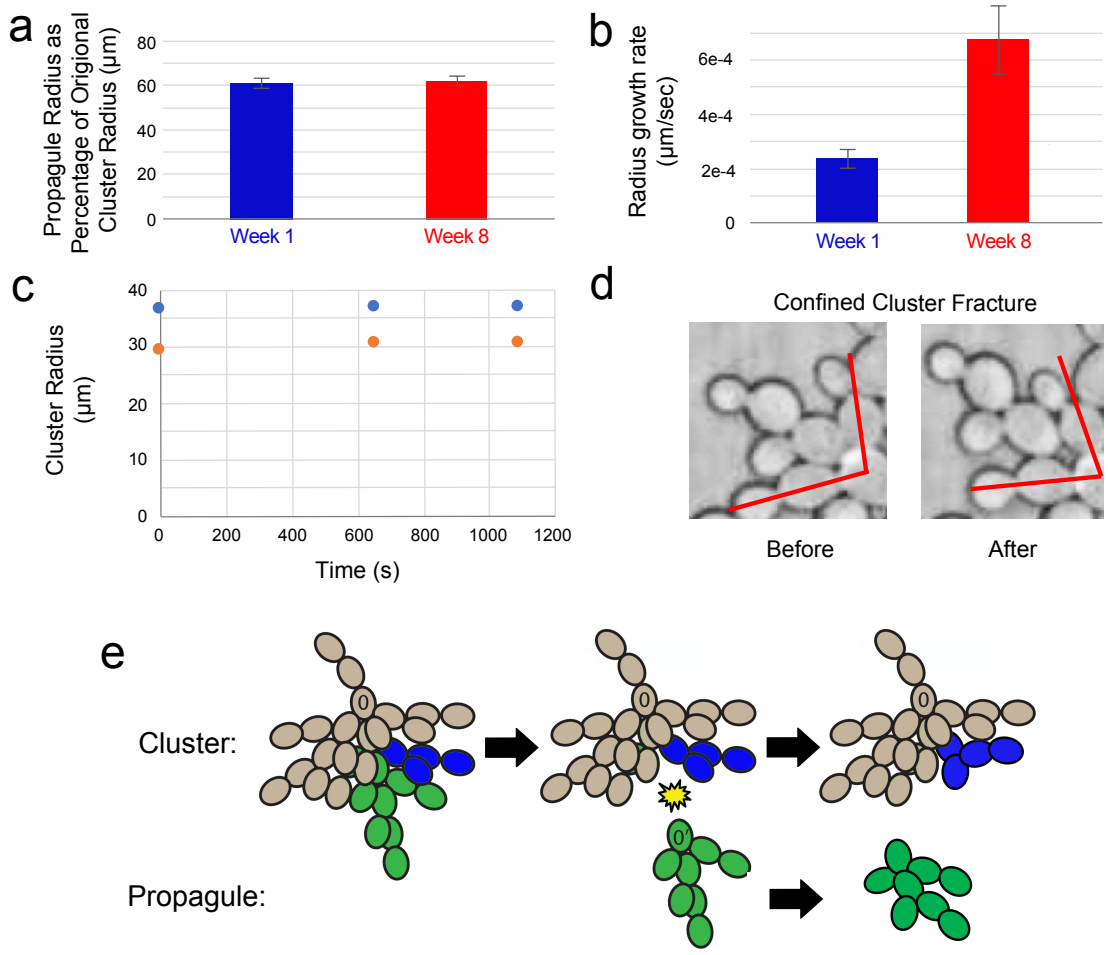

Figure A.2: (a) Propagule radius as a percentage of original cluster radius for week 1 and week 8 clusters. (b) Growth rate for week 1 and week 8 clusters. Bars denote one standard error of the mean. (c) Cluster size varies insignificantly as clusters move across the microscope field of view. Orange and blue circles represent different clusters. (d) A confined cluster fractures from the accumulation of internal stress. Neighboring cells relax upon propagule ejection (red lines). (e) Cartoon illustrating stress-relaxation of a cluster upon ejection of a propagule.

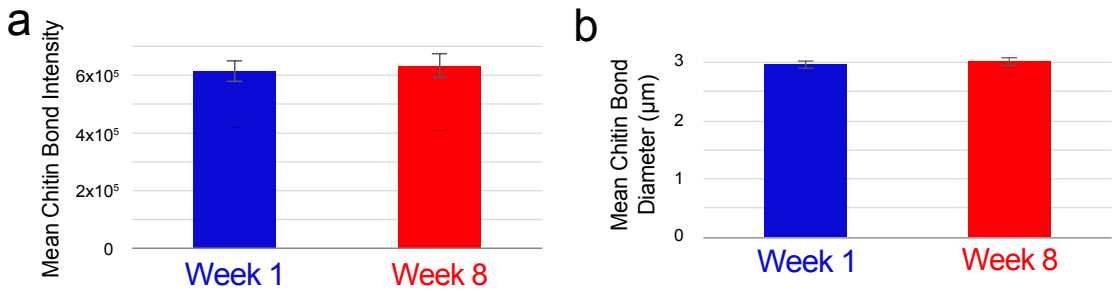

Figure A.3: (a) Mean fluorescence intensity of chitin bonds from week 1 and week 8 genotypes. (b) Mean bond diameter. Bars denote one standard error of the mean.

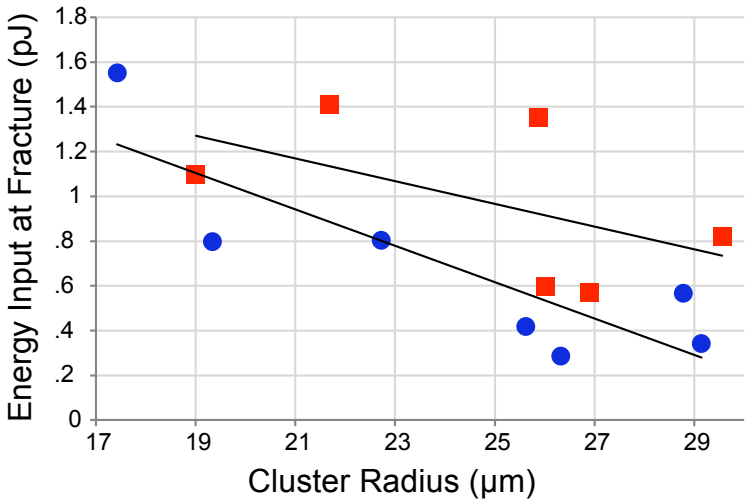

Figure A.4: Data for energy input at fracture vs. cluster radius for week 1 (blue) and week 8 (red) clusters using the aqueous environment AFM method.

acts as one plate, and the plastic wrap acts as the second. As a check to ensure that this method does not introduce unexpected artifacts, we also directly performed compression in an aqueous environment with a tipless cantilever; however this method has drawbacks of its own. In the absence of the plastic wrap, cantilevers with a lower spring constant were required, and as these were narrower, the application of force on the clusters was more localized, and therefore less globally uniform. Further, alignment of the cantilever and the cluster had to be performed using brightfield images, introducing a source of user error. Additionally, even when confined by the TEM grids, the clusters were far more susceptible to in-plane movement than they were under the plastic wrap. Thus, this direct compression serves as a consistency check.

The results of the aqueous method are shown in figure A.4. The linear trends are not as strong, likely a result of the force not being evenly distributed across the clusteras local environments within the snowflake become stressed at different rates, the internal stress inhomogeneity that results from failing to compress the entire cluster evenly likely explains, at least in part, the increased variance in fracture mechanics.

The superior uniformity of the plastic wrap approach (Regression, x variable: week 1

$t = -7.4$, $p = 0.0007$; Week 8 $t = -3.9$, $p = 0.012$) provides significant experimental advantages over the tip-only approach (regression, x variable: week 1 $t = -3.6$, $p = .016$; week 8 $t = -1.2$, $p = .28$). It is also the more traditional approach (compression between two plates), though such an approach is not traditionally used at this length scale. However, the two methods are consistent with each other. They both show that the energy input at fracture decreases with increasing size for week 1 and week 8. They both show that week 8 clusters take more energy to fracture than week 1 clusters of the same size. Furthermore, extrapolations of the linear fits of energy input at fracture versus radius from both approaches predict spontaneous fracture sizes that are within error bars of the independently measured value (Figure A.5a). This indicates that despite experimental uncertainty, we have captured the important characteristics of snowflake fracture under external compression.

Figure A.5b shows the distribution of spontaneous fracture sizes, with the values predicted by the AFM experiments overlaid.

Though measurement from flow cytometry lack units, the signals are proportional to size, facilitating direct comparisons across samples. The trend of larger clusters in the week 8 genotype is clearly visible (Figure A.5c).

The compression rate (2×10^{-7} m/s) and growth rates ($2 \times 10^{-1}0$ m/s and 7×10^{-10} m/s for week 1 and week 8, respectively, $t = 3.34$, $p = 0.003$, two-tailed t-test) are slow, especially when considered in the contest of cluster size (50+ microns). Further, the energy input trend lines in the compression experiments are consistent with the spontaneous fracture sizes. If kinetics played a large role in the process, one may have expected that increasing the rate of change by three orders of magnitude would cause fracture to occur earlier. Thus, the compression and growth rates are potentially in a quasi-static regime.

A.6 Volume Fraction

To measure volume fraction, snowflake yeast clusters were stained with CellTracker Blue vacuole stain (ThermoFisher Scientific catalogue no. C2110). Approximately $12\mu l$ of a

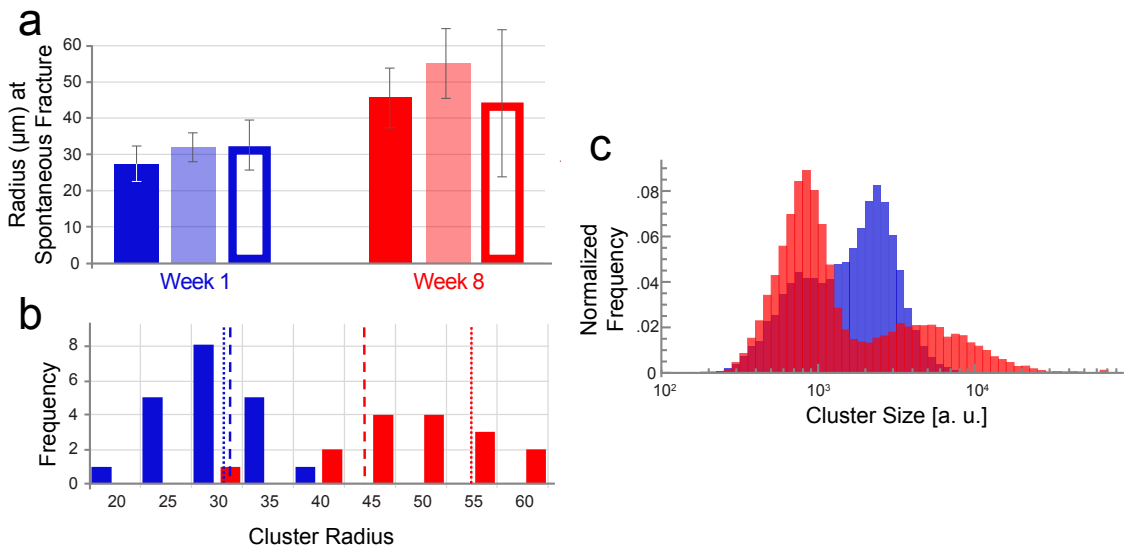

Figure A.5: (a) Comparison of spontaneous snowflake fracture size from experiment (solid fill) and linear extrapolations of linear fit lines from AFM data using the plastic wrap method (shaded fill) and the aqueous environment method (outlines). Error bars represent standard deviation for the spontaneous fracture size data and standard error from regression analysis of the AFM data. (b) Distribution of spontaneous fracture sizes for week 1 (blue) and week 8 (red). Predictions from linear extrapolation of AFM data shown as vertical lines for plastic wrap (dotted) and aqueous (dashed) methods. (c) Distribution of cluster size in population after 24 hours of growth measured via flow cytometry.

dilute sample of stained snowflake yeast clusters suspended in water was placed beneath an 18 m square coverslip on a glass slide. Images of individual clusters were taken and their in-plane area was measured. From this area, radius was calculated as $r = \sqrt{\frac{A}{\pi}}$, where r is radius and A is area; volumes were calculated using this radius and a spherical approximation.

Gradual evaporation of the water caused surface tension to pull the coverslip closer to the slide, compressing the snowflake clusters to a monolayer of cells. Cells were then counted via maxima identification in Fiji. Finally, volume fraction was calculated by multiplying the number of cells by the mean volume of a cell (see below for details) and then dividing by the volume of the cluster.

Despite the fact that genotypes isolated from a given week are not necessarily descendant from genotypes isolated from a prior week, we chose to include two intermediate points in our volume fraction measurement. As figure 6a shows, the distribution of cellular aspect ratio in the week 4 and week 6 genotypes are intermediate to those of week 1 and week 8 (Aspect Ratio Statistics: W1 vs. W8 $t = -26$, $p = 3 \times 10^{-136}$; W4 vs. W8 $t = -22$, $p = 1 \times 10^{-99}$; W6 vs. W8 $t = -18$, $p = 1 \times 10^{-69}$; W4 vs. W6 $t = -4.8$, $p = 2 \times 10^{-6}$; W1 vs. W6 $t = -9.5$, $p = 4 \times 10^{-21}$; W1 vs. W4 $t = -4.5$, $p = 6 \times 10^{-6}$, two-tailed t-tests). Figure 6b shows the high agreement between experiment and simulation for number of cells as a function of radius. Interestingly, mean cellular volume decreases from week 1 to 6 before increasing significantly in week 8, resulting in the overlap of the curves for weeks 1, 4 and 6 in figure 6b (Mean cell volume in cubic microns: W1 = 165, W4 = 149, W6 = 140, W8 = 274). Using the mean cellular volume for each genotype and a spherical approximation for cluster volume, this data is converted to volume fraction and plotted versus cluster radius in figure 6c. Figure 6d shows the mean volume fraction for weeks 1, 4, 6, and 8; volume fraction decreases by nearly 30 percent between weeks 1 and 8. Data was collected for 21 W8 clusters, 29 W4 clusters, 27 W6 clusters, and 26 W8 clusters (Volume Fraction Statistics: W1 vs W8 $t = 8.3$, $p = 6 \times 10^{-10}$; W1 vs W4 $t = 1.9$,

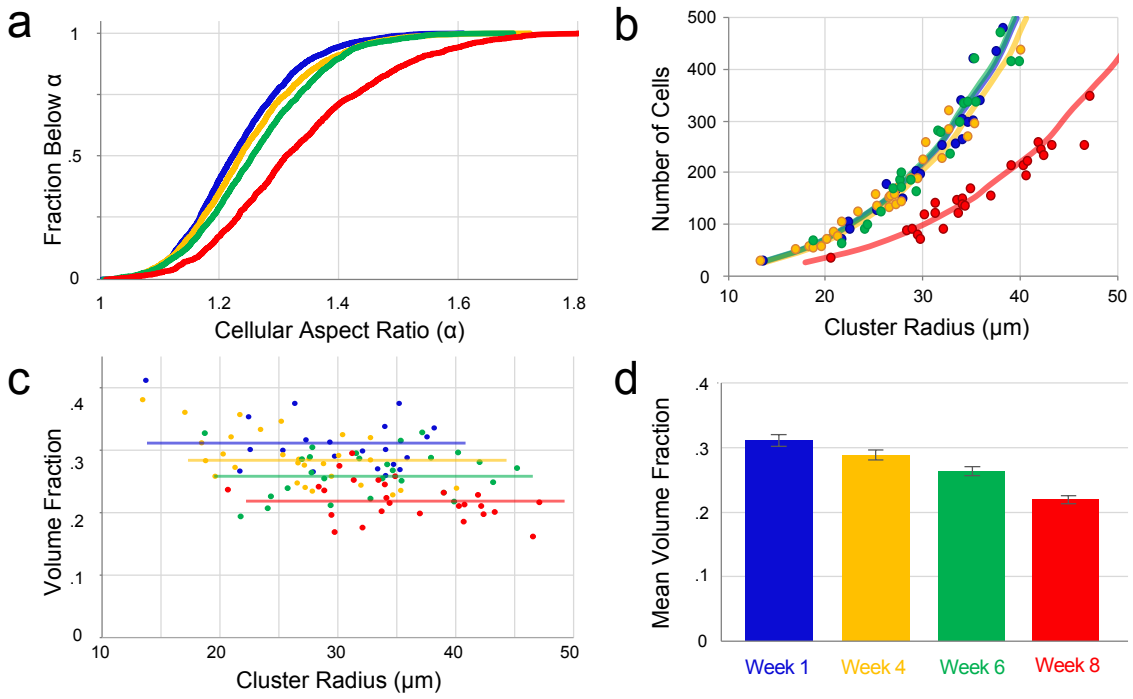

Figure A.6: Volume fraction of snowflake yeast decreases as they evolve. (a) Fraction of cells with aspect ratio below for week 1 (blue), week 4 (yellow), week 6 (green) and week 8 (red) genotypes. (b) Number of cells vs. cluster radius for all 4 genotypes from experiment (dots) and simulation (lines). (c) Volume fraction vs. cluster radius, with means indicated by horizontal lines. (d) Mean volume fraction. Bars denote the standard error of the mean.

$p = 0.06$; W4 vs W6 $t = 2.37$, $p = 0.02$; W6 vs W8 $t = 4.6$, $p = 2.6 \times 10^{-5}$; W1 vs W6 $t = 4.1$, $p = 0.0002$; W4 vs W8 $t = 6.9$, $p = 6.0 \times 10^{-9}$, two-tailed t-tests).

A.6.1 Calculations

Cluster radius

$$\text{Cluster radius (r)} = \sqrt{\frac{A}{\pi}} \tag{A.1}$$

where A is the in-plane area measured via microscopy.

Energy input at fracture

$$\text{Energy input at fracture} = \frac{fd}{2} \tag{A.2}$$

where f is the applied force at fracture and d is the displacement of the cantilever. As the forcedistance curves are essentially linear, this is a valid approximation of the total energy input.

Compressive modulus

$$\text{Compressive modulus} = \frac{f}{rd} \tag{A.3}$$

Cell volume

$$\text{Cell volume} = \frac{4}{3}\pi(\frac{W}{2})^2(\frac{L}{2}) \tag{A.4}$$

where width (W) and length (L) are mean values across the populationsingle-cell properties determined from genotypes reverted to unicellularity as described above in the section entitled 'Snowflake yeast genotypes and growth'.

Volume fraction

$$\text{Volume fraction} = \frac{(N_{cell} \cdot V_{cell})}{V_{cluster}} \tag{A.5}$$

where N_{cell} is the number of cells, V_{cell} is cell volume (see 'Cell volume' calculation) and $V_{cluster}$ is the volume of the cluster approximated from the cluster radius (see 'Cluster radius (r)' calculation).

All P values from t-tests are two-tailed.

A.7 Understanding constant force and decreasing energy input at fracture

To understand the counter-intuitive combination of decreasing energy input at fracture and constant applied force at fracture, consider the behavior of a 1-D system consisting of two springs attached to two separate walls, with a block between them (Figure A.7a). The springs are initially each compressed by a distance d; they each push the block with forces of magnitude $F = kd$. If an externally applied force pushes the block a distance d farther

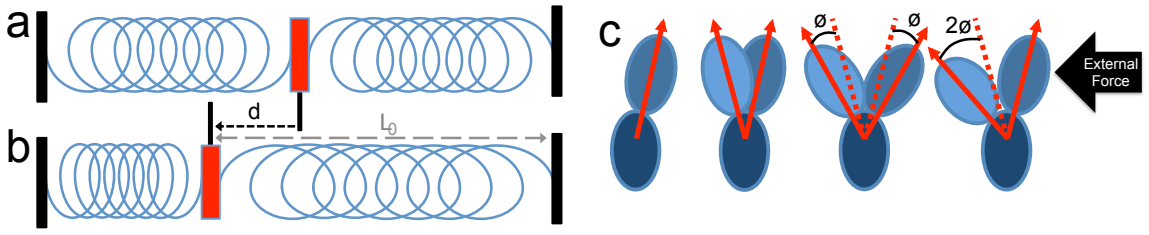

Figure A.7: Compression of spring system (a-b) is analogous to cellular deformations within a snowflake cluster (c).

to the left, the spring on the right is relaxed, and supplies no force. Instead, the entire force of F=k2d must be provided by the external force (Figure A.7b). However, this change only requires external energy input of $\Delta E = \frac{3}{2}kd^2$, rather than $\Delta E = 2kd^2$. Thus internal stresses in this block-spring model decrease the required energy input but not the required applied force to fracture.

This model captures the pertinent features of snowflake mechanics; namely, constant force at fracture and the inverse relationship between size and energy input at fracture. The block-spring system is potentially analogous to the trio of cells diagrammed in figure A.7c. A cell is perturbed from its equilibrium position by the growth of a second cell; they share the resultant stress by deforming from their equilibrium positions. With the application of a force external to the pictured 3-cell system, the cell on the left is pushed farther from equilibrium, while the cell on the right returns to its original, unperturbed position.

A.8 Angle of attachment measurement

The angle of attachment used in the simulations is extracted from experimental images of revertant cells via image analysis using the Fiji angle measurement tool. The mean angle was $42.4°$ with a standard deviation of $10.0°$ ($N = 20$). The rather large standard deviation is due to extracting the angle from a 2D image. Cells are selected for measurement if their entire perimeter is in focus, and their bud scar lies to the side, allowing the angle to be measured in-plane. While this measurement is sufficient to set an angle for the simulations (which do not qualitatively depend on the angle, and only exhibit a weak quantitative

dependence), full 3D images are necessary to better quantify this angle and its variance.

A.9 Simulation

Snowflake yeast are modelled as prolate spheroids in a geometric Python program. The program has a number of controllable parameters including size, allowed overlap, angle of attachment and aspect ratio.

In general, the program constructs a model of a snowflake yeast cluster one generation at a time starting with an initial basal parent cell. Each generation, every cell in the cluster is given the opportunity to attempt reproduction. A parent cell can spawn a daughter cell only if the centre-to-centre distance between the prospective daughter cell and its neighbours is less than a specified amount, which we call the overlap parameter. For the experiments reported here, the overlap parameter was set to 50% of the cells in-plane radius. This value was chosen as it approximates the minimum spacing set by the size of the chitin bonds. However, changing the overlap parameter does not qualitatively change the phenomena reported, it simply changes the magnitude of the effect.

The location on a parent cell at which a daughter is spawned is determined via the following protocol. Each cell, except the basal cell, has an 80% chance of spawning its first daughter at the distal pole (that is, directly opposite its own point of attachment) and a 20% chance of spawning a cell at a specified angle of attachment (Appendix A Fig. A.6). Subsequent daughters are spawned at a random location at this specified angle of attachment. Additionally, the model incorporates stochastic random variance (up to 10%) in the angles at which daughters are spawned. This helps to create clusters that realistically imitate the stochasticity of their biological counterparts. For the results reported here, the angle of attachment was set to $45°$, which is similar to what is observed experimentally ($42.4°$ with standard deviation of $10°$, $N = 20$ for both week 1 and week 8). Again, varying the angle of attachment (between 22.5 and $60°$) changed only the magnitude of the results, not the qualitative trends.

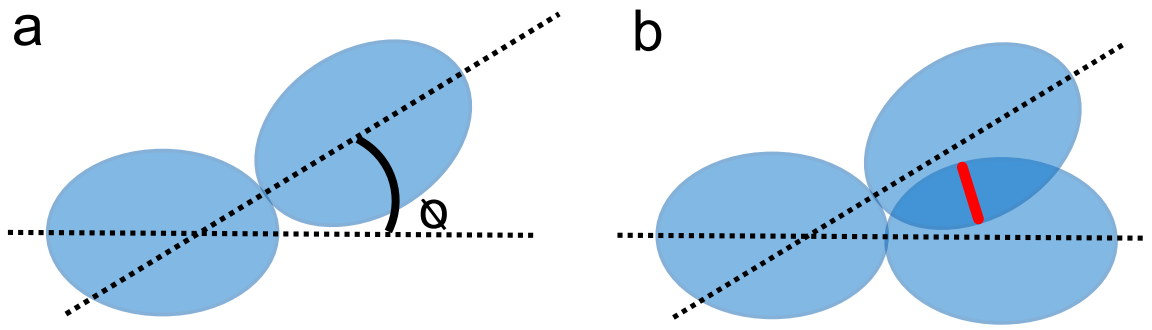

Figure A.8: (a) Angle of attachment, , between mother cell (blue) and daughter cell (green). (b) The value of the linear overlap between two cells is equal to the length of the red line.

To quickly determine the degree to which two cells overlap, we utilize a mathematical procedure to fill each ellipsoidal cell with five spheres that mimic the shape and extension of the cell. These spheres are concentric with the ellipsoids centre, foci and midpoints between the centre and the foci, and their radii are equal to that of the circular cross-section of the ellipsoid at their location. To measure overlap, the centre-to-centre distance, d, is compared with the sum of the radii of each pair of intercellular spheres, $r_1 + r_2$.

From the overlap between two cells, the effective elastic energy, U_{eff}, was calculated using both harmonic:

$$U_{eff} = (d - r_1 - r_2)^2 \tag{A.6}$$

and Hertzian models:

$$U_{eff} = (d - r_1 - r_2)^{2.5} \tag{A.7}$$

For 100 12-generation clusters constructed of cells with aspect ratios randomly chosen from the week 1, 4, 6, and 8 distributions with an angle of attachment of 45 degrees (Figure A.8a), the average cumulative overlap squared per cluster (a) and per cell (b) as a function of the number of cells are shown in figure A.9. Cumulative overlap squared is the sum of the square of the linear overlap (Figure A.8b) between each pair of cells.

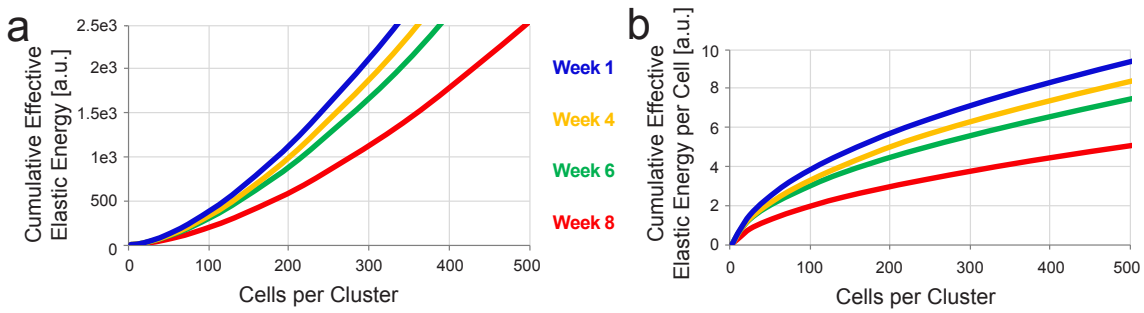

Figure A.9: Total average cumulative squared overlap, or effective elastic energy, in each cluster (a) and per cell (b) vs. number of cells for simulated clusters consisting of week 1 (blue), week 4 (yellow), week 6 (green) and week 8 cells (red).

For clusters of any size, those containing cells with aspect ratios drawn from the week 1 distribution have approximately twice the cumulative squared overlap of those consisting of cells from the week 8 distribution. Additionally, clusters consisting of cells from earlier evolutionary time points have more total cumulative overlap squared and more cumulative overlap squared per cell. Note that even though simulated clusters begin from a single cellwhereas real snowflake yeast clusters form from a propagulethe geometric simulations are unaffected by the starting point, as they are purely structural, and do not allow for dynamic relaxation. The model nonetheless accurately reproduces the geometry of snowflake yeast clusters because they grow according to simple rules, and previously published experiments examining clusters started from mechanically sheared single cells and recently-detached propagules show they have the same geometry (*Ratcliff et. al.*, 2015, Nature Communications) [35].

When using the simulation to predict spontaneous fracture size, we considered both harmonic and Hertzian models. Figure 3e shows the harmonic model; if we use a Hertzian model instead, the relative trends are nearly unchanged (Figure A.10). Since we are using the model to investigate relative differences between genotypes and not to predict physical values for the energy required to fracture a cluster, it makes no difference whether we use the Hertzian or harmonic model.

When investigating the packing of daughter cells on a single parent cell, the simulation

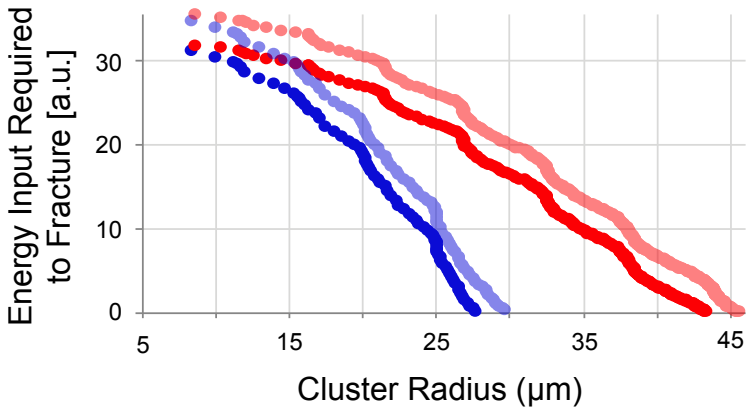

Figure A.10: From simulation, energy input required to fracture a cluster using a Hertzian model plotted versus cluster radius. The darker data series use the energy threshold set by the week 1 genotype, and the lighter series use the threshold set by the week 8 genotype.

was modified so that a single cell repeatedly attempted to reproduce until it failed 100 consecutive times, indicating that it was highly unlikely that another cell could be placed. The aspect ratio for all cells was randomly selected from distributions of cellular aspect ratios obtained from experiment. 1000 trials were performed from each of the distributions, and the results were averaged and are shown in figure A.11.

A.10 Evidence for the causal relationship between cellular elongation and increased cluster size

To examine this claim in detail, we separate it into 5 sub-claims:

1. Clusters evolved to have lower volume fractions.

2. Clusters evolved to accumulate internal stress during growth at a lower rate, which allows them to access larger sizes.

3. Individual cells evolve increased ellipticity.

4. The decrease in volume fraction is due to an increase in ellipticity at the individual cell level.

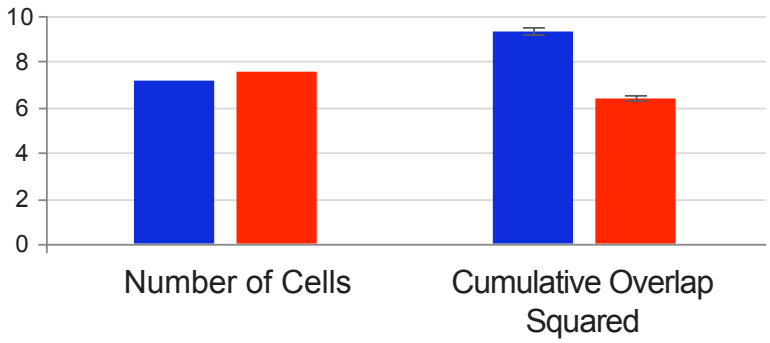

Figure A.11: Average number of cells added and cumulative overlap squared for maximally packed daughters on a single parent cell for week 1 (blue) and week 8 (red) cells. The units of cumulative overlap squared are arbitrary, and so values have been normalized so as to be on the same scale as the number of cells added. Error bars show standard error (error in number of cells too small to display).

5. The decrease in volume fraction facilitates the slower accumulation of internal stress.

Sub-claims 1, 2, and 3 are directly demonstrated in experiments, with data shown in Fig. 2.2b, 2.2d, and 2.3a, respectively. We directly observe a statistically significant decrease in volume fraction from week 1 to week 8 ($p = 6 \times 10^{-10}$). We directly observe a decrease in the rate of stress accumulation as a function of size between week 1 and week 8 ($p = 4.7 \times 10^{-5}$). We directly observe a statistically significant change in the distribution of ellipticity across individual cells ($p = 3 \times 10^{-136}$).

Support for sub-claim 4 comes from simulations and previously published experiments; however, while this is indirect, it is certainly strong enough to be compelling. In simulations, we show that the geometrical effect of this shift in aspect ratio is sufficient to account for the evolved decrease in volume fraction; in fact, with only the experimentally observed aspect ratios as input, the simulations predicts the experimentally observed volume fractions with remarkable accuracy - the slope of the best linear fit between experimental and simulated volume fractions is 0.998 with $r^2 = 0.94$. The application of the results of the simulations to the experimental system relies only on the robustness of the snowflake yeast growth form, which has been experimentally validated in previous exhaustive experiments across clusters with different sizes and from different weeks [35]. With the growth form

validated, this becomes a question of geometry: how does volume fraction change when the growth form is constant, but the distribution of aspect ratios changes?

Sub-claim 5 is also supported indirectly. However, it only requires that granular physics - related to the jamming transition - hold: for granular matter, the stiffness is directly proportional to the number of contacts between particles, which, in turn, is directly proportional to the volume fraction [70]. A recent publication in Nature Physics demonstrated that these physics do indeed hold for a different strain of yeast [138]. In our system, as clusters increase in size, individual cells produce more offspring, directly increasing the number of inter-cellular contacts. In fact, we directly observe that cluster stiffness increases with cluster size (Figure 2c - note that percent strain at fracture decreases as size increases). While our model is indeed minimal, it is remarkable that geometry alone captures much of the structural nature of snowflake yeast; in fact, as there are reasons to favor simple models over more complex ones [139, 140, 141].

APPENDIX B

SUPPLEMENT TO CHAPTER 3

B.1 Experimental Measurements

Experimental measurements used for comparisons with the model in this manuscript were originally reported in [42]. Measurements of cellular aspect ratio (α) and angle of attachment (θ) were performed on cells from populations of snowflake yeast cells that had been reverted to unicellularity using the lithium acetate / PEG / single-stranded carrier DNA method as described in Ratcliff *et. al.*[35]. This reversion was accomplished by replacing a single non-functional copy of ace2 (a mutation that arose during experimental evolution) with a functional, ancestral copy. Thus these revertants are thus genetically identical to their snowflake counterparts, with the exception that they are capable of normal mother-daughter cellular separation after mitosis. Revertants were used because they allow for precise measurements of cellular morphology that would have been far more difficult within three-dimensional snowflake clusters. A previous study confirmed that the geometry of revertant cells is not fundamentally different from those within snowflake clusters[42].

Aspect ratio was measured by imaging several fields of view with a Nikon A1R confocal microscope, and using the particle tracking feature in the image analysis software Fiji. (Statistics: week 1 N = 2128; week 8 N = 1961). To measure the angle of attachment, bud scars (attachment cites) were stained with calcoflour (Fluorescent Brightener 28 from MP Biomedicals, LLC) using the following procedure: a 1:10 dilution of cells from steady state was rinsed and resuspended in deionized water. Then calcoflour was added at a 1:100 dilution from a stock solution of 1 mg/mL calcoflour/water, and this mixture was incubated in the dark at room temperature for at least 10 minutes. Before imaging, the cells were again rinsed and resuspended in deionized water. θ measurements were obtained from 3D

confocal images of individual cells bearing at least 4 bud scars (Statistics: N = 10 for week 1 and week 8).

B.2 Model Validation

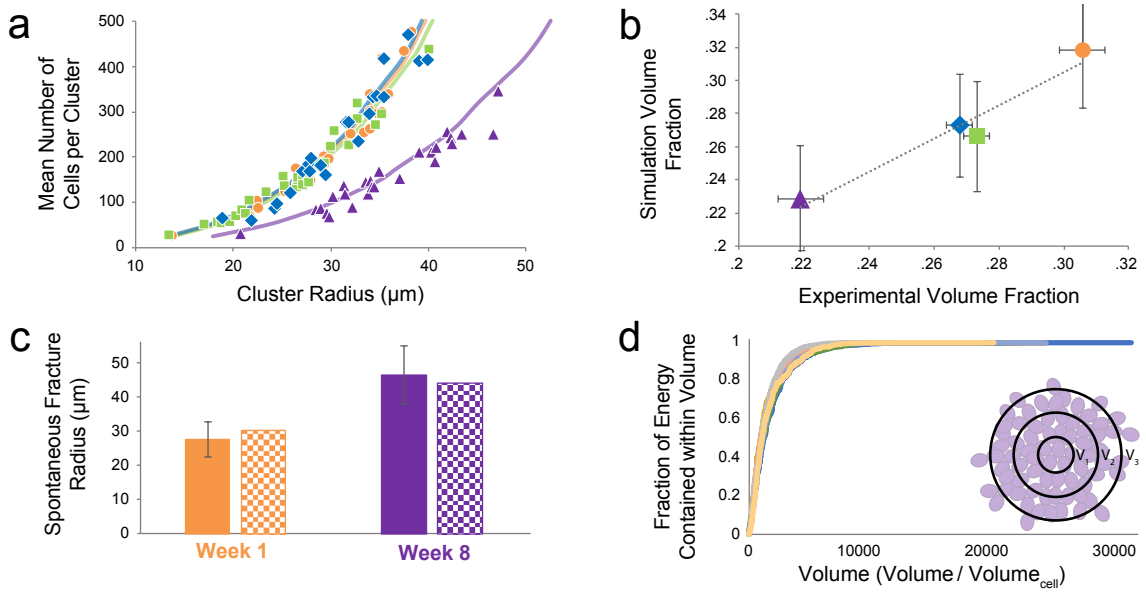

Figure B.1: (a) Number of cells versus cluster radius for genotypes isolated after 1 (orange circle), 4 (green square), 6 (blue diamond), and 8 (purple triangle) weeks of daily settling speed selection. Experimental (distinct points) and simulation (continuous lines) are shown, where the simulation data is the mean over 100 clusters. (b) Mean simulation versus mean experimental volume fraction; linear trendline slope $= .998$, $r^2 = .94$. (c) Experimentally observed (solid) and simulation-predicted (checkered) spontaneous fracture sizes for week 1 and week 8 clusters. Error bars represent standard deviation. This data was originally published in Jacobeen *et. al.*, 2018 [42] (d) Cumulative distribution plot of the fraction of energy contained in a given concentric spherical volume within a cluster (inset; concentric expanding volumes) for 10 trials of a simulation with $\alpha = 1.5$, $\theta = 54°$.

This validation was originally performed in Jacobeen *et. al.*, 2018, and further explanation of these experiments are contained therein[42]. To validate the minimal geometric model, we performed simulations utilizing experimentally observed values of θ and α, and compared several measurements of cluster properties across experiments and simulations. For the validation, θ was set to 45 degrees (with up to 10% random variance)–similar to what is observed experimentally[42]–and α was randomly seeded with experimentally-

obtained cellular aspect ratio distributions obtained from revertant cells from populations of snowflakes that had been isolated after 1, 4, 6, and 8 weeks of evolution. For each distribution, 100 independent clusters were simulated for 12 generations.

First we assessed the number of cells per cluster as a function of cluster radius. Cluster radius was obtained from a circular approximation of the in-plane area of an intact cluster. Cell counts were then obtained from microscopy images of clusters that had been compressed to a cellular monolayer. Figure 5a shows the remarkable agreement between simulation and experiment in the number of cells as a function of cluster radius for all 4 genotypes.

Next, we compared volume fraction, which was obtained by multiplying the number of cells by mean cell volume and dividing by the total volume of the cluster. Again, astounding similarity between experimental and simulated results is observed (Fig. B.1b); mean volume fraction from simulation is plotted versus that obtained from experiment (trendline slope $= .998$, $r^2 = .94$).

Finally, we used U to predict fracture size. Mean spontaneous fracture size of week 1 and week 8 genotypes was obtained from time-lapse microscopy videos of unconstrained cluster growth and fracture[42]. By setting U_c to the value predicted by the spontaneous fracture size of one genotype, the spontaneous fracture size of the other is predicted to well within one standard deviation (Fig. B.1c). In agreement with experimental observations [42], stress accumulation is concentrated in the core of the cluster (Fig. B.1d). Collectively, the remarkable agreement between simulation and experiment in number of cells versus radius, volume fraction, and fracture size offers compelling evidence that despite its lack of dynamics, our minimal geometric model accurately describes many of the structural aspects of snowflake yeast clusters. This in turn suggests that physically-imposed geometric constraints play a critical role in determining the structure and fitness of snowflake yeast.

B.3 'Magic Angle' packing

The optimal budding angle $\theta = 54^\circ$ observed in simulations can perhaps be understood through an analogy to the packing of cones. Daughters attach to a parent cell with an angle of attachment θ; this angle defines a budding ring along its surface (Fig B.2a). The set of all possible placements for daughter cells along this ring defines a cone-shaped volume (Fig. B.2b). If L is the length of the side of the cone, its volume is given by

$$V = \frac{1}{3} \cdot L^3 \cdot \sin^2\theta \cos\theta \tag{B.1}$$

.

Maximizing V while keeping the number of cells fixed is equivalent to minimizing volume fraction; V is maximized at the so-called 'magic angle,' $\theta = 54.7^\circ$ [81], independent of cell aspect ratio. Thus our simulations suggest that N is maximized when the volume of the cone defined by the accessible locations of each cell's daughters is maximized.

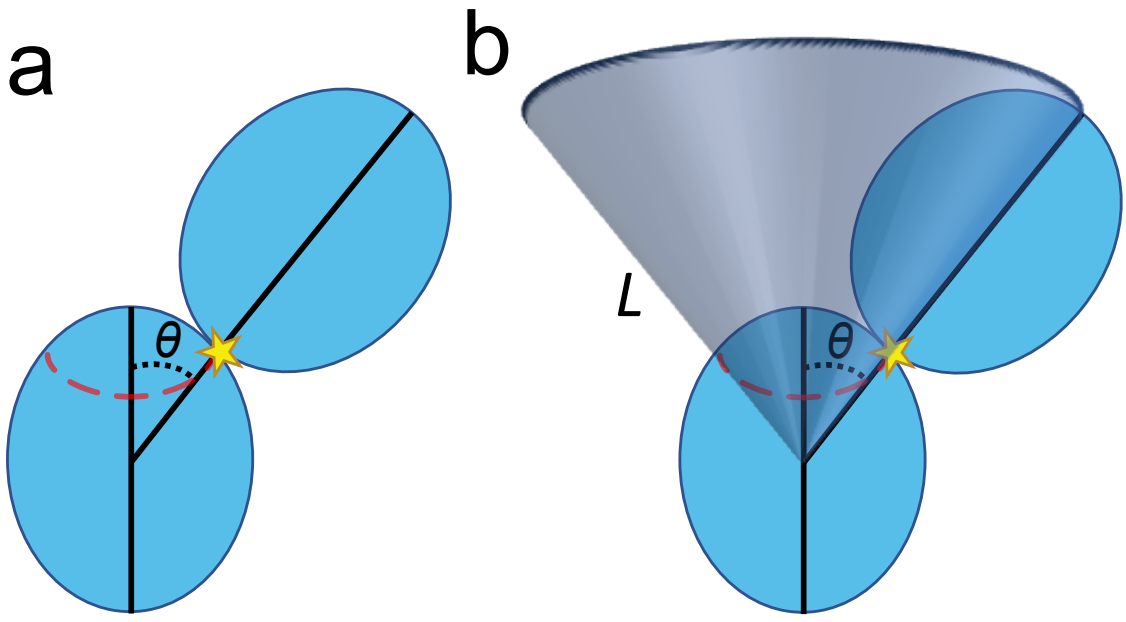

Figure B.2: (a) Parent cell with a budding ring (red dashed line) defined by angle of attachment θ, and daughter cell attached at the point marked by the yellow star. (b) A cone is formed by considering the set of possible placements for the daughter cell.

APPENDIX C

SUPPLEMENT TO CHAPTER 4

C.1 Evolution Protocol

C.1.1 Growth

Cultures were grown to steady state in a Symphony Incubating Orbital Shaker Model 3500I at 250 RPM and 30°C for 24 hours in 10 mL of YPD (10 $g \cdot l^{-1}$ yeast extract, 20 $g \cdot l^{-1}$ peptone and 20 $g \cdot l^{-1}$ dextrose) into which had been added 200mg/L G418 sulfate (VWR catalog number 97063-060). The antibiotic G418 was used because of the unavoidably high chance of contamination during the compression stage of the protocol; by using a G418-resistant strain of snowflake yeast and media that contained G418, contamination was avoided for the duration of the experiment.

C.1.2 Compression protocol

In order to compress a sufficiently large percentage of the population, steady state cultures were concentrated to a paste-like density via centrifugation in a 15 mL centrifuge tube at 6.5k g for 1 minute and the supernatant was removed. Next, 200 μL of this concentrated cluster paste was placed, in 2 100 μL drops, at 1/3 intervals on the long axis of a 50mm x 75mm glass slide. Another slide of the same dimensions was then placed on top of these, and the resulting slide-cluster-slide 'sandwich' was placed between the compression plates of a Zwick Universal Testing Machine and compressed for 15 seconds with a force of 1000N (using the force-controlled creep test protocol for 1000N, 15s). After compression, the crushed clusters were transferred via careful rinsing (performed with a 1000 μL pipette) with sterile H2O into a 1.5 mL micro centrifuge tube. Inevitably some clusters (no more than 10%) remained on the slides and were lost. Before selection, the total volume in the

centrifuge tube was brought to 1.5 mL by the addition of sterile H2O.

C.1.3 Settling speed selection

Settling speed selection was performed by allowing the tube to rest upright for 5 minutes after which the upper 1.4ml 93% of the volume was removed by pipette. The remaining 100 μL was transferred to a fresh tube containing 10 mL of YPD, thus re-initiating the growth phase.

C.1.4 Replicates and control

6 separate replicates were evolved under this protocol for 8 weeks, with checkpoint samples collected and frozen each week.

In addition, 6 replicates of a 'control' were evolved under a similar protocol that lacked the compression step. This was nearly identical to the evolution performed in *Ratcliff et. al., 2012*[34], we repeated it here so as to have a controlled comparison.

The control protocol is essentially the same as the compression protocol, except that compression was not performed. Though strictly unnecessary for settling speed selection and growth, for consistency the control protocol included the centrifugation of steady state culture into a dense paste. 180 μL of this paste was then transferred directly to a micro centrifuge tube, and the addition of sterile water brought the total volume to 1.5 mL. The 10% reduction in amount of paste used in the control protocol was intended to compensate for the clusters lost in transferring from the glass slides in the compression protocol. This compensation was motivated by an attempt to start the growth phase with roughly comparable numbers of clusters in both cases.

APPENDIX D

SUPPLEMENT TO CHAPTER 5

D.1 Simulation: Structure

This section provides a summary of the mathematical function of the simulation.

The fitness of each individual within a group is defined as:

$$W_i = A_i B_i \tag{D.1}$$

In order to model the costs of functional specialization of the individual units, we include a parameter, α, that allows us to vary the cost/benefit relationship of performing a particular function. The individual's output for each function is given by:

$$A_i = I_A^{\alpha_A}, B_i = I_B^{\alpha_B} \tag{D.2}$$

where I is the investment in each function, and each individual within the group is subject to the constraint

$$I_A + I_B = 1 \tag{D.3}$$

For simplicity, we have considered only the case where the functional returns are equal for both functions, that is:

$$\alpha_A = \alpha_B \tag{D.4}$$

We note that $\alpha = 1$ yields linear returns on the investment in specialization, while $\alpha > 1$ and $\alpha < 1$ yield super-linear and sub-linear returns, respectively. Thus, the evolutionary incentive for specialization increases with α.

For a group of autonomous, non-interacting individuals, the fitness of a group (W) is simply the sum of the fitness of each individual in the group:

$$W = \sum_{i=1}^{n} W_i = \sum_{i=1}^{n} A_i B_i \tag{D.5}$$

This is equivalent to the trace of the fitness matrix $\mathbf{W}$, or the sum of element-wise Hadamard product of $\mathbf{W}$ and the $n \times n$ identity matrix $\mathbf{I_n}$:

$$W = tr(\mathbf{W}) = sum(\mathbf{W} \circ \mathbf{I_n}) \tag{D.6}$$

where $\mathbf{W}$ is the product of $\mathbf{A}$ and $\mathbf{B^{-1}}$, column and row vectors containing the values of A and B for each of the individuals in the group:

$$\mathbf{W} = \mathbf{A}\mathbf{B^{-1}}, \mathbf{A} = \begin{bmatrix} A_1 \\ A_2 \\ \vdots \\ A_n \end{bmatrix}, \mathbf{B} = \begin{bmatrix} B_1 \\ B_2 \\ \vdots \\ B_n \end{bmatrix} \tag{D.7}$$

Equations D.5 and D.6 are equivalent because the trace and element-wise multiplication with the identity matrix eliminates all off-diagonal terms (those were $i \neq j$).

To allow for functional integration between individuals of a group, we generalize the identity matrix $\mathbf{I}$ in equation D.6 to a connectivity matrix $\mathbf{C}$. Equation D.5 can be similarly generalized by including a second sum and a connectivity term, $c_{i,j}$ which is the element at position i, j of the connectivity matrix $\mathbf{C}$:

$$W = sum(\mathbf{W} \circ \mathbf{C}) = \sum_{i=1}^{n} \sum_{j=1}^{n} A_i B_j c_{ij} \tag{D.8}$$

Note that for any $\mathbf{C}$, the diagonal ($c_{i=j}$) terms must always be 1 because of each individuals inherent self term. The off-diagonal entries in $\mathbf{C}$ can take any value between 0 and 1, and this value represents the functional integration strength between the interacting individuals,

or how much of their functional output is shared across connections. In order to make comparisons between fitness of groups with different $\mathbf{C}$s, $\mathbf{C}$ is always normalized by the sum of its entries; because we consider in this paper only cases in which all individuals have an equal number of connections, this normalization correctly distributes the functional outputs.

D.2 Specialization

In this simulation, specialization is measured by a mean quantity of the same name that ranges from 0 (for generalists) to 1 (for specialists). It is calculated as follows:

$$Specialization = \frac{\sum_{i=1}^{n} 2 \cdot (max(I_{A_n}, I_{B_n}). - 5)}{n} \tag{D.9}$$

where n is the number of individuals in the group. For the results reported here, 'specialization' refers to the mean specialization of the 10% of groups with the highest fitness. We say that specialization has occurred if this mean value is in excess of $.9$.

D.3 Connection Types

Here we expand on the discussion in the main text of the case in which $\alpha_{A,B} = 1$. In the case of a fully connected group ($\mathbf{C} = \mathbf{J_n}$), there is no fitness difference between the generalist and specialist configurations. For the generalist case, each connection-including self terms-contributes $I_A I_B = .5 \cdot .5 = .25$ to the fitness of the group. On the other hand, if all members of the group are specialists, $3/4$ of the terms in $\mathbf{WC}$ are zero, as half of each of the A_is and B_js are 0. The other $1/4$ of the terms, however (those for $A_i = B_j = 1$), have a value of 1. Therefore,

$$W_{gen} = .25 \cdot n^2 = W_{spc} = \frac{n^2}{4} \tag{D.10}$$

Since only $\frac{n^2}{4}$ of the terms in $\mathbf{W}$ contribute to the fitness in the specialist case, there

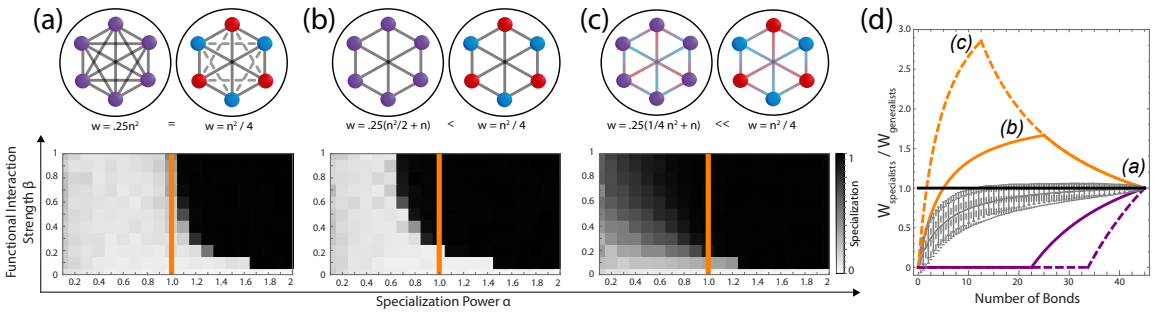

Figure D.1: CONNECTION TYPES (a) Heat map of specialization as a function of functional interaction strength and specialization power for a fully connected group. Orange line indicates the limit of super-linear returns on specialization ($P = 1$). Schematics show connection structure for a simplified 6-individual system, with generalists on the left (purple nodes) and specialists on the right (red and blue nodes). Dashed lines indicate edges in $\mathbf{C}$ that correspond to terms in $\mathbf{W}$ that do not contribute to fitness. (b) Specialization as a function of functional interaction strength and specialization power for a symmetric network optimized for the evolution of specialization. (c) Relaxing the symmetry constraint and removing all off-diagonal entries in $\mathbf{C}$ that do not contribute to the fitness yields the network best suited for the evolution of specialization. Here the color of the connections in the schematic indicates that connections are 'directed'; *e.g.* is if individual i specializes in parameter A and individual j specializes in B, the term $A_i B_j c_{ij}$ is included in the calculation of W, but $A_j B_i c_{ji}$ is omitted. All simulations performed on populations of 100 groups of 10 individuals for 100 rounds of evolution. (d) Ratio $\frac{W_{spc}}{W_{gen}}$ for a group of 10 individuals with $\alpha_A = \alpha_B = c_{ij} = 1$ for all i,j. If connections that contribute to W_{spc} are exclusively added first, specialization rapidly becomes favored (solid orange line). If connections that only contribute to W_{gen} are exclusively added first, specialization is never favored (solid purple line). These effects are exacerbated by allowing for non-mutual, directed interactions (dashed orange and purple lines, respectively). If connections are randomly added, specialization can occasionally be favored, but on average it is not (gray lines; solid for the mutual interaction case, and dashed for the directed case). Configurations explored in panels a-c are labeled at the appropriate location in panel d.

are terms in $\mathbf{C}$ whose value has no impact on the fitness of the group. This is because for (A_i, B_j) pairs $(1, 0)$ or $(0, 1)$ $W_{i,j} = A_i B_j c_{ij} = 0$, irrespective of the value of c_{ij}. Removing these connections from $\mathbf{C}$ therefore leaves the value of W_{spc} unchanged, but decreases W_{gen} by a factor of $.25(\frac{n^2}{2} - n)$, were the factor of n is the result of the inevitable self terms (Fig. D.1 a%b). Thus,

$$W_{gen} = .25(\frac{n^2}{2} + n) < W_{spc} = \frac{n^2}{4} \tag{D.11}$$

This inequality can be further exacerbated by relaxing the symmetry constraint such that we can drop the $(0,0)j,i$ pairs associated with the $(1,1)i,j$ pairs. In this case the fitness difference between the generalists specialists is maximized (Fig. D.1c):

$$W_{gen} = .25(\frac{n^2}{4} + n) \ll W_{spc} = \frac{n^2}{4} \tag{D.12}$$

Specialization is favored when $W_{spc} > W_{gen}$, or when the ratio $\frac{W_{spc}}{W_{gen}} > 1$. While the connection structure dictates the evolution of the group in our simulation, for purposes of illustration we now consider the case of a group of predetermined generalists or specialists. The value of the ratio $W_{spc} > W_{gen}$ depends highly on what type of connections exist within the group; if connections that contribute to fitness in the case of specialization–'specialist connections'–are exclusively added first, specialization quickly becomes favored (figure S1d). On the other hand, if only 'generalist connections' are added first, specialization is never favored. Again, the strength of this effect is exacerbated by breaking the symmetry of $\mathbf{C}$ and allowing for directed specialist connections. If connections are randomly added, specialization can be slightly favored due to the stochastic choice of connection type, but the mean value of the ratio $\frac{W_{spc}}{W_{gen}}$ never exceeds one.

To find the minimum value of $\alpha_{A,B}$ for which specialization can evolve, we remove our initial assumption that $\alpha_{A,B} = 1$ and replace $.25$ in W_{gen} with $(.5^P)^2$. Solving this general form of equation D.11 for $n > 0$ gives

$$\alpha_{min_sym} = \frac{\log(\frac{2(n+2)}{n})}{2\log(2)} \tag{D.13}$$

Likewise, solving the general form of equation D.12 for $n > 0$ gives

$$\alpha_{min_asym} = \frac{\log(\frac{n+4}{n})}{2\log(2)} \tag{D.14}$$

For $n = 10$ and $n = 100$, equation D.12 takes approximate values of $\alpha_{10min_sym} = .63$ and $\alpha_{100min_sym} = .51$ respectively, while equation D.13 yields $\alpha_{10min_asym} = .24$ and

$\alpha_{100min_asym} = .028$. These limits on complete specialization are consistent with the results in Figure 3. While this binary simplification of the system as either generalists or specialists exemplifies powerful role of group structure in the evolution of specialization, it must be noted here that our evolutionary algorithm does not treat these cases as binary. Rather it blindly optimizes groups under selection, and so may well settle on intermediate cases of 'partial specialization' as seen in figure 3b and 3c.

Finally, to discover the minimum exponent for which specialization is possible (in the infinitely large, symmetric case), we set the fitness advantage of adding a connection to a group of generalists equal to that of adding an unlike-specialists connection in a group of specialists

$$2 \times (.5^{\alpha})^2 = (1^{\alpha})^2 \tag{D.15}$$

Solving equation D.15 yields $\alpha = .5$, so for groups of any size, the α for which specialization is possible is $\alpha > .5$.

D.4 Simulation: Evolution Parameters

The 'deterministic' selection used throughout this work acts by selecting the fittest 10% of groups and coping them tenfold (with resource redistribution) to replenish the population for the next round of selection (figure 1b,c). To ensure that this was not influencing the final equilibrium configurations, we tested tested a 'probabilistic' evolution protocol that selected 10 groups via fitness-weighted random selection. We find that these selection protocols yield identical results; compare the heat maps in the first row of figure S2 to those in figures 2a, 2c, and S1c.

The evolution of groups in our simulation is controlled by 2 parameters: population size and number of steps. 100 was chosen for both population size and the number of rounds of selection as these values were sufficient for the system to reach stable, equilibrium configurations. To ensure stable final configurations were in fact reached, we ran the simulation

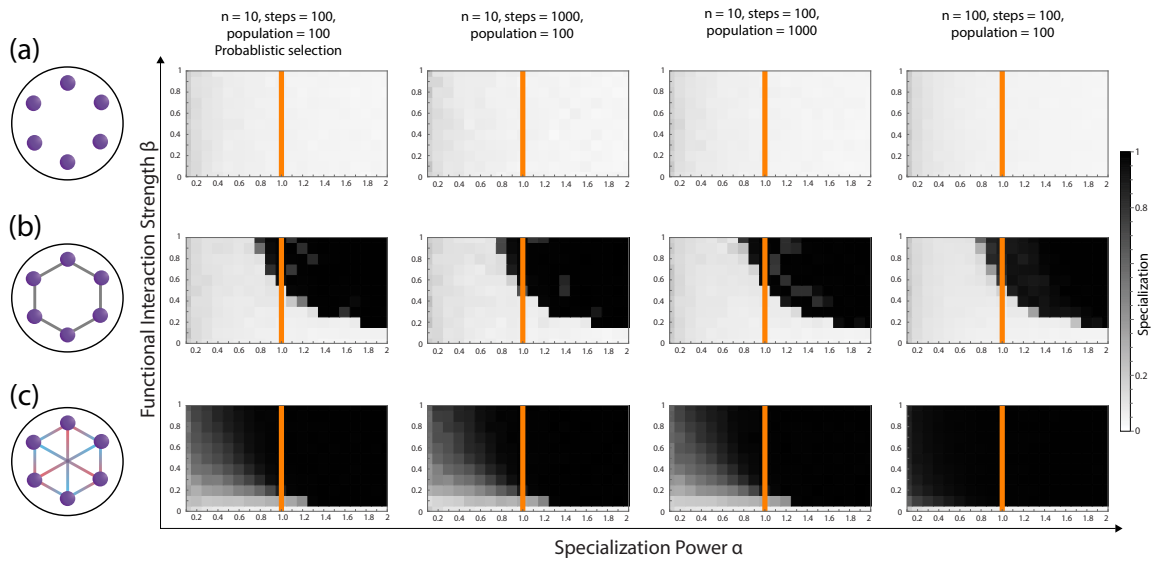

Figure D.2: SIMULATION PARAMETERS. Results of using probabilistic (versus deterministic) selection, increasing by a factor of 10 the number of steps, size of the population, or size of the groups in our simulation. In the cases of noninteracting individuals (a) and groups in which members are constantly connected to two 'neighbors' (b), there is no significant difference when any of these parameters are varied. (c) In the case of groups interacting via an asymmetric $\mathbf{C}$ optimized for specialization, we observe increased specialization with increased group size.

for both population size and selection steps of 1000 for the noninteracting case (S2a, figure 2a), the case of 2 constant connections (S2b, figure 2c), and the asymmetric case optimized for specialization (S2c, figure 3c). Note that there is no difference in the specialization of the final configuration when population size or number of steps are increased.

We also explored the result of increasing group size from 10 to 100 in each of the three cases mentioned above. Only in the third case is group size dependence demonstrated; consistent with previous work, specialization is more readily achieved with increased group size. When simulating groups of 100, the threshold for deleterious mutations was decreased to $.1\%$ of group fitness; this kept the simulation size-invariant by preserving at 10% the maximum possible loss in group fitness from one round of resource redistribution.

Finally, we tested the results of raising the threshold for the allowance of deleterious mutations; allowing mutations that were deleterious by 5 or 10 percent rather than the 1% (for groups of $n = 10$) used throughout this work resulted in noisier results (Fig. D.3).

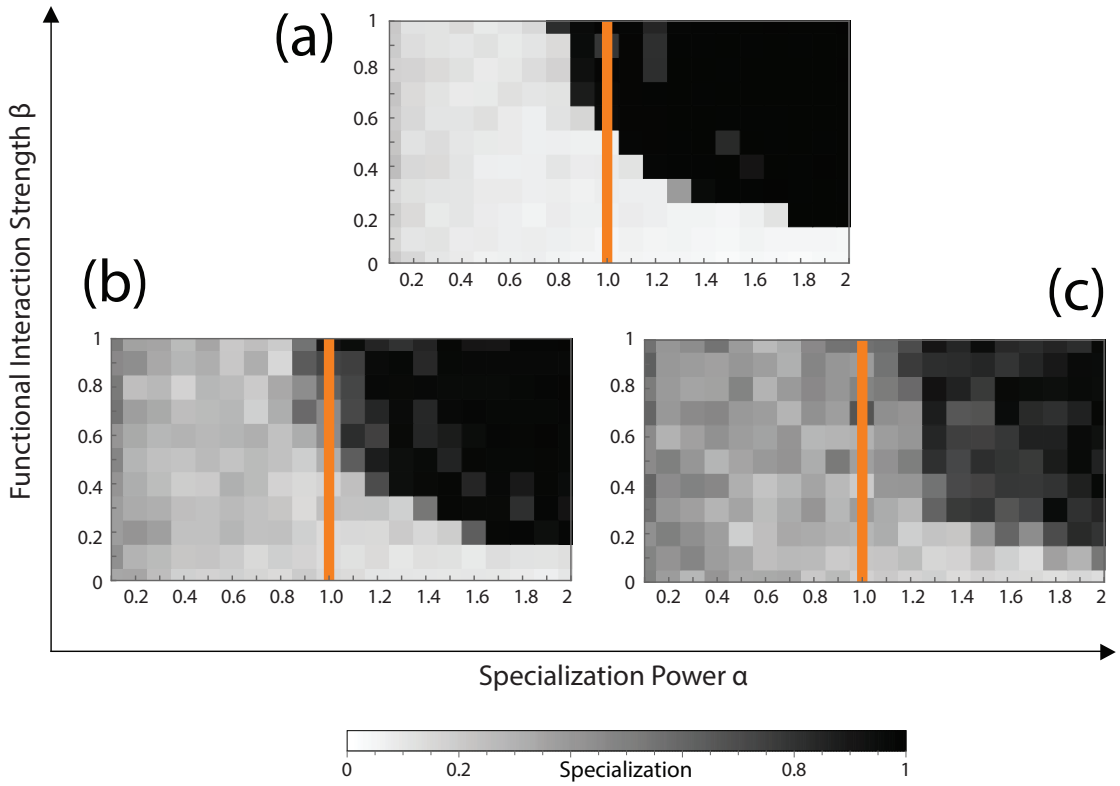

Figure D.3: DELETERIOUS MUTATIONS. (a) Heat map of specialization as a function of specialization power and functional interaction strength for two constant neighbors with a deleterious mutation threshold of 1%. As the deleterious mutation threshold is raised, the results become noisier; results when the threshold is 5% and 10% are shown in panels (b) and (c), respectively.

REFERENCES

[1] C. Darwin, *On the Origin of Species by Means of Natural Selection*. London: Murray, 1859, or the Preservation of Favored Races in the Struggle for Life.

[2] E. Szathmáry, "Toward major evolutionary transitions theory 2.0," *Proceedings of the National Academy of Sciences*, vol. 112, no. 33, pp. 10 104–10 111, 2015.

[3] E. Szathmary and J. M. Smith, "The major evolutionary transitions," *Nature*, vol. 374, no. 6519, pp. 227–232, Mar. 1995.

[4] E. Clarke, "Origins of evolutionary transitions," *Journal of Biosciences*, vol. 39, no. 2, pp. 303–317, Apr. 2014.

[5] R. B.S.M. L. Feynman R. P.; Leighton, *The Feynman lectures on physics*. Addison Wesley, 1963, ISBN: 9780201021165.

[6] S. R. Nagel, "Experimental soft-matter science," *Rev. Mod. Phys.*, vol. 89, p. 025 002, 2 Apr. 2017.

[7] D. L. Kirk, "A twelve-step program for evolving multicellularity and a division of labor," *BioEssays*, vol. 27, no. 3, pp. 299–310, 2005.

[8] M. Willensdorfer, "Organism size promotes the evolution of specialized cells in multicellular digital organisms," *Journal of evolutionary biology*, vol. 21, no. 1, pp. 104–110, Jan. 2008.

[9] J. T. Bonner, "The origins of multicellularity," *Integrative Biology: Issues, News, and Reviews*, vol. 1, no. 1, pp. 27–36, 1998.

[10] S. R. Fairclough, M. J. Dayel, and N. King, "Multicellular development in a choanoflagellate," *Current biology : CB*, vol. 20, no. 20, R875–R876, Oct. 26, 2010.

[11] R. K. Grosberg and R. R. Strathmann, "The evolution of multicellularity: A minor major transition?" *Annual Review of Ecology, Evolution, and Systematics*, vol. 38, pp. 621–654, 2007.

[12] L. W. Buss, *The Evolution of Individuality*. Princeton University Press, 1988, ISBN: 9781400858712.

[13] R. E. Michod and D. Roze, "Cooperation and conflict in the evolution of multicellularity," *Heredity*, vol. 86, 1 EP –, Jan. 1, 2001.

[14] S. A. Frank, *Foundations of Social Evolution*. Princeton University Press, 1998, ISBN: 9780691059341.

[15] R. Grosberg and R. Strathmann, "One cell, two cell, red cell, blue cell: The persistence of a unicellular stage in multicellular life histories," *Trends in Ecology & Evolution*, vol. 13, no. 3, pp. 112 –116, 1998.

[16] G. J. Velicer, L. Kroos, and R. E. Lenski, "Developmental cheating in the social bacterium myxococcus xanthus," *Nature*, vol. 404, 598 EP –, Apr. 6, 2000.

[17] R. E. MICHOD and M. D. HERRON, "Cooperation and conflict during evolutionary transitions in individuality," *Journal of Evolutionary Biology*, vol. 19, no. 5, pp. 1406–1409,

[18] S. P. Diggle, A. S. Griffin, G. S. Campbell, and S. A. West, "Cooperation and conflict in quorum-sensing bacterial populations," *Nature*, vol. 450, 411 EP –, Nov. 15, 2007.

[19] O. M. Gilbert, K. R. Foster, N. J. Mehdiabadi, J. E. Strassmann, and D. C. Queller, "High relatedness maintains multicellular cooperation in a social amoeba by controlling cheater mutants," *Proceedings of the National Academy of Sciences*, vol. 104, no. 21, pp. 8913–8917, 2007.

[20] R. C. Lewontin, "The units of selection," *Annual Review of Ecology and Systematics*, vol. 1, no. 1, pp. 1–18, 1970.

[21] S. Okasha, *Evolution and the Levels of Selection*. Clarendon Press, Nov. 2006, ISBN: 9780199267972.

[22] J. Griesemer, "The units of evolutionary transition," *Selection*, vol. 1, no. 1-3, pp. 67–80, 2001.

[23] P. Nonacs, "Monogamy and high relatedness do not preferentially favor the evolution of cooperation," *BMC Evolutionary Biology*, vol. 11, no. 1, p. 58, 2011.

[24] R. H. Kessin, G. G. Gundersen, V Zaydfudim, and M Grimson, "How cellular slime molds evade nematodes," *Proceedings of the National Academy of Sciences*, vol. 93, no. 10, pp. 4857–4861, 1996.

[25] M. E. Boraas, D. B. Seale, and J. E. Boxhorn, "Phagotrophy by a flagellate selects for colonial prey: A possible origin of multicellularity," *Evolutionary Ecology*, vol. 12, no. 2, pp. 153–164, 1998.

[26] S. Smukalla, M. Caldara, N. Pochet, A. Beauvais, S. Guadagnini, C. Yan, M. D. Vinces, A. Jansen, M. C. Prevost, J.-P. Latgé, G. R. Fink, K. R. Foster, and K. J.

Verstrepen, "¡em¿flo1¡/em¿ is a variable green beard gene that drives biofilm-like cooperation in budding yeast," *Cell*, vol. 135, no. 4, pp. 726–737, Nov. 2008.

[27] J. H. Koschwanez, K. R. Foster, and A. W. Murray, "Improved use of a public good selects for the evolution of undifferentiated multicellularity," *eLife*, vol. 2, D. Tautz, Ed., e00367, 2013.

[28] T. Pfeiffer and S. Bonhoeffer, "An evolutionary scenario for the transition to undifferentiated multicellularity," *Proceedings of the National Academy of Sciences*, vol. 100, no. 3, pp. 1095–1098, 2003.

[29] M. D. Herron, J. D. Hackett, F. O. Aylward, and R. E. Michod, "Triassic origin and early radiation of multicellular volvocine algae," *Proceedings of the National Academy of Sciences of the United States of America*, vol. 106, no. 9, pp. 3254–3258, Mar. 3, 2009.

[30] E. R. Hanschen, T. N. Marriage, P. J. Ferris, T. Hamaji, A. Toyoda, A. Fujiyama, R. Neme, H. Noguchi, Y. Minakuchi, M. Suzuki, H. Kawai-Toyooka, D. R. Smith, H. Sparks, J. Anderson, R. Bakarić, V. Luria, A. Karger, M. W. Kirschner, P. M. Durand, R. E. Michod, H. Nozaki, and B. J.S. C. Olson, "The gonium pectorale genome demonstrates co-option of cell cycle regulation during the evolution of multicellularity," *Nature Communications*, vol. 7, 11370 EP –, Apr. 22, 2016.

[31] J. B. Kirkegaard, A. Bouillant, A. O. Marron, K. C. Leptos, and R. E. Goldstein, "Aerotaxis in the closest relatives of animals," *eLife*, vol. 5, R. M. Berry, Ed., e18109, Nov. 2016.

[32] D. P. Anderson, D. S. Whitney, V. Hanson-Smith, A. Woznica, W. Campodonico-Burnett, B. F. Volkman, N. King, J. W. Thornton, and K. E. Prehoda, "Evolution of an ancient protein function involved in organized multicellularity in animals," *eLife*, vol. 5, J. D. Bloom, Ed., e10147, Jan. 2016.

[33] W. C. Ratcliff, R. F. Denison, M. Borrello, and M. Travisano, "Experimental evolution of multicellularity," *Proceedings of the National Academy of Sciences*, vol. 109, no. 5, pp. 201 115 323–1600, Jan. 2012.

[34] W. C. Ratcliff, J. T. Pentz, and M. Travisano, "Tempo and mode of multicellular adaptation in experimentally evolved Saccharomyces cerevisiae," *Evolution*, vol. 67, no. 6, pp. 1573–1581, Feb. 2013.

[35] W. C. Ratcliff, J. D. Fankhauser, D. W. Rogers, D. Greig, and M. Travisano, "Origins of multicellular evolvability in snowflake yeast," *Nature Communications*, vol. 6, pp. 6102+, Jan. 2015.

[36] M. D. Herron and R. E. Michod, "Evolution of complexity in the volvocine algae: Transitions in individuality through darwin's eye," *Evolution*, vol. 62, no. 2, pp. 436–451,

[37] M. Herron, "Many from one: Lessons from the volvocine algae on the evolution of multicellularity," *Communicative & Integrative Biology*, vol. 2, no. 4, pp. 368–370, 2009, PMID: 19721894.

[38] M. D. HERRON, "Origins of multicellular complexity: Volvox and the volvocine algae," *Molecular ecology*, vol. 25, no. 6, pp. 1213–1223, Mar. 2016.

[39] J. Pentz, M. Travisano, and W. Ratcliff, "Clonal development is evolutionarily superior to aggregation in wild-collected saccharomyces cerevisiae," *The 2018 Conference on Artificial Life: A Hybrid of the European Conference on Artificial Life (ECAL) and the International Conference on the Synthesis and Simulation of Living Systems (ALIFE)*, pp. 550–554, 2014.

[40] H. C. Plotkin, *The Role of Behavior in Evolution*. MIT Press, 1988, ISBN: 9780262161077.

[41] A. Donev, I. Cisse, D. Sachs, E. A. Variano, F. H. Stillinger, R. Connelly, S. Torquato, and P. M. Chaikin, "Improving the density of jammed disordered packings using ellipsoids," *Science*, vol. 303, no. 5660, pp. 990–993, 2004.

[42] S. Jacobeen, J. T. Pentz, E. C. Graba, C. G. Brandys, W. C. Ratcliff, and P. J. Yunker, "Cellular packing, mechanical stress and the evolution of multicellularity," *Nature Physics*, vol. 14, pp. 268–290, 2018.

[43] S. Jacobeen, E. C. Graba, C. G. Brandys, T. C. Day, W. C. Ratcliff, and P. J. Yunker, "Geometry, packing, and evolutionary paths to increased multicellular size," *Phys. Rev. E*, vol. 97, p. 050 401, 5 May 2018.

[44] D. T. Fraebel, H. Mickalide, D. Schnitkey, J. Merritt, T. E. Kuhlman, and S. Kuehn, "Environment determines evolutionary trajectory in a constrained phenotypic space," *eLife*, vol. 6, W. Shou, Ed., e24669, Mar. 2017.

[45] T. Nakayama, K. Yakubo, and R. L. Orbach, "Dynamical properties of fractal networks: Scaling, numerical simulations, and physical realizations," *Rev. Mod. Phys.*, vol. 66, pp. 381–443, 2 Apr. 1994.

[46] R. Orbach, "Dynamics of fractal networks," *Science*, vol. 231, no. 4740, pp. 814–819, 1986.

[47] S. Ornes, "Core concept: How nonequilibrium thermodynamics speaks to the mystery of life," *Proceedings of the National Academy of Sciences*, vol. 114, no. 3, pp. 423–424, 2017.

[48] S. C. Stearns, "Trade-offs in life-history evolution," *Functional Ecology*, vol. 3, no. 3, pp. 259–268, 1989.

[49] T. Brunet and N. King, "The origin of animal multicellularity and cell differentiation," *Developmental Cell*, vol. 43, no. 2, pp. 124–140, Oct. 23, 2017.

[50] T. Cavalier-Smith, "Origin of animal multicellularity: Precursors, causes, consequences—the choanoflagellate/sponge transition, neurogenesis and the cambrian explosion," *Philosophical Transactions of the Royal Society of London B: Biological Sciences*, vol. 372, no. 1713, 2017.

[51] D. C. Queller and J. E. Strassmann, "Beyond society: The evolution of organismality," *Philosophical Transactions of the Royal Society of London B: Biological Sciences*, vol. 364, no. 1533, pp. 3143–3155, 2009.

[52] L. Sagan, "On the origin of mitosing cells," *Journal of Theoretical Biology*, vol. 14, no. 3, pp. 225 –274, 1967.

[53] P. Godfrey-Smith, "Reproduction, symbiosis, and the eukaryotic cell," *Proceedings of the National Academy of Sciences*, vol. 112, no. 33, pp. 10 120–10 125, 2015.

[54] M. B. Dunn, "Evolutionary transitions in individuality and selection in societal evolution," in *Handbook on Evolution and Society*. Routledge, Jan. 2015, ISBN: 9781315634203.

[55] R. T.J. H. Maryanski Alexandra; Machalek, *Handbook on Evolution and Society: Toward an Evolutionary Social Science*. Routledge, Nov. 2015, ISBN: 9781317258322.

[56] R. E. Michod, "Darwinian dynamics: Evolutionary transitions in fitness and individuality," *Complexity*, vol. 5, no. 1, pp. 42–43, 1999.

[57] ——, "Evolution of individuality during the transition from unicellular to multicellular life," *Proceedings of the National Academy of Sciences*, vol. 104, no. suppl 1, pp. 8613–8618, 2007.

[58] M. P. Leslie, D. E. Shelton, and R. E. Michod, "Generation time and fitness trade-offs during the evolution of multicellularity," *Journal of Theoretical Biology*, vol. 430, pp. 92 –102, 2017.

[59] R. E. Michod and A. M. Nedelcu, "On the reorganization of fitness during evolutionary transitions in individuality1," *Integrative and Comparative Biology*, vol. 43, no. 1, pp. 64–73, 2003.

[60] H. J. Goldsby, D. B. Knoester, C. Ofria, and B. Kerr, "The evolutionary origin of somatic cells under the dirty work hypothesis," *PLOS Biology*, vol. 12, no. 5, pp. 1–11, May 2014.

[61] R. E. Michod, Y. Viossat, C. A. Solari, M. Hurand, and A. M. Nedelcu, "Life-history evolution and the origin of multicellularity," *Journal of Theoretical Biology*, vol. 239, no. 2, pp. 257 –272, 2006, Special Issue in Memory of John Maynard Smith.

[62] G. A. Cooper and S. A. West, "Division of labour and the evolution of extreme specialization," *Nature Ecology & Evolution*, 2018.

[63] I. Ispolatov, M. Ackermann, and M. Doebeli, "Division of labour and the evolution of multicellularity," *Proceedings of the Royal Society of London B: Biological Sciences*, vol. 279, no. 1734, pp. 1768–1776, 2012.

[64] C. A. Solari, J. O. Kessler, and R. E. Goldstein, "A general allometric and life-history model for cellular differentiation in the transition to multicellularity.," *The American Naturalist*, vol. 181, no. 3, pp. 369–380, 2013, PMID: 23448886.

[65] S. A. West, R. M. Fisher, A. Gardner, and E. T. Kiers, "Major evolutionary transitions in individuality," *Proceedings of the National Academy of Sciences*, vol. 112, no. 33, pp. 10 112–10 119, 2015.

[66] E. Pennisi, "The power of many," *Science*, vol. 360, no. 6396, pp. 1388–1391, 2018.

[67] P. Withers and H. Bhadeshia, "Residual stress. part 1 measurement techniques," *Materials Science and Technology*, vol. 17, no. 4, pp. 355–365, 2001.

[68] M. R. Ahmad*, M. Nakajima, S. Kojima, M. Homma, and T. Fukuda, "The effects of cell sizes, environmental conditions, and growth phases on the strength of individual w303 yeast cells inside esem," *IEEE Transactions on NanoBioscience*, vol. 7, no. 3, pp. 185–193, Sep. 2008.

[69] M. Delarue, J. Hartung, C. Schreck, P. Gniewek, L. Hu, S. Herminghaus, and O. Hallatschek, "Self-driven jamming in growing microbial populations," *Nature Physics*, vol. 12, 762 EP –, May 9, 2016.

[70] C. S. O'Hern, L. E. Silbert, A. J. Liu, and S. R. Nagel, "Jamming at zero temperature and zero applied stress: The epitome of disorder," *Phys. Rev. E*, vol. 68, p. 011 306, 1 Jul. 2003.

[71] E. Libby, W. Ratcliff, M. Travisano, and B. Kerr, "Geometry shapes evolution of early multicellularity," *PLOS Computational Biology*, vol. 10, no. 9, pp. 1–12, Sep. 2014.

[72] Y.-J. Sheu, Y. Barral, and M. Snyder, "Polarized growth controls cell shape and bipolar bud site selection in saccharomyces cerevisiae," *Molecular and Cellular Biology*, vol. 20, no. 14, pp. 5235–5247, 2000.

[73] W. P. J. Smith, Y. Davit, J. M. Osborne, W. Kim, K. R. Foster, and J. M. Pitt-Francis, "Cell morphology drives spatial patterning in microbial communities," *Proceedings of the National Academy of Sciences*, Dec. 2016.

[74] R. E. Lenski and M Travisano, "Dynamics of adaptation and diversification: A 10,000-generation experiment with bacterial populations," *Proceedings of the National Academy of Sciences*, vol. 91, no. 15, pp. 6808–6814, 1994.

[75] P. J. Gerrish and R. E. Lenski, "The fate of competing beneficial mutations in an asexual population," *Genetica*, vol. 102, no. 0, p. 127, Mar. 1998.

[76] A. H. Knoll, "The multiple origins of complex multicellularity," *Annual Review of Earth and Planetary Sciences*, vol. 39, pp. 217–239, 2011.

[77] B. Ilkanaiv, D. B. Kearns, G. Ariel, and A. Beer, "Effect of Cell Aspect Ratio on Swarming Bacteria," *Physical Review Letters*, vol. 118, no. 15, Apr. 2017.

[78] O. Guadayol, K. L. Thornton, and S. Humphries, "Cell morphology governs directional control in swimming bacteria," *Scientific Reports*, vol. 7, no. 2061, May 2017.

[79] J. Varennes, S. Fancher, B. Han, and A. Mugler, "Emergent versus individual-based multicellular chemotaxis," *Phys. Rev. Lett.*, vol. 119, p. 188 101, 18 Oct. 2017.

[80] W. C. Ratcliff, M. D. Herron, K. Howell, J. T. Pentz, F. Rosenzweig, and M. Travisano, "Experimental evolution of an alternating uni-and multicellular life cycle in chlamydomonas reinhardtii," *Nature Communications*, vol. 4, 2013.

[81] S. J. Erickson, R. W. Prost, and M. E. Timins, "The "magic angle" effect: Background physics and clinical relevance.," *Radiology*, vol. 188, no. 1, pp. 23–25, 1993, PMID: 7685531.

[82] A. J. Liu and S. R. Nagel, "The jamming transition and the marginally jammed solid," *Annual Review of Condensed Matter Physics*, vol. 1, no. 1, pp. 347–369, 2010.

[83] H. M. Jaeger, S. R. Nagel, and R. P. Behringer, "Granular solids, liquids, and gases," *Rev. Mod. Phys.*, vol. 68, pp. 1259–1273, 4 Oct. 1996.

[84] Y. Hosokawa, M. Hagiyama, T. Iino, Y. Murakami, and A. Ito, "Noncontact estimation of intercellular breaking force using a femtosecond laser impulse quantified by atomic force microscopy," *Proceedings of the National Academy of Sciences*, vol. 108, no. 5, pp. 1777–1782, 2011.

[85] S. Bajpai, Y. Feng, R. Krishnamurthy, G. D. Longmore, and D. Wirtz, "Loss of -catenin decreases the strength of single e-cadherin bonds between human cancer cells," *The Journal of Biological Chemistry*, vol. 284, no. 27, pp. 18 252–18 259, Jul. 3, 2009.

[86] Y. Hu, J. Ulstrup, and J. Zhang, "Bacterial biofilms investigated by atomic force microscopy and electrochemistry," PhD thesis, 2012.

[87] W. C. Ratcliff, M. Herron, P. L. Conlin, and E. Libby, "Nascent life cycles and the emergence of higher-level individuality," *Phil. Trans. R. Soc. B*, vol. 372, no. 1735, p. 20 160 420, 2017.

[88] J. T. Pentz, B. P. Taylor, and W. C. Ratcliff, "Apoptosis in snowflake yeast: Novel trait, or side effect of toxic waste?" *Journal of The Royal Society Interface*, vol. 13, no. 118, p. 20 160 121, 2016.

[89] D. W. McShea, "Functional complexity in organisms: Parts as proxies," *Biology and Philosophy*, vol. 15, no. 5, pp. 641–668, Nov. 2000.

[90] J. Smith and E. Szathmary, *The Major Transitions in Evolution*. OUP Oxford, 1997, ISBN: 9780198502944.

[91] H. J. Goldsby, A. Dornhaus, B. Kerr, and C. Ofria, "Task-switching costs promote the evolution of division of labor and shifts in individuality," *Proceedings of the National Academy of Sciences*, vol. 109, no. 34, pp. 13 686–13 691, 2012.

[92] P. A. Corning and E. Szathmry, "synergistic selectioni: A darwinian frame for the evolution of complexity," *Journal of Theoretical Biology*, vol. 371, pp. 45 –58, 2015.

[93] C. A. Hidalgo and R. Hausmann, "The building blocks of economic complexity," *Proceedings of the National Academy of Sciences*, vol. 106, no. 26, pp. 10 570–10 575, 2009.

[94] G. Boza, A. Szilágyi, Á. Kun, M. Santos, and E. Szathmáry, "Evolution of the division of labor between genes and enzymes in the rna world," *PLOS Computational Biology*, vol. 10, no. 12, pp. 1–9, Dec. 2014.

[95] M. Taborsky, J. G. Frommen, and C. Riehl, "Correlated pay-offs are key to cooperation," *Philosophical Transactions of the Royal Society of London B: Biological Sciences*, vol. 371, no. 1687, 2016.

[96] R. E. Page, R. Scheiner, J. Erber, and G. V. Amdam, "The development and evolution of division of labor and foraging specialization in a social insect (apis mellifera l.)," *Current Topics in Developmental Biology*, Current Topics in Developmental Biology, vol. 74, pp. 253 –286, 2006.

[97] C. Rueffler, J. Hermisson, and G. P. Wagner, "Evolution of functional specialization and division of labor," *Proceedings of the National Academy of Sciences*, vol. 109, no. 6, pp. 1830–1831, 2012.

[98] P. Szekely, H. Sheftel, A. Mayo, and U. Alon, "Evolutionary tradeoffs between economy and effectiveness in biological homeostasis systems," *PLOS Computational Biology*, vol. 9, no. 8, pp. 1–14, Aug. 2013.

[99] E. Clarke, "The problem of biological individuality," *Biological Theory*, vol. 5, no. 4, pp. 312–325, Dec. 2010.

[100] M. Montvil and M. Mossio, "Biological organisation as closure of constraints," *Journal of Theoretical Biology*, vol. 372, pp. 179 –191, 2015.

[101] L. A. Ferry-Graham, D. I. Bolnick, and P. C. Wainwright, "Using functional morphology to examine the ecology and evolution of specialization1," *Integrative and Comparative Biology*, vol. 42, no. 2, pp. 265–277, 2002.

[102] F. Galis, "The application of functional morphology to evolutionary studies," *Trends in Ecology & Evolution*, vol. 11, no. 3, pp. 124 –129, 1996.

[103] D. M. Dehling, P. Jordano, H. M. Schaefer, K. Böhning-Gaese, and M. Schleuning, "Morphology predicts species' functional roles and their degree of specialization in plant–frugivore interactions," *Proceedings of the Royal Society of London B: Biological Sciences*, vol. 283, no. 1823, 2016.

[104] S. Lidgard, M. C. Carter, M. H. Dick, D. P. Gordon, and A. N. Ostrovsky, "Division of labor and recurrent evolution of polymorphisms in a group of colonial animals," *Evolutionary Ecology*, vol. 26, no. 2, pp. 233–257, Mar. 2012.

[105] B. Allen, G. Lippner, Y.-T. Chen, B. Fotouhi, N. Momeni, S.-T. Yau, and M. A. Nowak, "Evolutionary dynamics on any population structure," *Nature*, vol. 544, 227 EP –, Mar. 2017.

[106] A. Pavlogiannis, J. Tkadlec, K. Chatterjee, and M. A. Nowak, "Construction of arbitrarily strong amplifiers of natural selection using evolutionary graph theory," *Communications Biology*, vol. 1, no. 1, p. 71, 2018.

[107] I. Berman-Frank, A. Quigg, Z. V. Finkel, A. J. Irwin, and L. Haramaty, "Nitrogen-fixation strategies and fe requirements in cyanobacteria," *Limnology and Oceanography*, vol. 52, no. 5, pp. 2260–2269, 2007.

[108] R. E. Michod, "On the transfer of fitness from the cell to the multicellularorganism," *Biology and Philosophy*, vol. 20, no. 5, pp. 967–987, Nov. 2005.

[109] Y. Ulrich, J. Saragosti, C. K. Tokita, C. E. Tarnita, and D. J. C. Kronauer, "Fitness benefits and emergent division of labour at the onset of group living," *Nature*, Aug. 2018.

[110] R. Jeanson, J. H. Fewell, R. Gorelick, and S. M. Bertram, "Emergence of increased division of labor as a function of group size," *Behavioral Ecology and Sociobiology*, vol. 62, no. 2, pp. 289–298, Dec. 2007.

[111] S. Bengtson, T. Sallstedt, V. Belivanova, and M. Whitehouse, "Three-dimensional preservation of cellular and subcellular structures suggests 1.6 billion-year-old crown-group red algae," *PLOS Biology*, vol. 15, no. 3, pp. 1–38, Mar. 2017.

[112] M. L. Droser and J. G. Gehling, "Synchronous aggregate growth in an abundant new ediacaran tubular organism," *Science*, vol. 319, no. 5870, pp. 1660–1662, 2008.

[113] B. Salamaga, T. K. Prajsnar, A. Jareo-Martinez, J. Willemse, M. A. Bewley, F. Chau, T. Ben Belkacem, A. H. Meijer, D. H. Dockrell, S. A. Renshaw, and S. Mesnage, "Bacterial size matters: Multiple mechanisms controlling septum cleavage and diplococcus formation are critical for the virulence of the opportunistic pathogen enterococcus faecalis," *PLOS Pathogens*, vol. 13, no. 7, pp. 1–26, Jul. 2017.

[114] M. McCarthy and B. Enquist, "Organismal size, metabolism and the evolution of complexity in metazoans," in *Evolutionary Ecology Research*, vol. 7, Jul. 2005, pp. 681–696.

[115] N. A. Heim, J. L. Payne, S. Finnegan, M. L. Knope, M. Kowalewski, S. K. Lyons, D. W. McShea, P. M. Novack-Gottshall, F. A. Smith, and S. C. Wang, "Hierarchical complexity and the size limits of life," *Proceedings of the Royal Society of London B: Biological Sciences*, vol. 284, no. 1857, 2017.

[116] C. R. McClain and A. G. Boyer, "Biodiversity and body size are linked across metazoans," *Proceedings of the Royal Society of London B: Biological Sciences*, vol. 276, no. 1665, pp. 2209–2215, 2009.

[117] C. E. Tarnita, C. H. Taubes, and M. A. Nowak, "Evolutionary construction by staying together and coming together," *Journal of Theoretical Biology*, vol. 320, pp. 10 –22, 2013.

[118] M. Abedin and N. King, "Diverse evolutionary paths to cell adhesion," *Trends in Cell Biology*, vol. 20, no. 12, pp. 734 –742, 2010, Special issue - CellBio-X.

[119] Q. Du, Y. Kawabe, C. Schilde, Z. hui Chen, and P. Schaap, "The evolution of aggregative multicellularity and cellcell communication in the dictyostelia," *Journal of Molecular Biology*, vol. 427, no. 23, pp. 3722 –3733, 2015, Cooperative Behaviour in Microbial Communities.

[120] A. Seb-Pedrs, M. Irimia, J. del Campo, H. Parra-Acero, C. Russ, C. Nusbaum, B. J. Blencowe, and I. Ruiz-Trillo, "Regulated aggregative multicellularity in a close unicellular relative of metazoa," *eLife*, vol. 2, D. Tautz, Ed., e01287, Dec. 2013.

[121] F. A. Smith, J. L. Payne, N. A. Heim, M. A. Balk, S. Finnegan, M. Kowalewski, S. K. Lyons, C. R. McClain, D. W. McShea, P. M. Novack-Gottshall, P. S. Anich, and S. C. Wang, "Body size evolution across the geozoic," *Annual Review of Earth and Planetary Sciences*, vol. 44, no. 1, pp. 523–553, 2016.

[122] J. L. Payne, A. G. Boyer, J. H. Brown, S. Finnegan, M. Kowalewski, R. A. Krause, S. K. Lyons, C. R. McClain, D. W. McShea, P. M. Novack-Gottshall, F. A. Smith, J. A. Stempien, and S. C. Wang, "Two-phase increase in the maximum size of life over 3.5 billion years reflects biological innovation and environmental opportunity," *Proceedings of the National Academy of Sciences*, vol. 106, no. 1, pp. 24–27, 2009.

[123] B. Rosslenbroich, "The evolution of multicellularity in animals as a shift in biological autonomy," *Theory in Biosciences*, vol. 123, no. 3, pp. 243 –262, 2005.

[124] J. F. Nash, "Equilibrium points in n-person games," *Proceedings of the National Academy of Sciences*, vol. 36, no. 1, pp. 48–49, 1950.

[125] J. M. Smith, "Evolution and the theory of games," in *Did Darwin Get It Right? Essays on Games, Sex and Evolution*. Boston, MA: Springer US, 1988, pp. 202–215, ISBN: 978-1-4684-7862-4.

[126] L. Chen, S. Xiao, K. Pang, C. Zhou, and X. Yuan, "Cell differentiation and germsoma separation in ediacaran animal embryo-like fossils," *Nature*, vol. 516, 238 EP –, Sep. 2014.

[127] B. E. Schirrmeister, A. Antonelli, and H. C. Bagheri, "The origin of multicellularity in cyanobacteria," *BMC Evolutionary Biology*, vol. 11, no. 1, p. 45, 2011.

[128] J. van Gestel and C. E. Tarnita, "On the origin of biological construction, with a focus on multicellularity," *Proceedings of the National Academy of Sciences*, vol. 114, no. 42, pp. 11 018–11 026, 2017.

[129] R. M. Fisher, C. K. Cornwallis, and S. A. West, "Group formation, relatedness, and the evolution of multicellularity," *Current Biology*, vol. 23, no. 12, pp. 1120 –1125, 2013.

[130] T. Poisot, J. D. Bever, A. Nemri, P. H. Thrall, and M. E. Hochberg, "A conceptual framework for the evolution of ecological specialisation," *Ecology Letters*, vol. 14, no. 9, pp. 841–851, Jun. 2011.

[131] D. G. Rand, M. A. Nowak, J. H. Fowler, and N. A. Christakis, "Static network structure can stabilize human cooperation," *Proceedings of the National Academy of Sciences*, vol. 111, no. 48, pp. 17 093–17 098, 2014.

[132] J. J. Kuzdzal-Fick, S. A. Fox, J. E. Strassmann, and D. C. Queller, "High relatedness is necessary and sufficient to maintain multicellularity in dictyostelium," *Science*, vol. 334, no. 6062, pp. 1548–1551, 2011.

[133] D. C. Queller, "Relatedness and the fraternal major transitions," *Philosophical Transactions of the Royal Society of London B: Biological Sciences*, vol. 355, no. 1403, pp. 1647–1655, 2000.

[134] S. A. West, A. S. Griffin, and A. Gardner, "Evolutionary explanations for cooperation," *Current Biology*, vol. 17, no. 16, R661 –R672, 2007.

[135] G. Uppal and D. C. Vural, "Shearing in flow environment promotes evolution of social behavior in microbial populations," *eLife*, vol. 7, J. Gore, Ed., e34862, May 2018.

[136] P. Nonacs, "Kinship, greenbeards, and runaway social selection in the evolution of social insect cooperation," *Proceedings of the National Academy of Sciences*, vol. 108, no. Supplement 2, pp. 10 808–10 815, 2011.

[137] D. C. Queller, "Cooperators since life began," *The Quarterly Review of Biology*, vol. 72, no. 2, pp. 184–188, 1997.

[138] M. Delarue, J. Hartung, C. Schreck, P. Gniewek, L. Hu, S. Herminghaus, and O. Hallatschek, "Self-driven jamming in growing microbial populations," *Nature physics*, vol. 12, no. 8, pp. 762–766, 2016.

[139] M. Buchanan, "Simple yet successful," *Nature Physics*, vol. 13, 720 EP –, Aug. 2, 2017.

[140] M. K. Transtrum, B. B. Machta, K. S. Brown, B. C. Daniels, C. R. Myers, and J. P. Sethna, "Perspective: Sloppiness and emergent theories in physics, biology, and beyond," *The Journal of Chemical Physics*, vol. 143, no. 1, p. 010 901, 2015.

[141] H. H. Mattingly, M. K. Transtrum, M. C. Abbott, and B. B. Machta, "Maximizing the information learned from finite data selects a simple model," *Proceedings of the National Academy of Sciences*, vol. 115, no. 8, pp. 1760–1765, 2018.

VITA

Born and raised in the Hershey, Pennsylvania, Shane Jacobeen graduated Summa Cum Laude from nearby Lebanon Valley College in the spring of 2014. Since enrolling in graduate school at the Georgia Institute of Technology in the fall of the same year, Jacobeen has been the recipient of several awards and honors, including the STAMI Graduate Fellowship, the Sam Nunn Security Program Fellowship, and as the student speaker for the innagural 2018 Graduate Student Convocation. Upon reception of his Ph.D. in physics, Jacobeen will begin a position as a Senior Consultant in Ernst & Young's division of Project Portfolio Management.